OBTAINING MODAL MODELS OF A NONLINEAR STRUCTURE USING FORCE-CONTROLLED FREQUENCY RESPONSE FUNCTIONS

A THESIS SUBMITTED TO
THE GRADUATE SCHOOL OF NATURAL AND APPLIED SCIENCES
OF
MIDDLE EAST TECHNICAL UNIVERSITY

BY

MUHAMMED FATİH GÜRBÜZ

IN PARTIAL FULFILLMENT OF THE REQUIREMENTS
FOR
THE DEGREE OF MASTER OF SCIENCE
IN
MECHANICAL ENGINEERING

JULY 2024

Approval of the thesis:

OBTAINING MODAL MODELS OF A NONLINEAR STRUCTURE USING FORCE-CONTROLLED FREQUENCY RESPONSE FUNCTIONS

submitted by **MUHAMMED FATİH GÜRBÜZ** in partial fulfillment of the requirements for the degree of **Master of Science** i**n Mechanical Engineering, Middle East Technical University** by,

Prof. Dr. Naci Emre Altun
Dean, **Graduate School of Natural and Applied Sciences** _____

Prof. Dr. M. A. Sahir Arıkan
Head of the Department, **Mechanical Engineering** _____

Assoc. Prof. Dr. M. Bülent Özer
Supervisor, **Mechanical Engineering, METU** _____

Prof. Dr. H. Nevzat Özgüven
Co-Supervisor, **Mechanical Engineering, METU** _____

Examining Committee Members:

Prof. Dr. Yiğit Yazıcıoğlu
Mechanical Engineering, METU _____

Assoc. Prof. Dr. M. Bülent Özer
Mechanical Engineering, METU _____

Prof. Dr. Ender Ciğeroğlu
Mechanical Engineering, METU _____

Assist. Prof. Dr. Orkun Özşahin
Mechanical Engineering, METU. _____

Assoc. Prof. Dr. Can Ulaş Doğruer
Mechanical Engineering, Hacettepe University _____

Date: 08.07.2024

I hereby declare that all information in this document has been obtained and presented in accordance with academic rules and ethical conduct. I also declare that, as required by these rules and conduct, I have fully cited and referenced all material and results that are not original to this work.

Name, Last name: Muhammed Fatih Gürbüz

Signature:

ABSTRACT

OBTAINING MODAL MODELS OF A NONLINEAR STRUCTURE USING FORCE-CONTROLLED FREQUENCY RESPONSE FUNCTIONS

Gürbüz, Muhammed Fatih
Master of Science, Mechanical Engineering
Supervisor: Assoc. Prof. Dr. M. Bülent Özer
Co-Supervisor: Prof. Dr. H. Nevzat Özgüven

July 2024, 124 pages

Identification of physical and modal parameters of an engineering structure is important in the field of structural dynamics in order to establish input and output (i.e. forcing and displacement) relationships of the structure. Linear structure identification is a rather well-established field thanks to the research performed on it over several decades. Modal analysis is the most widespread approach used in this area. On the other hand, nonlinear system identification is significantly more challenging and there has been great interest in it over the recent years. There are several different and novel identification approaches proposed by different researchers in the nonlinear structural dynamics field. Response-controlled stepped sine testing (RCT) is one of these methods which is implemented by keeping the response amplitude of a degree of freedom constant over different excitation frequencies. It offers important advantages such as not needing to know nonlinearity infected coordinates and the type of nonlinearities in the structure, and provides a modal model for the whole nonlinear structure. However, most of the experimental methods and testing hardware are compatible with constant amplitude forcing tests rather than constant response tests. This thesis aims to introduce a new approach that extends the use of the response-controlled nonlinear structural identification method to the structural response data acquired with constant amplitude forcing tests. The

proposed approach first forms a harmonic force surface (HFS) which is obtained from the measured response through constant force amplitude tests. The constant-response frequency response functions (FRFs) are obtained from this surface data and the modal parameters of the nonlinear structure are identified. The proposed method is validated using numerical case studies, experimental data shared by other researchers as well as the experiments performed as a part of this thesis. This study has the potential to extend the applicability of nonlinear structural identification with response-controlled testing by making it compatible with constant amplitude force data and testing equipment.

Keywords: Nonlinear System Identification, Nonlinear Experimental Modal Analysis, Response-Controlled Stepped-Sine Testing, Force-Controlled Stepped-Sine Testing, Harmonic Force Surface

ÖZ

KUVVET KONTROLLÜ FREKANS CEVAP FONKSİYONLARI KULLANILARAK DOĞRUSAL OLMAYAN BİR YAPININ MODAL MODELLERİNİN ELDE EDİLMESİ

Gürbüz, Muhammed Fatih
Yüksek Lisans, Makina Mühendisliği
Tez Yöneticisi: Doç. Dr. M. Bülent Özer
Ortak Tez Yöneticisi: Prof. Dr. H. Nevzat Özgüven

Temmuz 2024, 124sayfa

Bir mühendislik yapısının fiziksel ve modal parametrelerinin tanımlanması, yapının giriş ve çıkış (yani zorlayıcı ve yer değiştirme) ilişkilerini kurmak amacıyla yapısal dinamikler alanında önemlidir. Doğrusal yapı tanımlama, üzerinde yapılan onlarca yıllık araştırmalar sayesinde oldukça iyi kurulmuş bir alandır. Modal analiz, bu alanda kullanılan en yaygın yaklaşımdır. Diğer yandan, doğrusal olmayan sistem tanımlama önemli ölçüde daha zordur ve son yıllarda büyük ilgi görmektedir. Doğrusal olmayan yapısal dinamikler alanında farklı araştırmacılar tarafından önerilen birkaç farklı ve yenilikçi tanımlama yaklaşımı bulunmaktadır. Yanıt kontrollü adımlı sinüs testi (RCT), farklı uyarım frekansları boyunca bir serbestlik derecesinin yanıt genliğini sabit tutarak uygulanan bu yöntemlerden biridir. Yapıdaki doğrusal olmayanlık etkilenmiş koordinatları ve doğrusal olmayanlık türlerini bilmeye gerek duymamak gibi önemli avantajlar sunar ve tüm doğrusal viii olmayan yapı için modal bir model sağlar. Ancak, çoğu deneysel yöntem ve test donanımı, sabit yanıt testlerinden ziyade sabit genlik zorlayıcı testlerle uyumludur. Bu tez, sabit genlik zorlayıcı testlerle elde edilen yapısal yanıt verilerini kullanarak yanıt kontrollü doğrusal olmayan yapısal tanımlama yönteminin kullanımını genişleten yeni bir yaklaşım tanıtmayı amaçlamaktadır. Önerilen yaklaşım, ilk olarak

sabit zorlayıcı genlik testleri ile ölçülen yanıt üzerinden elde edilen harmonik zorlayıcı yüzeyini (HFS) oluşturur. Bu yüzey verilerinden sabit yanıt frekans yanıt fonksiyonları (FRF'ler) elde edilir ve doğrusal olmayan yapının modal parametreleri tanımlanır. Önerilen yöntem, sayısal vaka çalışmaları, diğer araştırmacılar tarafından paylaşılan deneysel veriler ve bu tezin bir parçası olarak gerçekleştirilen deneylerle doğrulanmıştır. Bu çalışma, sabit genlik zorlayıcı veri ve test ekipmanları ile uyumlu hale getirerek yanıt kontrollü testlerle doğrusal olmayan yapısal tanımlamanın uygulanabilirliğini genişletme potansiyeline sahiptir.

Anahtar Kelimeler: Doğrusal Olmayan Sistem Tanımlama, doğrusal olmayan deneysel modal analiz, Tepki Kontrollü Kademeli Sinüs Testi, Kuvvet Kontrollü Kademeli Sinüs Testi, Harmonik Kuvvet Yüzeyi

To my beloved family, whose unwavering support and boundless love have been my guiding light.

ACKNOWLEDGMENTS

Firstly, I am deeply honored to have had the opportunity to work with Prof. Dr. H. Nevzat Özgüven and Assoc. Prof. Dr. M. Bülent Özer. Their guidance and support throughout the thesis process have been invaluable, and I have learned immensely from them. I am profoundly grateful to be one of their students.

Furthermore, I extend my gratitude to SAGE for providing the experimental setups and the space necessary for this research. Lastly, I would like to thank ODTÜ-DİMER for offering a workspace whenever I needed it.

TABLE OF CONTENTS

ABSTRACT v

ÖZ vii

ACKNOWLEDGMENTS x

TABLE OF CONTENTS xi

LIST OF TABLES xiii

LIST OF FIGURES xiv

LIST OF ABBREVIATIONS xx

LIST OF SYMBOLS xxii

CHAPTERS

1 INTRODUCTION 1

1.1 Motivation of the Thesis 1

1.2 Literature Review 2

1.3 Outline of Thesis 8

2 NONLINEAR RESPONSE OF DYNAMIC SYSTEMS 9

2.1 Nonlinear Equation of Motion 9

2.2 Quasi-Linearization of Nonlinear Equation of Motion 10

2.2.1 Describing Function Method (DFM) 10

2.3 Solution Techniques of Nonlinear Equation Sets 13

2.3.1 Newton Raphson Method 14

2.3.2 Newton's Method Coupled with Arclength Continuation 14

3 THEORY AND NUMERICAL APPLICATIONS OF THE FCT-HFS FRAMEWORK 19

3.1 Theory of FCT-HFS Framework 19

3.1.1 Single Nonlinear Normal Mode Theory 20
3.1.2 Theory of Response-Controlled Stepped-Sine Testing (RCT) and Harmonic Force Surface (HFS) 22
3.2 Numerical Applications and Procedure of FCT-HFS Framework 32
3.2.1 Multi Degree of Freedom (MDOF) System with Cubic Stiffness 1 . 32
3.2.2 Multi Degree of Freedom (MDOF) System with Cubic Stiffness 2 . 42
3.3 Summary 47
4 EXPERIMENTAL APPLICATIONS OF THE FCT-HFS FRAMEWORK .. 49
4.1 Brake-Reuß Beam Tests Conducted in TÜBİTAK SAGE 51
4.1.1 Test Setup 51
4.1.2 Test 1: Test with Tightening Torque of 10 Nm 54
4.1.3 Test 2: Test with Tightening Torque of 25 Nm 70
4.2 The Orion Beam 74
4.2.1 Third Bending Mode 74
4.2.2 Sixth Bending Mode 79
4.3 The Length Modified Brake-Reuß Beam (LBRB) 91
4.3.1 Mode 1 91
4.3.2 Mode 2 94
4.4 The Half-Brake-Reuß Beam 97
4.4.1 Mode 1 98
5 SUMMARY AND DISCUSSION 101
REFERENCES 105
APPENDICES
A. Conference Paper 113

LIST OF TABLES

TABLES

Table 3-1. System Properties of SDOF system 23
Table 3-2. Piecewise Polynomial Equations to Modal Constant 27
Table 3-3. System Parameters of 3 Degree of Freedom System 32
Table 4-1. Summary of the Experimental Setups 51

LIST OF FIGURES

FIGURES

Figure 2-1. Typical Discrete MDOF System with any Type of Nonlinearity Element 10
Figure 2-2. Transfer and Describing Functions 11
Figure 2-3. Graphical Representation of Arclength Continuation Method 16
Figure 3-1. SDOF example of RCT-HFS Method 23
Figure 3-2. Harmonic Force Spectra 24
Figure 3-3. Quasi-Linear FRFs 25
Figure 3-4. Displacement Dependent Modal Parameters 28
Figure 3-5. Creating Harmonic Force Surface 29
Figure 3-6. Harmonic Force Surface 29
Figure 3-7. Extraction of Constant Force Response Amplitude Curves from the HFS 30
Figure 3-8. Comparison of Different techniques 31
Figure 3-9. Flowchart of Procedure of RCT-HFS Framework 31
Figure 3-10. Multi-Degree of Freedom 32
Figure 3-11. Constant Force Receptance Amplitude Curves of MDOF System- Cubic Stiffness Example 1 33
Figure 3-12. Resultant HFS after Merging Constant Force Frequency-Response Amplitude Curves- Cubic Stiffness Example 1 34
Figure 3-13. Extraction of Harmonic Force Spectra from the HFS 34
Figure 3-14. Quasi Linear FRFs of MDOF System- Cubic Stiffness Example 1 ... 35
Figure 3-15. Identified Modal Parameters- Cubic Stiffness Example 1 36
Figure 3-16. Comparison of Measured and Synthesized Frequency-Response Amplitude Plots- Cubic Stiffness Example 1 37
Figure 3-17. Refined Force Controlled Tests 38
Figure 3-18. Modal Parameters Comparison Extracted Using Different Sampling Frequencies of Force 39

Figure 3-19. a) FRF Comparison b) Detailed View 39
Figure 3-20. Comparison of Modal Parameters using Different Curve Fitting Methods..... 40
Figure 3-21. Comparison of FRFs Using Different Curve Fitting Methods..... 41
Figure 3-22. FRFs Comparison Using Different Curve Fit Types- Extended Frequency Sweep 41
Figure 3-23. Modal Parameter Extrapolation 42
Figure 3-24. Frequency-Response Amplitude Curves-Cubic Stiffness Example 2 43
Figure 3-25. Harmonic Force Surface- Cubic Stiffness Example 2 43
Figure 3-26. Quasi-Linear FRFs Extracted from HFS- Cubic Stiffness Example 244
Figure 3-27. Quasi-Linear FRFs Modal Fit- Cubic Stiffness Example 2 45
Figure 3-28. Identified Modal Parameters- Cubic Stiffness Example 2 45
Figure 3-29. Comparison of Measured and Synthesized Frequency- Response Amplitude Curves-Cubic Stiffness Example 2 46
Figure 3-30. Flowchart of the Proposed Nonlinear System Identification Method 48
Figure 4-1. Whole Test Setup Including Data Acquisition, Power Amplifier and Test Specimen 53
Figure 4-2. Detailed View of Test Setup Photo of Brake-Reuß Beam test setup in TÜBİTAK-SAGE 53
Figure 4-3. Fish Line of The Setup 54
Figure 4-4. Constant Force Response Amplitude Curves of Data Set 1 of Test 1 of BRB a) Accelerance data from LMS b) MATLAB plot using displacement data . 55
Figure 4-5. Harmonic Force Surface of Data Set 1 of Test 1 of BRB 55
Figure 4-6. a) Quasi-Linear FRFs Extracted from HFS b) Applied Curve Fitting of Data Set 1 of Test 1 of BRB-Curve Fit Type 1..... 56
Figure 4-7. Identified Modal Parameters of Data Set 1 of Test 1 of BRB-Curve Fit Type 1 57
Figure 4-8. Comparison of Synthesized FRFs and Measured Ones of Data Set 1 of Test 1 of BRB-Curve Fit Type 1..... 58
Figure 4-9. Quasi-Linear FRFs after *lsqcurvefit*-Curve Fit Type 2 60

Figure 4-10. Identified Modal Parameters of Data Set 1 of Test 1 of BRB-Curve Fit Type 2 60
Figure 4-11. Comparison of Synthesized FRFs and Measured Ones of Data Set 1of Test 1 of BRB-Curve Fit Type 2 62
Figure 4-12. Constant Force Response Amplitude Curves of Data Set 2 of Test 1 of BRB a) from LMS (detailed view) b) from MATLAB 63
Figure 4-13. Harmonic Force Surface of Data Set 2 of Test 1 of BRB 64
Figure 4-14. a) Quasi-Linear FRFs Extracted from HFS b) Applied Curve Fitting to Data Set 2 of Test 1 of BRB 64
Figure 4-15. Identified Modal Parameters of Data Set 2 of Test 1 of BRB- Curve Fit Type 1 65
Figure 4-16. Comparison of Synthesized FRFs and Measured Ones of Data Set 2 of Test 1 of BRB- Curve Fit Type 1 66
Figure 4-17. Quasi-Linear FRFs after *lsqcurvefit*-Curve Fit Type 2 67
Figure 4-18. Identified Modal Parameters of Data Set 1 of Test 2 of BRB-Curve Fit Type 2 68
Figure 4-19. Comparison of Synthesized FRFs and Measured Ones of Data Set 2 of Test 1 of BRB- Curve Fit Type 2 69
Figure 4-20. Constant Force Response Amplitude Curves of Test 2 of BRB a) from LMS b) from MATLAB 70
Figure 4-21. a) Harmonic Force Surface b) Quasi-Linear FRFs Extracted from HFS of Test 2 of BRB 71
Figure 4-22. Identified Modal Parameters of Test 2 of BRB 71
Figure 4-23. Comparison of Synthesized and Measured FRFs of Test 2 of BRB 73
Figure 4-24. Orion Beam a) Experimental Setup b) Schematic Representation 74
Figure 4-25. a) Measured Constant Force Frequency-Response Amplitude Curves b) Harmonic Force Surface- The Orion Beam Third Bending Mode 20 cNm Torque 75
Figure 4-26. Quasi-Linear FRFs Extracted from HFS- The Orion Beam Third Bending Mode 20 cNm Torque 76

Figure 4-27. Identified Modal Parameters- The Orion Beam Third Bending Mode 20 cNm Torque 76
Figure 4-28. Comparison of Measured and Synthesized Frequency-Response Amplitude Curves- The Orion Beam Third Bending Mode 20 cNm Torque..... 77
Figure 4-29. a) Measured Constant Force Frequency-Response Amplitude Curves b) Harmonic Force Surface- The Orion Beam Third Bending Mode 80 cNm Torque 77
Figure 4-30. Quasi-Linear FRFs Extracted from HFS- The Orion Beam Third Bending Mode 80 cNm Torque 78
Figure 4-31. Identified Modal Parameters- The Orion Beam Third Bending Mode 80 cNm Torque 78
Figure 4-32. Comparison of Measured and Synthesized Frequency-Response Amplitude Plots- The Orion Beam Third Bending Mode 80 cNm Torque 79
Figure 4-33. a) Measured Constant Force Frequency-Response Amplitude Curves b) Harmonic Force Surface- The Orion Beam Sixth Bending Mode 10 cNm Torque 80
Figure 4-34. Quasi-Linear FRFs Extracted from HFS -The Orion Beam Sixth Bending Mode 10 cNm Torque 80
Figure 4-35. Identified Modal Parameters - The Orion Beam Sixth Bending Mode 10 cNm Torque 81
Figure 4-36. Comparison of Measured and Synthesized Frequency-Response Amplitude Curves-The Orion Beam Sixth Bending Mode 10 cNm Torque 82
Figure 4-37. a) Measured Constant Force Frequency-Response Amplitude Curves b) Harmonic Force Surface- The Orion Beam Sixth Bending Mode 20 cNm Torque 82
Figure 4-38. Quasi-Linear FRFs Extracted from HFS -The Orion Beam Sixth Bending Mode 20 cNm Torque 83
Figure 4-39. Identified Modal Parameters - The Orion Beam Sixth Bending Mode 20 cNm Torque 83

Figure 4-40. Comparison of Measured and Synthesized Frequency-Response Amplitude Curves -The Orion Beam Sixth Bending Mode 20 cNm Torque.....84
Figure 4-41. a) Measured Constant Force Frequency-Response Amplitude Curves b) Harmonic Force Surface- The Orion Beam Sixth Bending Mode 30 cNm Torque 84
Figure 4-42.Quasi-Linear FRFs Extracted from HFS -The Orion Beam Sixth Bending Mode 30 cNm Torque.....85
Figure 4-43. Identified Modal Parameters – The Orion Beam Sixth Bending Mode 30 cNm Torque.....85
Figure 4-44. Comparison of Measured and Synthesized Frequency-Response Amplitude Curves -The Orion Beam Sixth Bending Mode 30 cNm Torque.....86
Figure 4-45. a) Measured Constant Force Frequency-Response Amplitude Curves b) Harmonic Force Surface- The Orion Beam Sixth Bending Mode 80 cNm Torque 87
Figure 4-46. Quasi-Linear FRFs Extracted from HFS -The Orion Beam Sixth Bending Mode 80 cNm Torque.....87
Figure 4-47. Identified Modal Parameters - The Orion Beam Sixth Bending Mode 80 cNm Torque.....88
Figure 4-48. Comparison of Measured and Synthesized Frequency-Response Amplitude Curves -The Orion Beam Sixth Bending Mode 80 cNm Torque.....88
Figure 4-49. a) Measured Constant Force Frequency-Response Amplitude Curves b) Harmonic Force Surface- The Orion Beam Sixth Bending Mode 1000 cNm Torque.....89
Figure 4-50. Quasi-Linear FRFs Extracted from HFS -The Orion Beam Sixth Bending Mode 1000 cNm Torque.....89
Figure 4-51. Identified Modal Parameters - The Orion Beam Sixth Bending Mode 1000 cNm Torque.....90
Figure 4-52. Comparison of Measured and Synthesized Frequency-Response Amplitude Curves-The Orion Beam Sixth Bending Mode 1000 cNm Torque.....90
Figure 4-53. The Length Modified Brake-Reuß Beam Setup [64] 91

Figure 4-54. a) Measured Constant Force Frequency-Response Amplitude Curves b) Harmonic Force Surface- The Length Modified Brake-Reuß Beam Mode 1 92
Figure 4-55. Quasi-Linear FRFs Extracted from HFS -The Length Modified Brake-Reuß Beam Mode 1 92
Figure 4-56. Identified Modal Parameters-The Length Modified Brake-Reuß Beam Mode 1 93
Figure 4-57. Identified Frequency Response Plots from [64]..... 93
Figure 4-58. Comparison of Measured and Synthesized Frequency-Response Amplitude Curves -The Length Modified Brake-Reuß Beam Mode 1 94
Figure 4-59. a) Measured Constant Force Frequency-Response Amplitude Plots b) Harmonic Force Surface-The Length Modified Brake-Reuß Beam Mode 2..... 95
Figure 4-60. Quasi-Linear FRFs Extracted from HFS-The Length Modified Brake-Reuß Beam Mode 2 95
Figure 4-61. Identified Modal Parameters-The Length Modified Brake-Reuß Beam Mode 2 96
Figure 4-62. Comparison of Measured and Synthesized Frequency-Response Amplitude Curves -The Length Modified Brake-Reuß Beam Mode 2 96
Figure 4-63. Identified Frequency Response Curve from the Literature [64] 97
Figure 4-64. Experimental Setup of Forced Control Testing of HBRB[65]..... 97
Figure 4-65. a) Measured Constant Force Frequency-Response Amplitude Curves b) Harmonic Force Surface- The Half-Brake-Reuß Beam Mode 1 98
Figure 4-66. Quasi-Linear FRFs Extracted from HFS- The Half-Brake-Reuß Beam Mode 1 99
Figure 4-67. Identified Modal Parameters- The Half-Brake-Reuß Beam Mode 1 . 99
Figure 4-68. Comparison of Measured and Synthesized FRFs - The Half-Brake-Reuß Beam Mode 1 99

LIST OF ABBREVIATIONS

ABBREVIATIONS

FRF	Frequency Response Function
RCT	Response-Controlled Stepped-Sine Testing
FRC	Frequency Response Curve
NLAE	Nonlinear Algebraic Equations
EOM	Equation of Motion
DOF	Degree of Freedom
HFS	Harmonic Force Surface
FCT	Force Controlled Stepped-Sine Testing
PLL	Phase-Locked-Loop
CBC	Control-Based Continuation
SDOF	Single Degree of Freedom
MDOF	Multi Degree of Freedom
RFS	Restoring Force Surface
NNM	Nonlinear Normal Mode
SNNM	Single Nonlinear Normal Mode

DF	Describing Function
BRB	Brake-Reuß Beam
LBRB	The Length Modified Brake-Reuß Beam
HBRB	The Half-Brake-Reuß Beam

LIST OF SYMBOLS

SYMBOLS

ω	Frequency
$\boldsymbol{M}$	Mass Matrix
$\boldsymbol{K}$	Stiffness Matrix
$\boldsymbol{H}$	Structural (Hysteric) Damping Matrix
$\boldsymbol{C}$	Viscous Damping Matrix
$\boldsymbol{x}$	Generalized Coordinates vector
$_{ij}$	i'th row j'th column in a matrix
$\dot{x}$	Time derivative of displacement
$\ddot{x}$	Second time derivative of displacement
F_N	Nonlinear Force
k	Stiffness
c	Viscous Damping
h	Hysteric Damping
$f_{ext}(t)$	External Force Acting on a System
$q(t)$	Response of Vibrating System

E_a	Actual Error
$iter_{max}$	Maximum Iteration
λ	Relaxation Constant
k_c	Cubic Stiffness
$\boldsymbol{J}$	Jacobian Matrix
$r(\boldsymbol{x}, \omega)$	Residual Vector
s	Hypothetical Radius in Arclength Method
N	Number of Iterations Performed
$N_{optimum}$	Number of Optimum Iterations
n_r	Nonlinear Internal Force
Δ_{rr}	Diagonal Elements of Describing Function
Δ_{rj}	Off-Diagonal Elements of Describing Function

CHAPTER 1

INTRODUCTION

1.1 Motivation of the Thesis

Different engineering disciplines design and analyze various complex systems for several purposes. Specifically, civil engineers design buildings, including tall ones, which may experience high amplitudes of vibrations due to their height. Furthermore, mechanical and aerospace engineers design and analyze systems such as aircraft, rockets, and automobiles. To understand the behavior of such systems, they need to be modeled using mathematics. Therefore, system identification is used to find the parameters of the system which relate the system's input to its output. Various methods [1] have been utilized for linear system identification to understand the dynamics of natural or man-made systems. However, these systems may behave nonlinearly (in general, they behave nonlinearly). For instance, in structural vibrations, different types of nonlinearities exist. Geometric nonlinearity occurs due to the extensive amount of displacement. Nonlinear material behavior might be recognized due to the constitutive law related to nonlinear stress and strain. Damping is also one of the main contributors to nonlinearity in natural systems whose actual behavior can be highly complicated [2]. One can add other sources of nonlinearity from the literature to this list.

These nonlinear behaviors make the analysis of the actual systems harder and complicated. To analyze nonlinear system behavior, researchers have developed several methods for the identification of nonlinear systems.

A nonlinear system identification process generally includes three stages [3]:

- Checking existing nonlinearities in the system and their detection.
- Determining the location of the nonlinearity and characterizing its type.

- Obtaining the values of the nonlinear system parameters.

A literature review of nonlinear system identification is conducted in the following section.

1.2 Literature Review

As discussed in section 1.1, various approaches and techniques are available for nonlinear system identification. The literature on non-linear system identification is quite extensive, so this section reviews relevant literature on nonlinear system identification in structural dynamics.

This review is based on Kerschen et al.'s [2] classification of nonlinear system identification methods, which can be grouped into seven categories: *linearization*, *time and frequency domain methods*, *modal methods*, *time-frequency analysis*, *black-box modeling*, and *structural model updating*. The review first summarizes each category by selecting the primary references from the review papers [2, 4], followed by a detailed explanation of three recently proposed methods at the end of the section.

1. Linearization methods: When dealing with harmonic forcing and response of systems, two methods commonly used as a basis for nonlinear system identification in structural dynamics are the *harmonic balance method* and the *describing function method*. For instance, Wang and Zheng [5] developed the equivalent dynamic stiffness mapping technique, and the method was validated on a metal mesh damper. Moreover, some researchers made use of time varying models by applying small time steps to achieve linear identification. Interesting research has been published by Sracic and Allen [6] using linear time-periodic approximations.

2. Time-domain methods: When data are represented as a time series, such as force or acceleration, the method used for identification is referred to as a time-domain method. Masri and Caughey [7] proposed a restoring force surface (RFS) method to identify nonlinear systems. The method was helpful for a single degree of freedom

systems having nonlinearities and requires the system's displacement, velocity, and restoring force acting to create the RFS. SDOF application with a sinusoidal forcing was examined in their paper. Another method is the time-domain nonlinear subspace identification (TNSI) technique applied to nonlinear mechanical systems with smooth nonlinearities by Marchesiello and Garibaldi [8]. Furthermore, an application to an aircraft with non-smooth nonlinearities has been performed by Noel et al. [9] using TNSI.

3. Frequency-domain methods: The data analyzed in frequency-domain identification exhibit greater diversity than those analyzed in the time domain. These data can manifest in various forms, such as Fourier spectra, frequency response, transmissibility functions, or power spectral densities. One of the promising frequency-domain methods is the nonlinear identification through feedback of the outputs (NIFO) developed by Adams [10]. Ozer et al. [11] proposed a new approach that involves using the describing function method to detect nonlinearity in a multi-degree of freedom system and then identifying the type and parameters of the system. This method can be utilized when nonlinearity exists between the ground and any degree of freedom of the system. The frequency domain nonlinear subspace identification method developed by Noël and Kerschen [12] was applied to the benchmark for nonlinear structural identification (BENSI) by Carri and Ewins [13].

4. Time-frequency methods: Nonlinear vibrations are characterized by the fact that the system's natural frequency and damping coefficient can vary with time, depending on the type of nonlinearity present. For instance, techniques like the *wavelet* and *Hilbert* transforms have been consistently employed to identify the backbone curves of the systems, such as beams with localized nonlinearities [14] and jointed structures [15].

5. Black-box methods: If one has difficulty in determining a nonlinearity model that is accurate enough, relying on physical insight can be very helpful. However, if physical insight is not available or the results are not satisfactory, it is advisable to turn to nonlinear black-box modeling. A nonlinear black-box model is a type of

model that can be used to describe almost any kind of nonlinear dynamics using only data. Some methods under this subsection for nonlinear system identification are *artificial neural networks*, *wavelet networks*, and *neuro-fuzzy models*. However, neural network methods are the most appealing ones. A neural network method has been applied to a semi-active damper [16], and two case studies, Box and Jenkins gas furnace, and an experimental ball-and-tube system [17] for nonlinear system identification.

6. Structural model updating: Resorting to models with many degrees of freedom (DOFs) becomes necessary when investigating more complex structures in a wider frequency range. However, estimating all the model parameters from experimental measurements can quickly become unmanageable. To solve this problem, structural modeling techniques that calculate the model parameters based on the known geometrical and mechanical properties of the structure can be used. Enhancing structural models by comparing them with vibration measurements conducted on the actual structure is essential. This process is commonly known as *structural model updating*. Based on the Bayesian inference, some nonlinear system identification methods as a model updating framework are applied to a mechanism that uses rotational energy to generate electricity [18] and to a numerical three-floor shear building model [19].

7. Modal methods: Modal methods offer a highly advanced technique for system identification, where the system is defined using modal natural frequencies, modal damping, and mode shapes. Thanks to the pioneering work of Rosenberg [20-22], nonlinear normal mode (NNM) theory has become the benchmark for modal methods in nonlinear system identification. By framing to find nonlinear modal parameters presented in NNM theory as nonlinear system identification, NNM theory provides a means to identify the nonlinear modal parameters that govern the system's response. As an example, for this category, a nonlinear resonant decay method was proposed. The method was validated using a 5 degree of freedom system and nonlinear panel structure [23], wing/pylon/store experimental setup [24], and a real airplane test data [25].

Review papers [2, 4] provided detailed explanations and references for nonlinear system identification methods to conclude these subcategories.

More specifically, three trending nonlinear system identification and testing techniques have been proposed and appealed to researchers from both industry and academia. Those are response-controlled stepped sine testing (RCT), control-based continuation (CBC), and phase-locked loop (PLL). All three have common features; they do not need prior knowledge of nonlinearity types, locations, and numbers. Therefore, this powerful property makes these nonlinear system identification methods promising and appealing. Details of those are given in the following paragraphs.

Firstly, Renson et al. [26] proposed a robust method (control-based continuation, CBC) to extract the backbone curve of the nonlinear systems and compared it with the resonant-decay method. For verification and validation purposes, a single degree of freedom oscillator with base excitation was used with a single point, one harmonic. It was proven that CBC overcame the presence of bifurcations and stability changes that might face the system. Finally, the method not only extracted the backbone curve of the underlying system but also gave the periodic solution of the system. Some works that have used and extended the technique of CBC are listed in these refs. [27-34].

Secondly, Peter and Leine [35] developed phase-locked-loop (PLL) technique. They introduced an innovative nonlinear mode indicator function based on power, which is simple to implement. The PLL controller automates the tuning of the excitation phase, resulting in significant time savings with this closed-loop controller. The methodology was tested on a clamped steel beam to demonstrate its effectiveness, which showed faster and more robust tracking of the backbone curve with this controller. Additional works building on this technique can be found in refs. [36-39].

Finally, Karaağaçlı and Özgüven [40] generalized the response-controlled testing method proposed by Arslan and Özgüven [41] for systems with nonlinear elements between a single coordinate and ground, to systems with many distributed nonlinear

elements. The RCT (Response-Controlled stepped sine Testing) method developed for obtaining nonlinear modal parameters (modal model) of a nonlinear system is also the basis that is used in this study. It makes use of the exciting outcome of single NNM theory that was proposed by Szemplinska-Stupnicka [42, 43], in which it was shown that using a single nonlinear normal mode is sufficient for representing the response of a nonlinear system around a resonance. With this, the proposed method first constructs a modal model of a nonlinear system by exciting the system at the n^{th} degree of freedom at constant displacement amplitude levels for a single NNM. The nonlinear system resulted in quasi-linear frequency response functions at the end due to constant displacement amplitude testing, which makes it easier to calculate modal parameters using linear modal fitting techniques such as the peak-picking method. Afterward, these quasi-linear FRFs measured at different displacement amplitude levels are used to obtain amplitude-dependent modal parameters by curve fitting to these experimental points. Furthermore, the harmonic force surface (HFS) proposed in this study is constructed by merging the quasi-linear FRFs (the x-axis is the frequency, and the y-axis is displacement after converting FRFs to displacement) along the force axis. One can extract force controlled, classical FRFs by cutting HFS surface with constant force planes. The RCT-HFS concept later used by Karaağaçlı and Özgüven [44] to obtain backbone curves of strongly nonlinear systems. They used a 5-degree-of-freedom discrete system with cubic stiffness, and an experimental T-Beam system to verify and validate the technique. The method is also applied to a control fin actuator mechanism in the same paper, to a geometrically nonlinear structure [45], and to a stack-type piezoelectric actuator mechanism that exhibits high stiffness and damping nonlinearity [46]. Moreover, Karaağaçlı and Özgüven [47] used the RCT-HFS approach successfully for a nonlinear system with highly nonlinear damping. Recently, Ekinci et al. [48] proposed a new nonlinear structural modification method based on RCT-HFS framework and the structural modification method proposed for linear systems [49].

To conclude, these three recent nonlinear system identification methods are powerful and promising in the context of nonlinear system identification. Furthermore, the

RCT-HFS method requires a more basic controller strategy to perform, which makes it outstanding among the others.

New nonlinear system identification methods are required to be developed due to the nature of the nonlinear mechanical systems. A novel method is proposed in this study. The aim of the method is to construct nonlinear modal models of nonlinear mechanical systems using force-controlled frequency response functions. The RCT-HFS method [40] developed by Karaağaçlı and Özgüven is extended to this end. Hence, this thesis leverages the RCT-HFS method and aims to extend the advantages of the RCT-HFS concepts to the conventionally used constant force sine testing method. The harmonic force surface concept is first utilized to achieve that goal by merging the constant force frequency-displacement curves conducted at different forcing levels. Cutting the resultant harmonic force surface at constant displacement planes gives quasi-linear FRFs, from which nonlinear modal parameters can be determined.

The theory of the method is explained in detail in Chapter 3 with a summary of main points: single nonlinear normal mode theory, response-controlled step sine testing and harmonic force surface concepts. Furthermore, some numerical examples are given to validate and verify the proposed method. Afterward, an experimental validation and verification are made using a benchmark beam from the literature in TÜBİTAK-SAGE. Finally, some real experimental data from the nonlinear mechanical system literature is exploited to validate and verify the method further.

An output of the thesis is also given in [50], which is the experimental data-based validation of the proposed method, the force controlled stepped sine testing-harmonic force surface (FCT-HFS) framework.

Hence, this study is believed to provide the RCT-HFS methodology to a broader community of researchers from industry and academia with experimental capabilities.

1.3 Outline of Thesis

The organization theme of the thesis is as follows:

Chapter 2 details nonlinear systems, quasi-linearization of nonlinear equation of motions and solution strategies for solving nonlinear systems of equations.

Chapter 3 first gives an insight into the RCT-HFS method and provides the procedure of the proposed novel method which links FCT-HFS and RCT-HFS methods. Numerical applications of the method are also provided for validation and verification purposes.

Chapter 4 gives the application of the proposed method to real systems. First experiments are conducted on a nonlinear structure called the Brake-Reuß beam in TÜBİTAK-SAGE to validate the proposed approach. Then, three systems are taken from the literature to verify further and validate the method. These systems are the Orion beam, the half Brake-Reuß beam, and the length-modified Brake-Reuß beam. They are studied using the data provided in the literature.

The thesis is closed with Chapter 5, which contains the summary and conclusion on the results of the proposed method.

CHAPTER 2

NONLINEAR RESPONSE OF DYNAMIC SYSTEMS

After demonstrating the significance of mathematical modeling of real engineering systems, it becomes crucial to solve them. This chapter focuses on the solution of the nonlinear equation of motion. Firstly, the nonlinear equation of motion is presented briefly. Then, harmonic balance and describing function methods are introduced for converting the nonlinear equations of motion to the algebraic equations. Finally, various approaches to solving the nonlinear equations are discussed.

2.1 Nonlinear Equation of Motion

The differential equation of motion of a nonlinear MDOF system can be written as

$$\boldsymbol{M}\ddot{\boldsymbol{x}}(\boldsymbol{t}) + \boldsymbol{C}\dot{\boldsymbol{x}}(t) + i\boldsymbol{H}\boldsymbol{x}(t) + \boldsymbol{K}\boldsymbol{x}(t) + \boldsymbol{f}_{\boldsymbol{N}}(\boldsymbol{x}(t), \dot{\boldsymbol{x}}(t), \dots) = \boldsymbol{f}_{\boldsymbol{ext}}(t) \qquad (2.1)$$

where $\boldsymbol{M}, \boldsymbol{C}, \boldsymbol{H}$ and $\boldsymbol{K}$ are the mass, viscous damping, structural (hysteric) damping and stiffness matrices of the underlying linear system, respectively. Furthermore, in equation (2.1), $\boldsymbol{x}(t)$ is the response vector while $\boldsymbol{f}_{\mathbf{ext}}(t)$ is the external forcing vector acting on each degree of freedom of the system. Finally, $\boldsymbol{f}_{\boldsymbol{N}}(\boldsymbol{x}(t), \dot{\boldsymbol{x}}(t), \dots)$ is the vector that contains the nonlinear internal forces in the system. One observes that the nonlinear force in the system may be a function of displacement, velocity, and other factors, depending on the physics of the problem. Under harmonic forcing, the external forcing for the linear part of the problem can be expressed as

$$\boldsymbol{f}_{\mathbf{ext}}(t) = \begin{cases} Im\left(\boldsymbol{f}e^{i\omega t}\right), & \text{if sinusoidal forcing} \\ Re\left(\boldsymbol{f}e^{i\omega t}\right), & \text{if cosine forcing} \end{cases} \qquad (2.2)$$

Then, the response of the system is expressed as

$$\boldsymbol{x(t)} = \begin{cases} Im\left(\boldsymbol{x}e^{i\omega t}\right), & \text{if sinusoidal forcing} \\ Re\left(\boldsymbol{x}e^{i\omega t}\right), & \text{if cosine forcing} \end{cases} \tag{2.3}$$

Expanding equation (2.1) gives

$$(-\omega^2\boldsymbol{M} + i\omega\boldsymbol{C} + i\boldsymbol{H} + \boldsymbol{K})\boldsymbol{x}e^{i\omega t} + \boldsymbol{f_N}(\boldsymbol{x}(t)) = \boldsymbol{f_{ext}}(t) \tag{2.4}$$

A typical example of a nonlinear system is schematically illustrated in Figure 2-1.

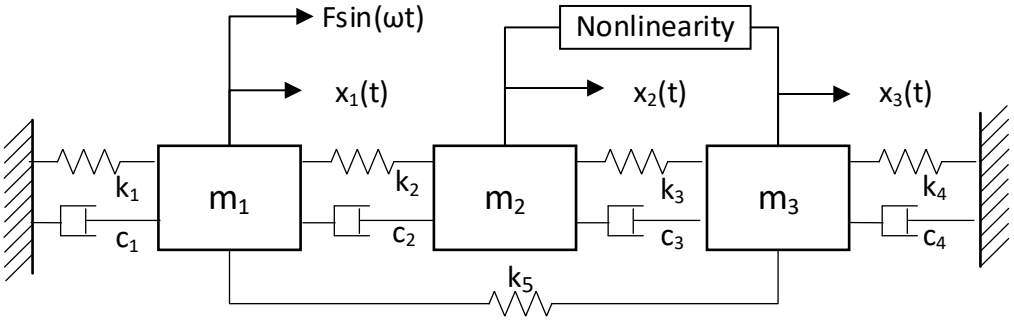

Figure 2-1. Typical Discrete MDOF System with any Type of Nonlinearity Element

2.2 Quasi-Linearization of Nonlinear Equation of Motion

2.2.1 Describing Function Method (DFM)

The concept of describing functions has its basis in control engineering. On the other hand, Tanrikulu et al. [51] developed a describing function methodology-based method. In linear systems, input and output can be related to transfer functions. However, this transfer function cannot be defined in nonlinear systems due to the nonlinear behavior of the system. Therefore, they proposed a method to relate the input and output in nonlinear systems. Figure 2-2 shows how describing function and transfer function work.

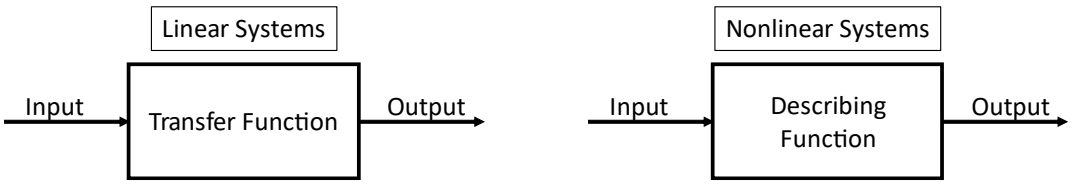

Figure 2-2. Transfer and Describing Functions

Recall (2.1),

$$\boldsymbol{M}\ddot{\boldsymbol{x}}(t) + \boldsymbol{C}\dot{\boldsymbol{x}}(t) + i\boldsymbol{H}\boldsymbol{x}(t) + \boldsymbol{K}\boldsymbol{x}(t) + \boldsymbol{f_N}(\boldsymbol{x}(t), \dot{\boldsymbol{x}}(t), \dots) = \boldsymbol{f_{ext}}(t) \qquad (2.5)$$

'r[th]' row in nonlinear force vector '$\boldsymbol{f_N}$' is expressed as

$$f_{N_r}(t) = \sum_{r=1}^{n} n_{rj}\,(t) \qquad (2.6)$$

Where $n_{rj}(t)$ is the resultant nonlinear internal force due to nonlinear elements existing in the system between coordinate 'r' and 'j', and n is the number of DOFs. This nonlinear force then can be rewritten as

$$n_{rj}(t) = n_{rj}\big(y_{rj}(t), \dot{y}_{rj}(t), \dots\big), \quad \begin{cases} y_{rj}(t) = x_r(t) - x_j(t), & \text{if r} \neq \text{j} \\ y_{rj}(t) = x_r(t), & \text{if r} = \text{j} \end{cases} \qquad (2.7)$$

Assuming periodic excitation of external force in sine and bias terms as

$$\boldsymbol{f_{ext}}(t) = \boldsymbol{f_0} + Im\left(\sum_{m=1}^{\infty} \boldsymbol{f_m}\, e^{im\omega t}\right) \qquad (2.8)$$

where '$\boldsymbol{f_m}$' is 'm^{th}' harmonic's amplitude vector of external forcing. Since the system is assumed to vibrate periodically, the displacement can be written as

$$\boldsymbol{x}(t) = \boldsymbol{x_0} + Im\left(\sum_{m=1}^{\infty} \boldsymbol{x_m}\, e^{im\omega t}\right) \qquad (2.9)$$

where '$\mathbf{x}_{\boldsymbol{m}}$' is '$m^{th}$' harmonic's amplitude vector of displacement. Furthermore, nonlinear forcing is written as

$$y_{rj}(t) = y_{rj_0} + Im\left(\sum_{m=1}^{\infty} y_{rj_m} e^{im\omega t}\right) \tag{2.10}$$

$$\left(y_{rj}\right)_m = \begin{cases} (x_r)_m - \left(x_j\right)_m, & if\ r \neq j \\ (x_r)_m, & if\ r = j \end{cases} \tag{2.11}$$

$$n_{rj}(t) = a_{rj_0} + Im\left(\sum_{m=1}^{\infty} a_{rj_m} e^{im\omega t}\right) \tag{2.12}$$

$$a_{rj_0} = \frac{i}{\pi}\int_0^{2\pi} n_{rj}\left(y_{rj}(t), \dot{y}_{rj}(t), \dots\right) d\phi\,, \qquad m = 0 \tag{2.13}$$

$$a_{rj_m} = \frac{i}{2\pi}\int_0^{2\pi} n_{rj}\left(y_{rj}(t), \dot{y}_{rj}(t), \dots\right) e^{-im\phi} d\phi\,, \qquad m = 1, 2, 3, \dots \tag{2.14}$$

Where '$\phi = \omega t$'. Elements of '$\boldsymbol{\Delta}$' is then expressed as

$$\left(v_{rj}\right)_m = \frac{\left(a_{rj}\right)_m}{\left(y_{rj}\right)_m} \tag{2.15}$$

Insert (2.15) into (2.12), one gets

$$n_{rj}(t) = \left(v_{rj}\right)_0\left(y_{rj}\right)_0 + Im\left(\sum_{m=1}^{\infty}\left(v_{rj}\right)_m\left(y_{rj}\right)_m e^{-im\omega t}\right) \tag{2.16}$$

Therefore, nonlinear restoring force is expressed as

$$\boldsymbol{f_N}(\boldsymbol{x}(t), \dot{\boldsymbol{x}}(t), \dots) = \sum_{m=0}^{\infty} \boldsymbol{n_m}\, e^{-im\omega t} \tag{2.17}$$

In (2.17) $\boldsymbol{n_m}$ can be written in matrix form using DFM as

$$\boldsymbol{n_m} = \boldsymbol{\Delta_m x_m} \tag{2.18}$$

Where $\boldsymbol{\Delta}$ is the response dependent nonlinearity matrix due to nonlinear elements in the analyzed systems. Elements of '$\boldsymbol{\Delta}$' are then expressed using the above-mentioned rules as

$$\begin{aligned} \Delta_{rr} &= v_{rr} + \sum_{\substack{j=1 \\ j \neq r}}^{k} v_{rj} \quad r = 1,2, \dots k \\ \Delta_{rj} &= -v_{rj} \quad r \neq j, \quad r = 1,2, \dots k \end{aligned} \tag{2.19}$$

Inserting this into (2.5) yields

$$(-(m\omega)^2 \boldsymbol{M} + i(m\omega)\boldsymbol{C} + i\boldsymbol{H} + \boldsymbol{K} + \boldsymbol{\Delta_m})\boldsymbol{x_m} = \boldsymbol{f}_m \tag{2.20}$$

Taking '*m=1'* in the describing function method is mathematically equivalent to the first order harmonic balance method $\boldsymbol{\Delta_m}$ is the response-dependent matrix in DFM, which results in quasi-linear form as seen in equation (2.20). Further, it is possible to determine the nonlinear behavior of the system by DFM in a computationally efficient manner contrary to the time integration methods. However, still an iterative solution scheme is required to calculate the nonlinear response amplitudes. Hence, in the following section, solution procedures of nonlinear algebraic equations are reviewed.

2.3 Solution Techniques of Nonlinear Equation Sets

Throughout this thesis, it is necessary to solve sets of nonlinear equations. Specifically, in Chapter 3, the forced response of nonlinear equations of motions requires numerical solutions, and in Chapter 4, forced nonlinear equation sets need to be synthesized using response dependent modal parameters. In this sub-section, some approaches to solve these equations are discussed.The Newton-Raphson method and Newton's method coupled with the arclength-continuation method are explained, respectively. Hence, this subsection details the solution of the nonlinear

algebraic equations in frequency domain. The following chapters use these methods to determine the nonlinear frequency response functions.

2.3.1 Newton Raphson Method

The Newton-Raphson method, also known as Newton's method, is an alternative technique widely used for solving nonlinear algebraic equations due to its speed and fewer convergence issues compared to fixed-point iteration. This method utilizes the slope of a line tangent to the curve of interest, i.e., first-order Taylor series expansion. This method can be applied to the classical nonlinear equation presented earlier as follows

$$\boldsymbol{r}(\boldsymbol{x},\omega) = (-\omega^2\boldsymbol{M} + i\omega\boldsymbol{C} + i\boldsymbol{H} + \boldsymbol{K})\boldsymbol{x} + \boldsymbol{f_N} - \boldsymbol{f_{ext}} = \boldsymbol{0} \tag{2.21}$$

Taylor series expansion of residual vector gives

$$r(\boldsymbol{x} + \Delta\boldsymbol{x},\omega) = \boldsymbol{r}(\boldsymbol{x},\omega) + \boldsymbol{J}(\boldsymbol{x},\omega)\Delta\boldsymbol{x} + O(\Delta\boldsymbol{x^2}) \tag{2.22}$$

Ignoring the 2nd order and higher order terms appearing in (2.22) and setting $\boldsymbol{s}(\boldsymbol{x} + \Delta\boldsymbol{x},\omega) = \boldsymbol{0}$ where $\boldsymbol{J}(\boldsymbol{x},\omega) = \frac{\partial \boldsymbol{r}(\mathbf{x},\omega)}{\partial \boldsymbol{x}}$ is the Jacobian matrix.

$$\boldsymbol{r}(\boldsymbol{x},\omega) = -\boldsymbol{J}(\boldsymbol{x},\omega)\Delta\boldsymbol{x} \tag{2.23}$$

Solving for $\boldsymbol{x_{i+1}}$ from $\Delta\boldsymbol{x}$ gives

$$\boldsymbol{x_{i+1}} = \boldsymbol{x}_i - \boldsymbol{J}(\boldsymbol{x},\omega)^{-1}\boldsymbol{r}(\boldsymbol{x},\omega) \tag{2.24}$$

Newton's method is widely used to find system roots, with other works using the Newton-Raphson method found in literature, including [52, 53] and many others.

2.3.2 Newton's Method Coupled with Arclength Continuation

Neither fixed-point iteration nor the classical Newton-Raphson method can track the path in the case of a strong nonlinearity since the Jacobian matrix is close to singular

at the turning point. Some modifications are made to the nonlinear equation. First, frequency is added as an additional parameter shown in the following equation. Adding frequency as an additional unknown increases the number of unknowns, and one more equation is needed to solve the system of equations. To solve that, an additional parameter known as the arclength parameter is introduced and the radius of the hypothetical sphere is shown in Figure 2-3.

$$\boldsymbol{q} = \begin{bmatrix} \boldsymbol{x} \\ \omega \end{bmatrix} \tag{2.25}$$

$$\left(\boldsymbol{x^k} - \boldsymbol{x^{k-1}}\right)^2 + (\omega^k - \omega^{k-1})^2 = s^2 \tag{2.26}$$

Equation (2.26) can be expressed as

$$\delta \boldsymbol{x^k} = \boldsymbol{x^k} - \boldsymbol{x^{k-1}} \;\; \& \;\; \delta\omega_k = \omega^k - \omega^{k-1} \tag{2.27}$$

$$\delta \boldsymbol{q^k} = \begin{bmatrix} \delta \boldsymbol{x^k} \\ \delta \omega^k \end{bmatrix} \tag{2.28}$$

Inserting (2.28) into (2.26) gives

$$h\left(\boldsymbol{x^k}, \omega^k\right) = \delta \boldsymbol{q^k}^{\mathrm{T}} \, \delta \boldsymbol{q^k} - s^2 = 0 \tag{2.29}$$

With this new equation the iterative solution becomes

$$\boldsymbol{q_{i+1}^k} = \boldsymbol{q_i^k} - \begin{bmatrix} \dfrac{\partial \boldsymbol{r}(\boldsymbol{x_i^k}, \omega_i^k)}{\partial \boldsymbol{x_i^k}} & \dfrac{\partial r(\boldsymbol{x_i^k}, \omega_i^k)}{\partial \omega} \\ \dfrac{\partial h\left(\boldsymbol{x_i^k}, \omega_i^k\right)}{\partial \boldsymbol{x_i^k}} & \dfrac{\partial h}{\partial \omega} \end{bmatrix}^{-1} \begin{Bmatrix} r(\boldsymbol{x_i^k}, \omega_i^k) \\ h(\boldsymbol{x_i^k}, \omega_i^k) \end{Bmatrix} \tag{2.30}$$

Equation (2.30) is rewritten by defining new parameters to have a neater representation of it.

$$\bar{J}\left(\boldsymbol{x_i^k}, \omega_i^k\right) = \begin{bmatrix} \dfrac{\partial \boldsymbol{r}(\boldsymbol{x_i^k}, \omega_i^k)}{\partial \boldsymbol{x_i^k}} & \dfrac{\partial R\left(\boldsymbol{x_i^k}, \omega_i^k\right)}{\partial \omega} \\ \dfrac{\partial h\left(\boldsymbol{x_i^k}, \omega_i^k\right)}{\partial \boldsymbol{x_i^k}} & \dfrac{\partial h}{\partial \omega} \end{bmatrix}$$

$$\bar{\boldsymbol{r}}\left(\boldsymbol{x_i^k}, \omega_i^k\right) = \begin{bmatrix} \boldsymbol{r}\left(\boldsymbol{x_i^k}, \omega_i^k\right) \\ h\left(\boldsymbol{x_i^k}, \omega_i^k\right) \end{bmatrix} \tag{2.31}$$

Rewriting equation (2.30) gives

$$\boldsymbol{q_{i+1}^k} = \boldsymbol{q_i^k} - \bar{\boldsymbol{J}}\left(\boldsymbol{x_i^k}, \omega_i^k\right)^{-1} \bar{\boldsymbol{r}}\left(\boldsymbol{x_i^k}, \omega_i^k\right) \tag{2.32}$$

The Solution point is denoted by ‘k’ whereas ‘i’ denotes the iteration counter. As mentioned, the initial guess is crucial when solving the nonlinear equation sets. Providing a good initial guess results in a fast convergence rate. Therefore, one can use a tangent predictor to have a fast convergence rate [54, 55], while others can utilize different predictors methods as well.

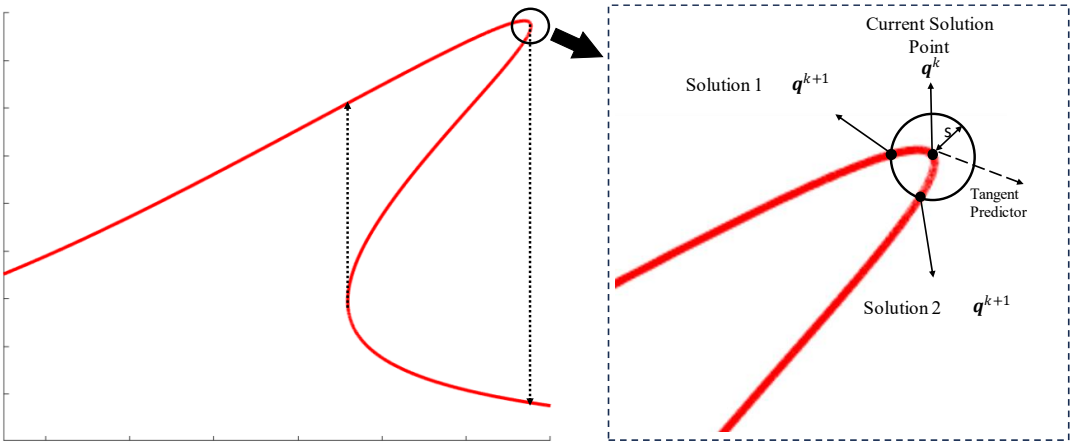

Figure 2-3. Graphical Representation of Arclength Continuation Method

The arclength continuation method is graphically illustrated in Figure 2-3. As mentioned, it involves defining an arclength that crosses two possible solution points at each step. The subsequent frequency can be selected using the method described above to follow the path. The frequency sweep can be performed from lower to upper and vice versa. Figure 2-3 illustrates the possible jump phenomenon paths.

Finally, what happens about resonance, and how does one follow the path around that? The radius of the hypothetical sphere needs to be small enough to catch the sharp turns. However, this leads to long computational times. To not sacrifice the computational time, the adaptive step size is proposed [54].

$$\epsilon = \frac{N_{optimum}}{N} \tag{2.33}$$

Where $N_{optimum}$ is set by the user and N is the number of iterations performed at each solution step. Then,

$$\bar{\epsilon} = \begin{cases} 0.5, & \text{if } \epsilon < 0.5 \\ \epsilon, & \text{if } 0.5 \leq \epsilon \leq 2 \\ 2, & \text{if } \epsilon > 2 \end{cases} \tag{2.34}$$

$$s_{new} = \bar{\epsilon}\, s_{old} \tag{2.35}$$

One can further modify by converting $\bar{\epsilon}$ to exponential number as

$$s_{new} = \bar{\epsilon}^{1/n} s_{old} \tag{2.36}$$

Where n is a positive real number.

Some studies performed by researchers in the field can be found in the literature [56-60].

CHAPTER 3

THEORY AND NUMERICAL APPLICATIONS OF THE FCT-HFS FRAMEWORK

Chapter 2 presents methods one might need to solve the nonlinear system equations. Specifically, the Describing Function (DF) and Harmonic Balance (HB) methods are discussed, which result in converting nonlinear equations of motion into algebraic equations. Once algebraic equations are obtained, various techniques can be applied to solve them.

This chapter first delves into the single nonlinear normal mode theory, which provides a means of expressing the system's response. Explanations of this theory are provided in detail. As touched on in Chapter 1, the RCT-HFS framework utilizes the single nonlinear normal mode theory [42]. Furthermore, a more detailed explanation and implementation, as well as a numerical example of the RCT-HFS method, are meticulously analyzed. The approach for the FCT-HFS framework, the proposed method, is then explained, building on these concepts. To conclude, numerical examples of the FCT-HFS framework are presented.

3.1 Theory of FCT-HFS Framework

As the proposed method is an extension of the RCT-HFS framework, reviewing first the single nonlinear normal mode (SNNM) theory and then the RCT and HFS concepts are necessary. After that, the FCT-HFS framework is explained in detail.

3.1.1 Single Nonlinear Normal Mode Theory

The theory of single nonlinear normal mode (SNNM) [42] states that in nonlinear systems one mode is sufficient to make good predictions near resonance by assuming that the modes are distinctly separated and no significant coupling occurs. In this subsection, the theory behind it is briefly discussed.

As indicated in Chapter 2, nonlinear systems are solved by converting the nonlinear terms to nonlinearity matrix as explained. Equation (3.1) is the frequency domain representation of the MDOF lumped system.

$$(-\omega^2\boldsymbol{M} + i\boldsymbol{H} + \boldsymbol{K} + \boldsymbol{\Delta})\boldsymbol{x} = \boldsymbol{f} \tag{3.1}$$

where $\boldsymbol{M}, \boldsymbol{H}, \boldsymbol{K}$ and $\boldsymbol{\Delta}$ are the mass, structural (hysteric) damping, stiffness, and nonlinearity matrices of any MDOF system, respectively. The solution of this MDOF system can be written as

$$\boldsymbol{x} = q_r\boldsymbol{\phi}(q_r)_r \tag{3.2}$$

Where q_r is the amplitude of the r^{th}modal coordinate. $\boldsymbol{\phi}(q_r)_r$ is the r^{th} nonlinear normal mode. Inserting (3.2) to (3.1) and multiplying with $\boldsymbol{\phi}(q_r)_r$, then arranging it gives the following:

$$\boldsymbol{\phi}(q_r)_r^T(-\omega^2\boldsymbol{M} + i\boldsymbol{H} + \boldsymbol{K} + \boldsymbol{\Delta})q_r\boldsymbol{\phi}(q_r)_r = \boldsymbol{\phi}(q_r)_r^T\boldsymbol{f} \tag{3.3}$$

$$\left(-\omega^2 m_r(q_r) + i h_r(q_r) + k_r(q_r)\right)q_r = \boldsymbol{\phi}(q_r)_r^T\boldsymbol{f} \tag{3.4}$$

Where $m_r(q_r) = \boldsymbol{\phi}(q_r)_r^T\boldsymbol{M}\boldsymbol{\phi}(q_r)_r$, $k_r(q_r) = \boldsymbol{\phi}(q_r)_r^T(\boldsymbol{K} + \boldsymbol{\Delta_{re}})\boldsymbol{\phi}(q_r)_r$, $h_r(q_r) = \boldsymbol{\phi}(q_r)_r^T(\boldsymbol{H} + \boldsymbol{\Delta_{im}})\boldsymbol{\phi}(q_r)_r$. Furthermore, $m_r(q_r)$, $k_r(q_r)$ and $h_r(q_r)$ are modal mass, stiffness, and damping, respectively.

It is essential to recognize that, $m_r(q_r)$, $k_r(q_r)$ and $h_r(q_r)$ are functions of q_r, r^{th}modal amplitude.

Equation (3.4) can be taken into parenthesis of $m_r(q_r)$ which leads to the following:

$$m_r(q_r)\left(-\omega^2 + i\eta_r(q_r)\omega_r^2(q_r) + \omega_r^2(q_r)\right)q_r = \boldsymbol{\phi}(q_r)_r^T\boldsymbol{f} \tag{3.5}$$

where $\omega_r^2(q_r) = k_r(q_r)/m_r(q_r)$, $\eta_r(q_r) = h_r(q_r)/(m_r(q_r)\omega_r^2(q_r))$

From here, modal amplitude, q_r, can be determined as:

$$q_r = \frac{\boldsymbol{\phi}(q_r)_r^T\boldsymbol{f}}{m_r(q_r)\left(-\omega^2 + i\eta_r(q_r)\omega_r^2(q_r) + \omega_r^2(q_r)\right)} \tag{3.6}$$

Inserting (3.6) into (3.2) gives

$$\boldsymbol{x} = \frac{\boldsymbol{\phi}(q_r)_r\boldsymbol{\phi}(q_r)_r^T\boldsymbol{f}}{m_r(q_r)\left(-\omega^2 + i\eta_r(q_r)\omega_r^2(q_r) + \omega_r^2(q_r)\right)} \tag{3.7}$$

Normalizing the nonlinear normal mode as

$$\bar{\boldsymbol{\phi}}(q_r)_r = \boldsymbol{\phi}(q_r)_r/\sqrt{m_r(q_r)} \tag{3.8}$$

Inserting this into (3.7) gives

$$\boldsymbol{x} = \frac{\bar{\boldsymbol{\phi}}(q_r)_r\bar{\boldsymbol{\phi}}(q_r)_r^T\boldsymbol{f}}{\left(-\omega^2 + i\eta_r(q_r)\omega_r^2(q_r) + \omega_r^2(q_r)\right)} \tag{3.9}$$

Then, receptance can be written as for j^{th}coordinate of interest, and force is applied at k^{th} coordinate for lumped (discrete) systems as

$$\alpha_{jk} = \frac{\bar{\boldsymbol{\phi}}(q_r)_r\bar{\boldsymbol{\phi}}(q_r)_r^T}{\left(-\omega^2 + i\eta_r(q_r)\omega_r^2(q_r) + \omega_r^2(q_r)\right)} \tag{3.10}$$

For viscous damping instead of hysteric damping, receptance can be written as

$$\alpha_{jk} = \frac{\bar{\boldsymbol{\phi}}(q_r)_r\bar{\boldsymbol{\phi}}(q_r)_r^T}{\left(-\omega^2 + i2\zeta_r(q_r)\omega\omega_r(q_r) + \omega_r^2(q_r)\right)} \tag{3.11}$$

3.1.2 Theory of Response-Controlled Stepped-Sine Testing (RCT) and Harmonic Force Surface (HFS)

The concept behind the method is worth mentioning. Firstly, consider equations (3.10) and (3.11); the force spectrum is measured for the determined frequency interval by keeping the response amplitude constant for several response levels at the excitation point.

Secondly, the corresponding FRFs, which will be quasi-linear, are used to make linear modal analysis using the FRFs' quasi-linearity behavior for each response amplitude level. Following this procedure, by including all the amplitude levels, one gets the modal parameters as a function of response amplitude. The measured harmonic force spectra at those different response amplitude levels are composed together resulting in harmonic force surface (HFS). The details of the HFS' construction are shown in Figure 3-5 with an example. The measured harmonic force spectra at each response amplitude level are plotted along with the third axis, i.e., the response amplitude axis.

Finally, constant force response amplitude plots are obtained by directly cutting the HFS with the constant force amplitude planes (which will be experimentally measured ones) or using the extracted modal parameters (which will give the synthesized ones). The extraction of constant force response amplitudes from the HFS is simulated in Figure 3-7.

Now, to better understand the underlying methodology behind the RCT-HFS framework [40], it is worth working on an example and presenting a flowchart at the end.

The system shown in Figure 3-1 is a forced SDOF system with cubic nonlinearity. Its equation of motion is given by equation (3.12).

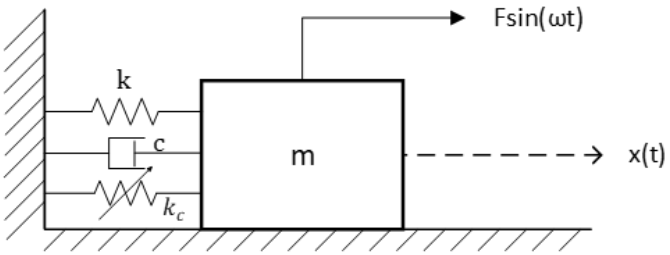

Figure 3-1. SDOF example of RCT-HFS Method

$$m\ddot{x}(t) + ihx(t) + kx(t) + k_c x(t)^3 = Fsin(\omega t) \tag{3.12}$$

Using the DF expression for cubic stiffness, the equation of motion can be written as:

$$(-\omega^2 m + ih + k + 0.75k_c x^2)x = fsin(\omega t) \tag{3.13}$$

where x is the response amplitude of the oscillations in the system. where $x = \sqrt{x_{re1}^2 + x_{im1}^2}$ is the amplitude of the coordinate. The equation turns out the following expression as

$$\begin{bmatrix} k-\omega^2 m & -h \\ -h & k-\omega^2 m \end{bmatrix} \begin{Bmatrix} x_{re1} \\ x_{im1} \end{Bmatrix} + 0.75k_c \begin{bmatrix} x_{re1}^2 + x_{im1}^2 & 0 \\ 0 & x_{re1}^2 + x_{im1}^2 \end{bmatrix} \begin{Bmatrix} x_{re1} \\ x_{im1} \end{Bmatrix} - \begin{Bmatrix} f_{re1} \\ f_{im1} \end{Bmatrix} = \begin{Bmatrix} 0 \\ 0 \end{Bmatrix} \tag{3.14}$$

The values tabulated in the following table as

Table 3-1. System Properties of SDOF system

m [kg]	**k [N/m]**	**h [N/m]**	$\boldsymbol{k_c}$ $[\boldsymbol{N/m^3}]$
1	1e4	1000	1e6

For the solution of Eq. 3.16, the literature generally uses a constant force as the input and aims to solve the response amplitudes. However, the numerical implementation of the RCT approach treats the response amplitude as constant and finds the forcing

required to achieve this constant response amplitude at a certain degree of freedom. Therefore, the amplitude of the response is substituted with no phase since the response is the input and the forcing real and imaginary parts are solved using equation (3.16). Next, the aforementioned procedure is repeated for several response levels. In this context, RCT is employed at seven amplitude levels: 10, 20, 30, 40, 50, 60, and 70 mm. The resulting harmonic force spectra are depicted in Figure 3-2. To generate the quasi-linear FRFs, each displacement value must be divided by its respective forcing values, and the results are illustrated in Figure 3-3. It is shown that by keeping the driving point's displacement amplitude, the FRFs come out as quasi-linear. For each receptance curve, linear modal analysis can be performed to find the modal parameters at each displacement level of interest. Throughout this thesis, the peak-picking method is utilized to determine the modal parameters in general.

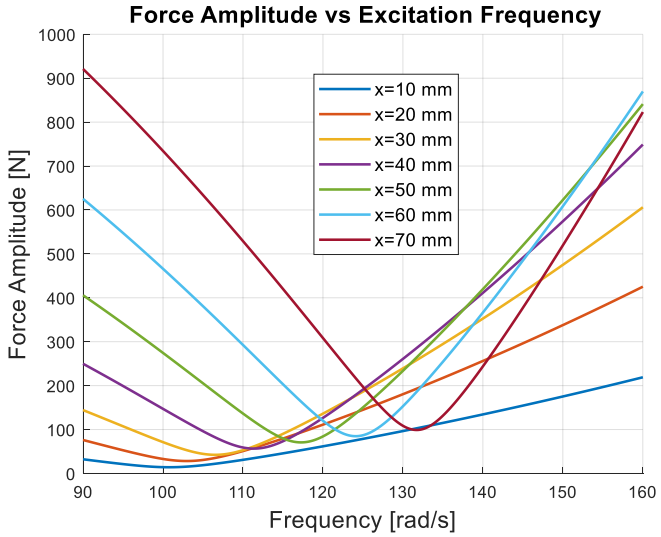

Figure 3-2. Harmonic Force Spectra

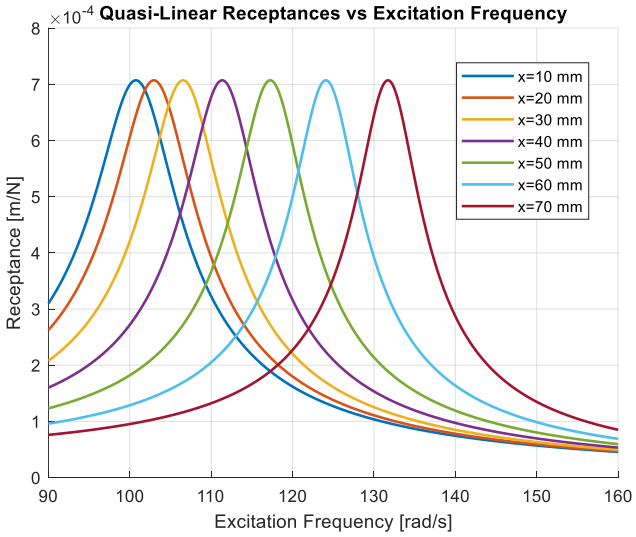

Figure 3-3. Quasi-Linear FRFs

Basically peak-picking method used here can be summarized in the following sentences.

1. Resonance peaks are determined in the measured FRFs.
2. Frequencies at the half power points (which are the points where the receptance amplitude is equal to $\frac{1}{\sqrt{(2)}}$ of the maximum receptance amplitude) are determined.
3. Hysteric damping is estimated from

$$\gamma_r = \frac{\omega_2^2 - \omega_1^2}{2\omega_r^2} \approx \frac{\omega_2 - \omega_1}{\omega_r} \tag{3.15}$$

4. Modal constant is estimated from

$$\alpha_{jk} = \sum_{r=1}^{n} \frac{\phi_j^r \phi_k^r}{\omega_r^2 - \omega^2 + i\eta_r\omega_r^2} = \sum_{r=1}^{n} \frac{A_{jk}^r}{\omega_r^2 - \omega^2 + i\gamma_r\omega_r^2} \tag{3.16}$$

Making SDOF assumption around resonance gives

$$|A_{jk}^r| = \left|\alpha_{jk}\right|_{max} \gamma_r \omega_r^2 \tag{3.17}$$

One finds the modal parameters, namely natural frequency, modal damping and modal constant using this procedure presented. The next step is to use these parameters and obtain a fitting function for them.

In the figure below, the markers represent calculated points of modal parameters, and the solid lines are the *smoothingspline* curves fitted to those points. The mathematical background of smoothingspline is given as

$$p\sum_{i} w_i\left(y_i - s(x_i)\right)^2 + (1-p)\int\left(\frac{d^2s}{dx^2}\right)^2 dx \tag{3.18}$$

Where $w_i, p\ and\ s$ are weight, smoothing parameter and smoothing spline, respectively. Generally, p is taken as 1, in which case it stands as a cubic spline that should give the markers in the fitted curve. However, p is determined based on the experimental data. For example, in this example, p is determined as 0.99. Therefore, the fitted curve does not pass through some of the experimental points. Furthermore, smoothing spline generates piecewise polynomials across the measured points. These polynomials are presented for the modal constants in Table 3-2 for brevity. There are 13 measured points so 12 polynomial functions are utilized. An important point to be mentioned here is what happens at the boundaries. For the sake of understanding take 0.02 m constant displacement level, although polynomial functions take two same values at that point, they do not give the measured point. This happens since smoothingspline determines the value of the function so that a smooth transition between the intervals is obtained. These modal parameters will be used to synthesize constant-force frequency-response amplitude plots. Equation (3.11) needs to be solved to get the constant force frequency-response amplitude graphs. To achieve that, an iterative solution scheme such as Newton's method with arclength continuation is required since displacement amplitude dependent functions are at each side of the equality.

Table 3-2. Piecewise Polynomial Equations to Modal Constant

Interval [m]	**Polynomial Equation**
[0.01, 0.02]	$-206.593326\ (x\ -\ 0.01)\text{^}3\ -0.043400\ (x\ -\ 0.01)\ +\ 1.003614$
[0.02, 0.03]	$328.383209\ (x\ -\ 0.02)\text{^}3\ +\ -6.1978\ (x\ -\ 0.02)\text{^}2\ +\ -0.105378\ (x\ -\ 0.02)\ +\ 1.002973$
[0.03, 0.04]	$-28.142507(x\ -\ 0.03)\text{^}3\ +\ 3.653696\ (x\ -\ 0.03)\text{^}2\ -0.130819(x\ -\ 0.03)\ +\ 1.001628$
[0.04, 0.05]	$-64.218514(x\ -\ 0.04)\text{^}3\ +\ 2.809421\ (x\ -\ 0.04)\text{^}2\ -0.066188\ (x\ -\ 0.040000)\ +\ 1.000657$
[0.05, 0.06]	$-23.539119\ (x\ -\ 0.05)\text{^}3\ +\ 0.882866\ (x\ -\ 0.05)\text{^}2\ +\ -0.029265\ (x\ -\ 0.05)\ +\ 1.000212$
[0.06, 0.07]	$-5.889742\ (x\ -\ 0.06)\text{^}3\ +\ 0.176692\ (x\ -\ 0.06)\text{^}2\ -0.018669\ (x\ -\ 0.06)\ +\ 0.999984$

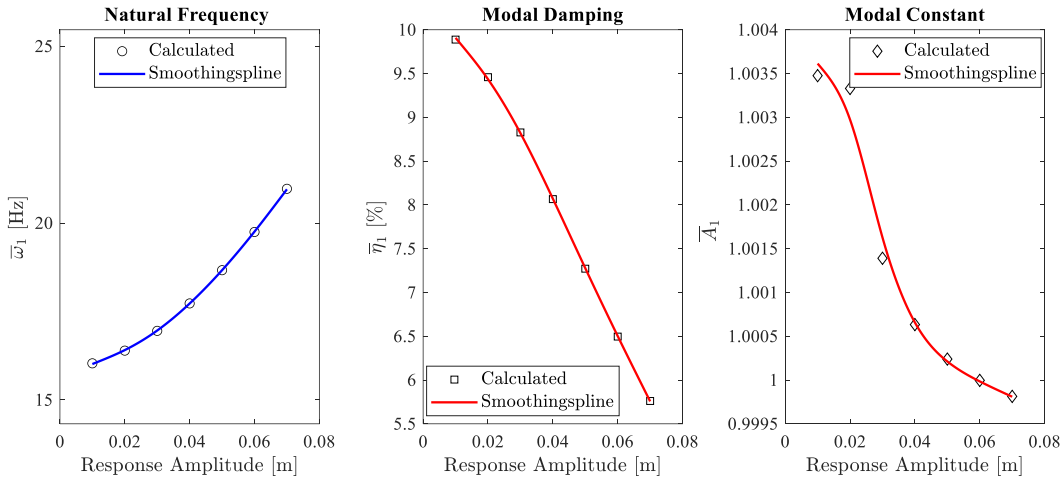

Figure 3-4. Displacement Dependent Modal Parameters

Furthermore, one can construct the harmonic force surface associated with the system at the same time. Harmonic force spectra are plotted for each displacement amplitude level in the 3D plot in Figure 3-5. The HFS is then constructed with the help of linear interpolation between those curves. That is, a linear interpolation is performed between each response amplitude level shown in Figure 3-5 to create a surface. Figure 3-6 shows the created harmonic force surface. This HFS is used to extract the constant force frequency-response amplitude curves. Those are extracted by cutting the HFS with constant force amplitude planes. Figure 3-7 shows how constant force frequency-response amplitude curves are extracted from the HFS. A constant plane corresponding to F=40 N is drawn as seen, then the interception of the HFS and the plane gives the constant force frequency-response amplitude curves at that level of forcing.

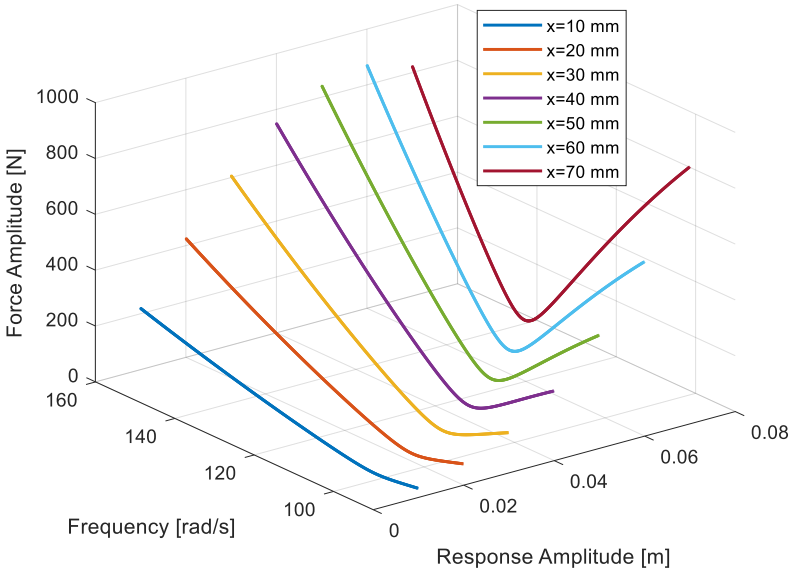

Figure 3-5. Creating Harmonic Force Surface

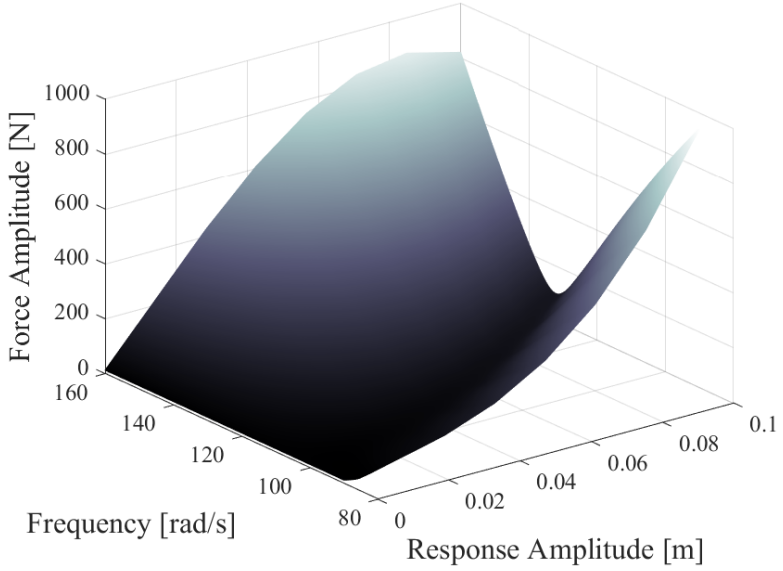

Figure 3-6. Harmonic Force Surface

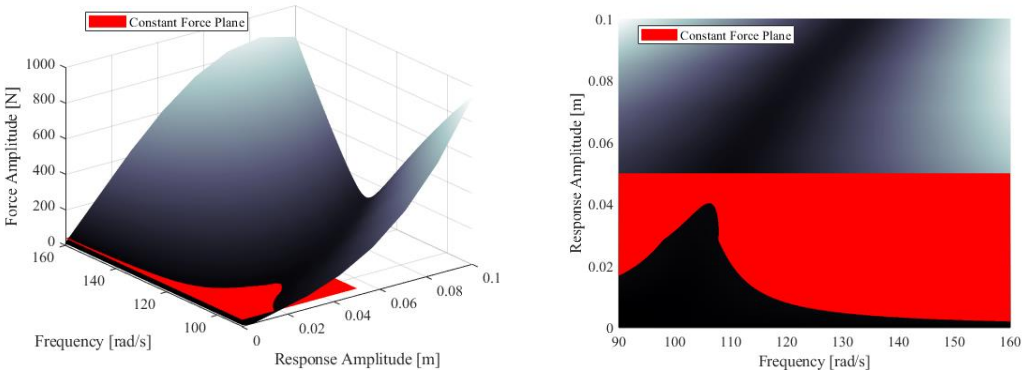

Figure 3-7. Extraction of Constant Force Response Amplitude Curves from the HFS

Three different forcing values are chosen as an example: 25, 40, and 70 N. These are synthesized first directly by cutting the HFS and using nonlinear modal parameters. Figure 3-8 compares the three approaches: constant force, harmonic force surface, and response-controlled stepped sine testing. As seen from the figure, there is a good agreement between constant force-controlled testing and the remaining two methods. Even though RCT is defined for a numerical case study with a single-degree-of-freedom system, a similar approach can be utilized for experimental studies with a controller which tries to maintain a constant displacement on the related degree of freedom. Hence, the RCT-HFS framework can be summarized in Figure 3-9 flowchart.

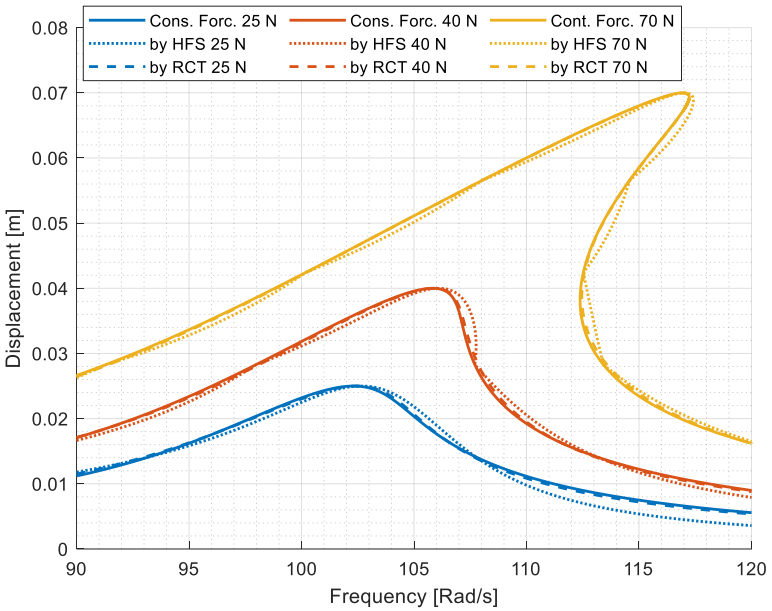

Figure 3-8. Comparison of Different techniques

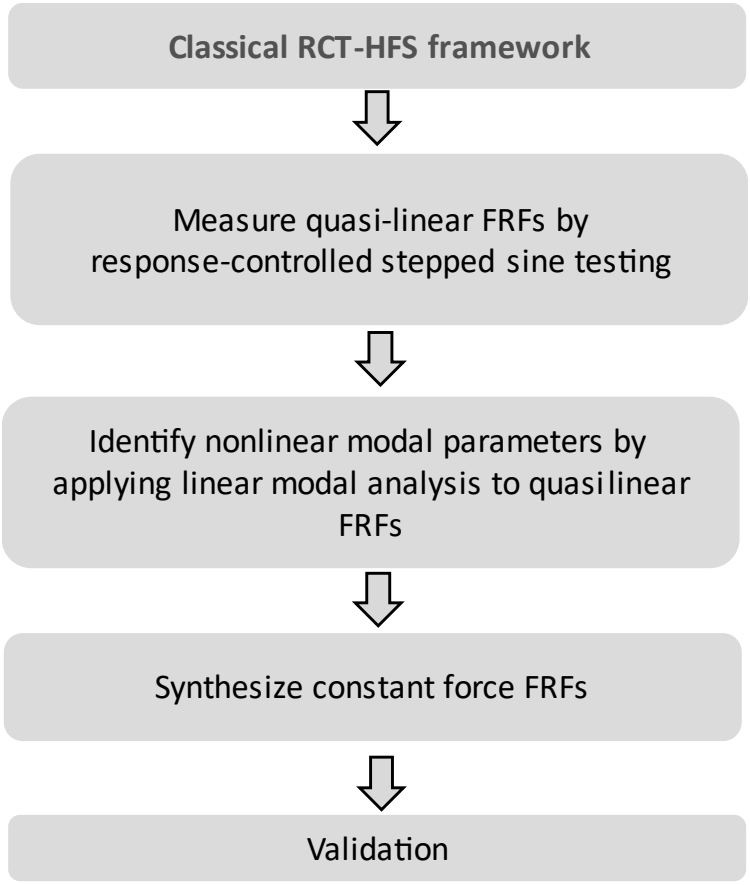

Figure 3-9. Flowchart of Procedure of RCT-HFS Framework

3.2 Numerical Applications and Procedure of FCT-HFS Framework

In order to conceptually explain the RCT-HFS method, a simple numerical example is given in the previous subsection. Now, the FCT-HFS method is utilized in this section by giving more complex examples. Two three-degree of-freedom systems with cubic stiffness are examined before the experimental work is discussed. The types of nonlinearities can be increased, but two examples are given here for the brevity of the numerical application part. The other reason is that there are various examples of real experimental data.

3.2.1 Multi Degree of Freedom (MDOF) System with Cubic Stiffness 1

First, consider the following three-degree of freedom lumped system. The system is excited at the first degree of freedom with the sinusoidal force with an amplitude of *F*. The nonlinear force due to cubic spring can be written as shown in equation (3.19). Further, numerical values of the system parameters are tabulated in Table 3-3.

$$F_{cubic} = k_c x^3 \tag{3.19}$$

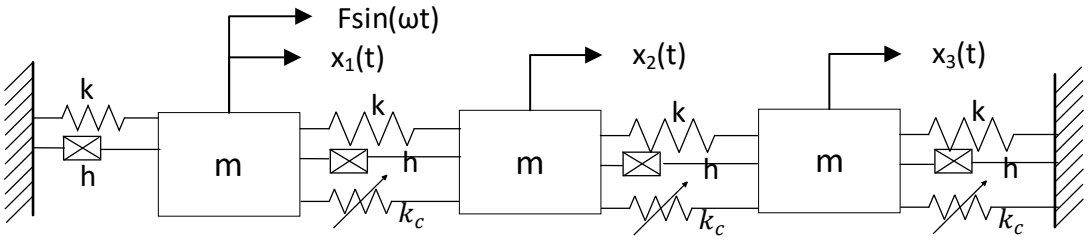

Figure 3-10. Multi-Degree of Freedom

Table 3-3. System Parameters of 3 Degree of Freedom System

m [kg]	k [N/m]	h [N/m]	k_c $[N/m^3]$
1	1e4	5e2	1e7

Natural frequencies are determined as 76.53 rad/s, 141.42 rad/s, and 184.77 rad/s using the linear part of the system by solving the eigenvalue problem. Let's take the frequency interval as 60-90 rad/s.

In the RCT-HFS method, the system is excited at a constant displacement amplitude level; conversely, the classical constant force-frequency response functions are used in this new framework. Detailed information will be given since this is the first example of the new method.

So first, excite the system at several forcing levels, 9, 11, 13, and 15 N's. The measured displacement amplitudes are given in Figure 3-11.

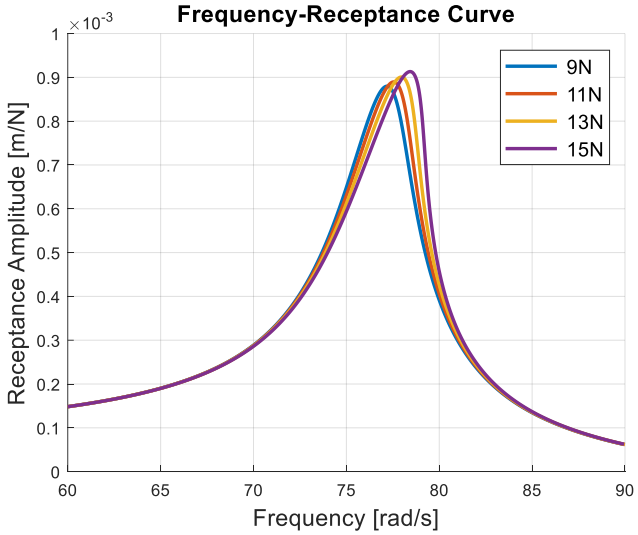

Figure 3-11. Constant Force Receptance Amplitude Curves of MDOF System-Cubic Stiffness Example 1

Merging these constant force FRFs to get the harmonic force surface results in:

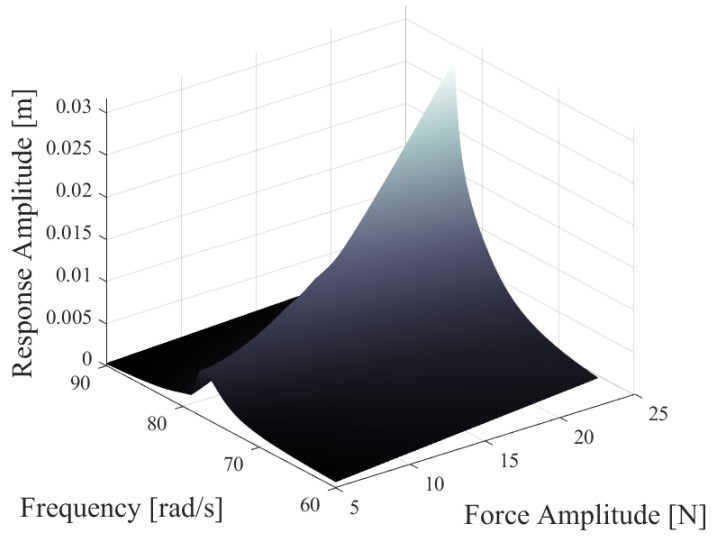

Figure 3-12. Resultant HFS after Merging Constant Force Frequency-Response Amplitude Curves- Cubic Stiffness Example 1

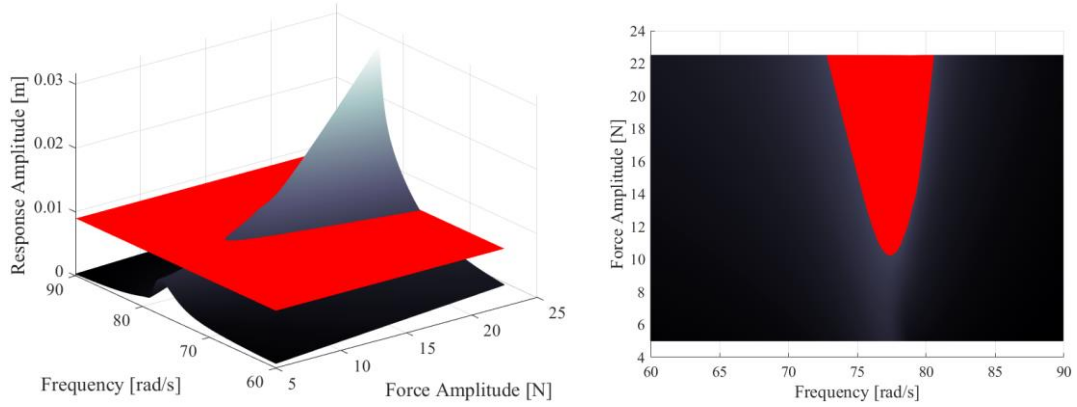

Figure 3-13. Extraction of Harmonic Force Spectra from the HFS

Constant displacement amplitude planes are utilized to determine the corresponding quasi-linear FRFs of the system. The associated harmonic force spectra are extracted from the HFS using constant displacement amplitude planes. Finally, the correspondent quasi-linear FRFs are found by dividing the response amplitude by the harmonic force spectra as shown in Figure 3-14. One should remember that these quasi-linear FRFs determined here are indirect (obtained from constant force input

simulations) since the system is excited with the constant displacement amplitude levels to get the quasi-linear FRFs while using the RCT method.

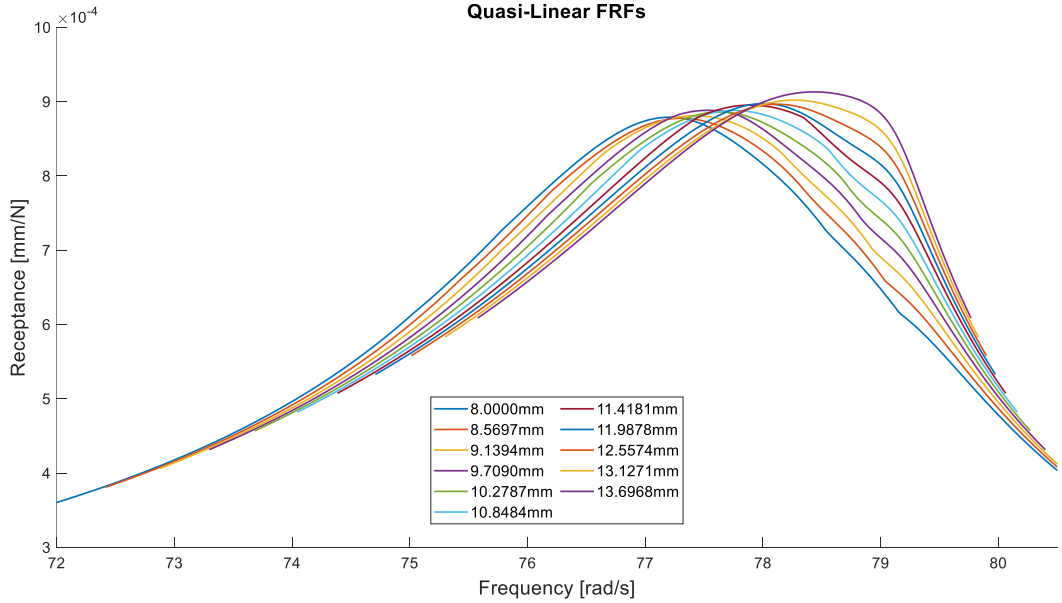

Figure 3-14. Quasi Linear FRFs of MDOF System- Cubic Stiffness Example 1

As a side note, the peak-picking method generally determines the modal parameters throughout this thesis. In some cases, the results of the peak-picking method, the modal parameters, are used as an initial guess to the least square method to find the closest values of the modal parameters extracted from the quasi-linear FRFs.

The peak-picking method is utilized to demonstrate the FCT-HFS method in this example. Then, it is necessary to perform curve fitting during post-processing to synthesize the force-controlled frequency-response amplitude curves, as illustrated in Figure 3-15.

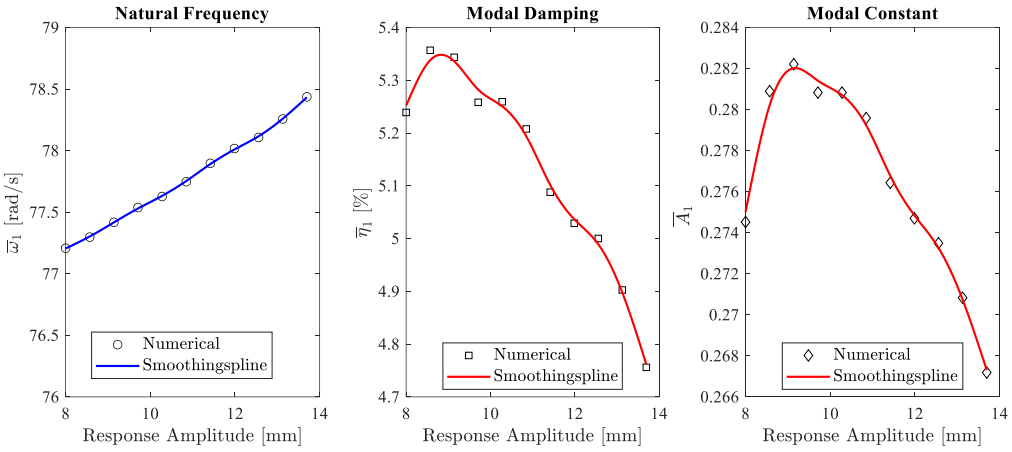

Figure 3-15. Identified Modal Parameters- Cubic Stiffness Example 1

One mode is used to synthesize the frequency response functions, which are then verified using the algebraic solution of the frequency domain non-linear equations with constant force amplitude as the input using the arc-length continuation method, as shown in Figure 3-16. As anticipated, the agreement between the original and synthesized functions near the resonance frequency is good.

Here, one can observe that at low forcing levels, the match between the original and the synthesized frequency-response amplitude plots is not so good at the off-resonance region compared to that at high forcing levels. This may be due to the nature of the construction of HFS. That is, force-controlled frequency-response amplitude curves are merged to get the correspondent HFS. One might need to extrapolate the HFS to get the quasi-linear FRFs at low displacement amplitude levels, which results in some deviation from the actual values to get the modal parameters at that displacement amplitude level. Also, the level of success of the modal fit of the RCT receptances determines the success of the constant amplitude force receptance simulations.

Until this point, the procedure of the proposed method is examined step by step for the ease of the following procedure for the following sections.

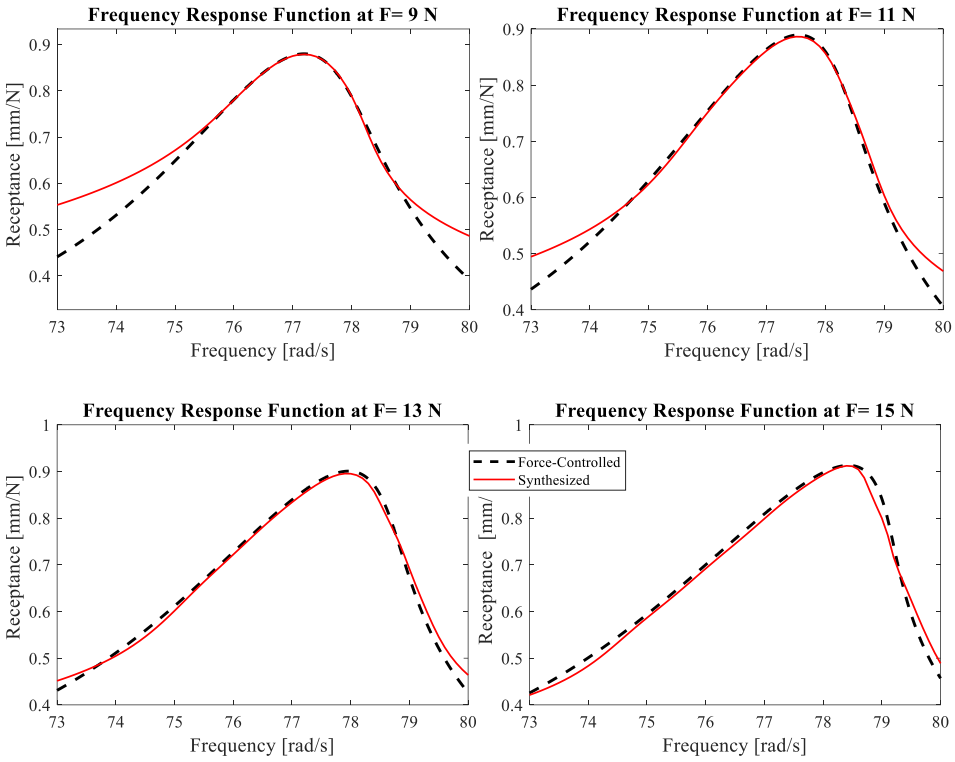

Figure 3-16. Comparison of Measured and Synthesized Frequency-Response Amplitude Plots- Cubic Stiffness Example 1

One might investigate the effects of the following on the constant force receptance estimations:

1. Taking intermediate force levels.
2. Trying different curve fits to the modal parameters.

3.2.1.1 Adding Intermediate Force Levels

Remember that under section 3.2.1 force-controlled tests are performed at 9,11,13 and 15 N. Now, let's excite the same system at forcing levels from 9 N to 15 N with an increment of 0.5 N to investigate the result of the taking more force between the boundaries.

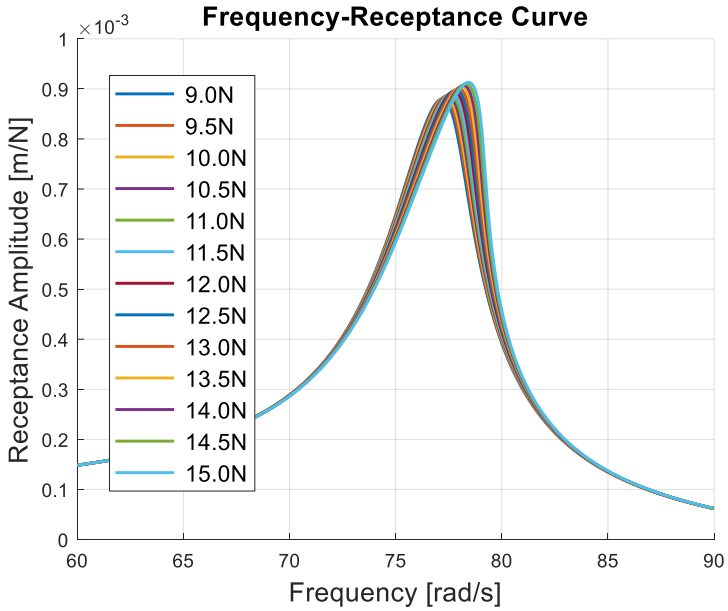

Figure 3-17. Refined Force Controlled Tests

Figure 3-18 gives an insight into the modal parameters. A smoothingspline type of curve fit is utilized for the sake of comparison in terms of force sampling. Firstly, circles represent the identified modal parameters from the HFS created using the test with less number of forcing levels, whereas the plus signs represent the tests with more forcing levels. Secondly, blue curves are for the coarse forcing levels, while reds are for the refined forces. As seen from the figure, taking more force did not affect the natural frequency values much. On the other hand, the effect of the increased force levels can be observed for modal damping and modal constant.

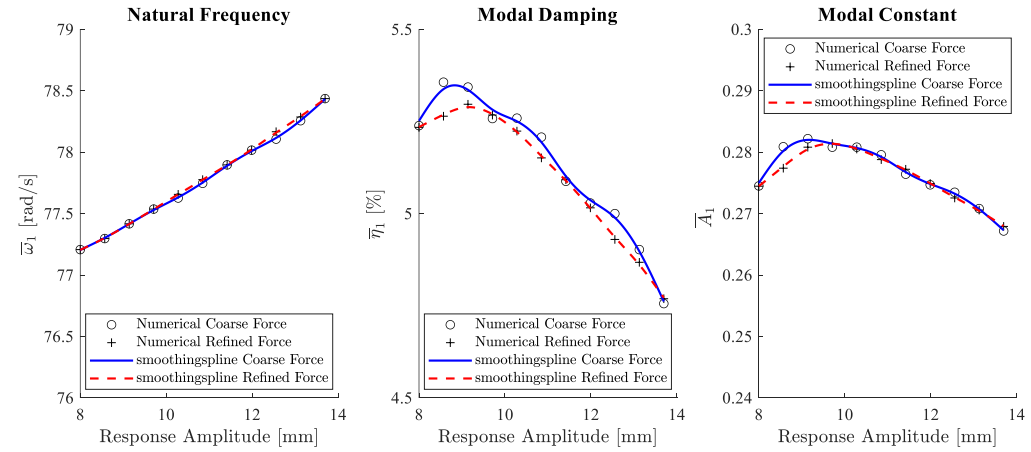

Figure 3-18. Modal Parameters Comparison Extracted Using Different Sampling Frequencies of Force

Then, the frequency response curves are synthesized at a single forcing level, 14 N, that is untested force level at the first test. Figure 3-19 compares the two synthesized FRFs using FCT-HFS with the simulated one numerically. As seen from the graph, the more force data sampled case gives more accurate synthesis around the off-resonance region. Hence, tests at a higher number of forcing levels provide minor improvements around resonance but significant improvements around off-resonance which makes test force level planning important based on the desired accuracy level.

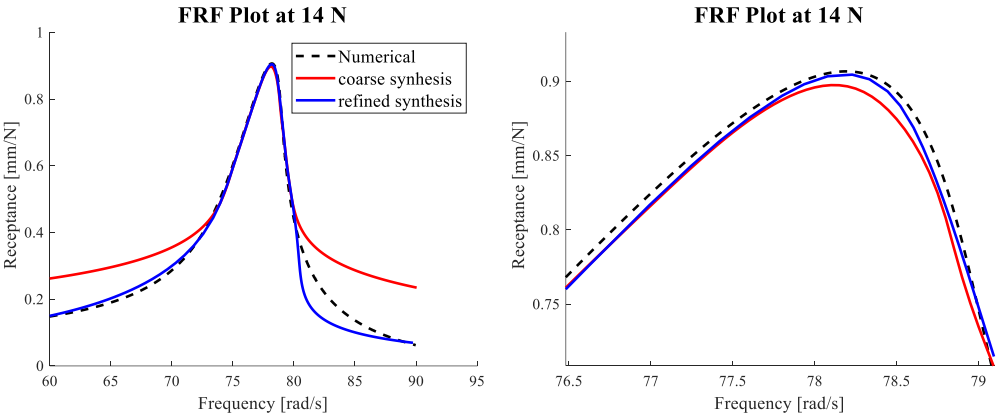

Figure 3-19. a) FRF Comparison b) Detailed View

3.2.1.2 Different Curve Fits to the Modal Parameters

In this section, the same data set of 9,11,13, and 15 is utilized, and the effect of the type of fit on the synthesis is examined. Figure 3-20 compares the curve fits to the modal parameters. Figure 3-21 compares the synthesized FRFs obtained using different curve fit types between 75-79 rad/s, around resonance. As observed from the figure, The closest curve fit type to the actual FRF is cubic spline curve fit, followed by smoothingspline and polynomial fits.

Afterward, another point that can be considered is what happens when increasing the frequency sweep in all cases from interval 75-79 rad/s to 75-80 rad/s, using the same modal parameter curve fits. Figure 3-22 gives an insight into this case. Cubic spline fit case starts to give inaccurate results frequencies from 79 rad/s to 80 rad/s. Furthermore, since not all the data points that are extracted from the HFS do not cover the whole displacement range of the frequency response amplitude curves, an extrapolation is inevitable as seen in Figure 3-23. In addition, as marked in Figure 3-22 the point where the deviation starts is an extrapolated point.

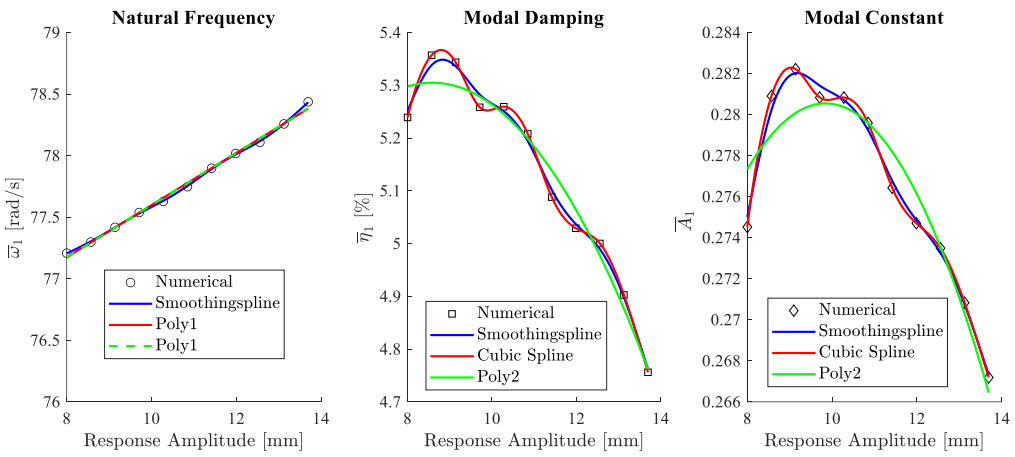

Figure 3-20. Comparison of Modal Parameters using Different Curve Fitting Methods

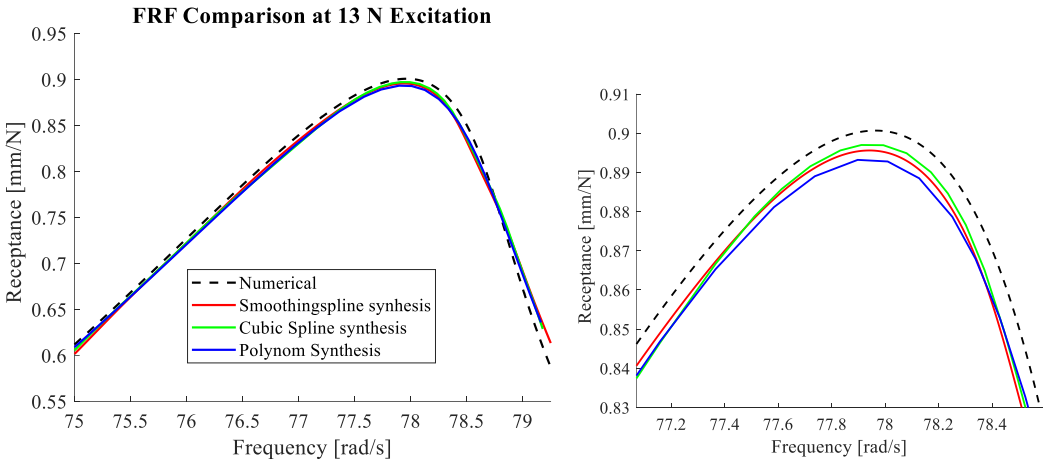

Figure 3-21. Comparison of FRFs Using Different Curve Fitting Methods

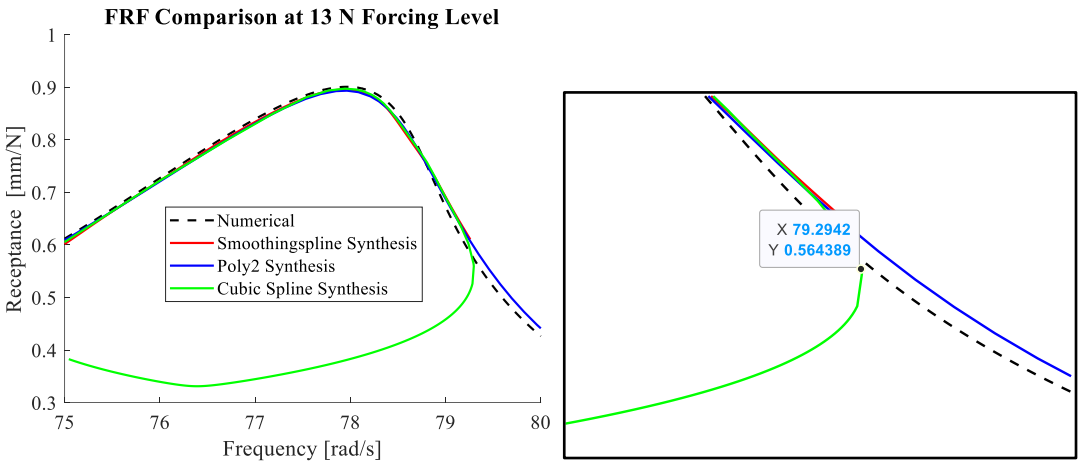

Figure 3-22. FRFs Comparison Using Different Curve Fit Types- Extended Frequency Sweep

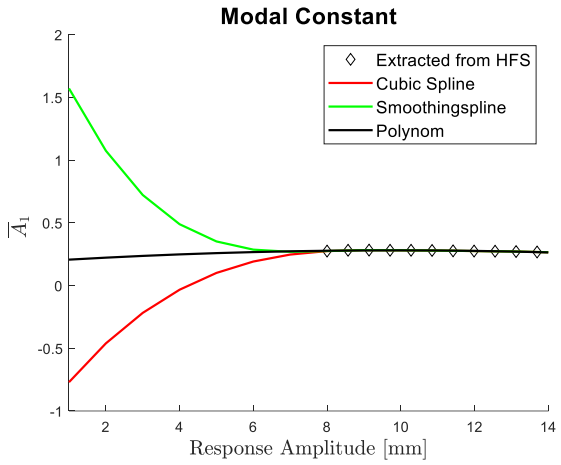

Figure 3-23. Modal Parameter Extrapolation

It is apparent that cubic spline fit predicts an unnatural behavior due to the built-in behavior of boundary conditions in the cubic spline command of MATLAB. On the other hand, smoothingspline and polynomial curve fits predict this natural behavior correctly. Although using polynomial and smoothingspline curve fits give accurate results, one should hesitate to extrapolate these curves and should be prudent while doing this.

3.2.2 Multi Degree of Freedom (MDOF) System with Cubic Stiffness 2

Now, consider the system in Figure 3-10, subjected to different amplitudes of forcing levels - 10, 15, 20, and 25 N. The system is excited between 60 and 100 rad/s. In the previous example, no unstable branches were observed in frequency-response amplitude curves. The resulting curves are listed in Figure 3-24 as dashed lines. The solid line of the forcing level 25 N shows a jump behavior in its response curve, while the dashed is the frequency response amplitude curve with the unstable branch. Therefore, the harmonic force surface is constructed using the frequency-response amplitude curves with a jump (solid lines), as shown in Figure 3-25.

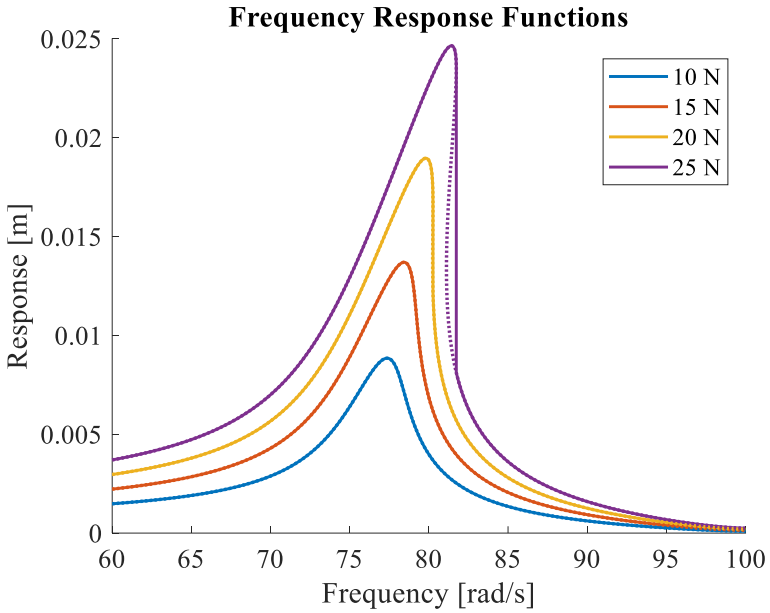

Figure 3-24. Frequency-Response Amplitude Curves-Cubic Stiffness Example 2

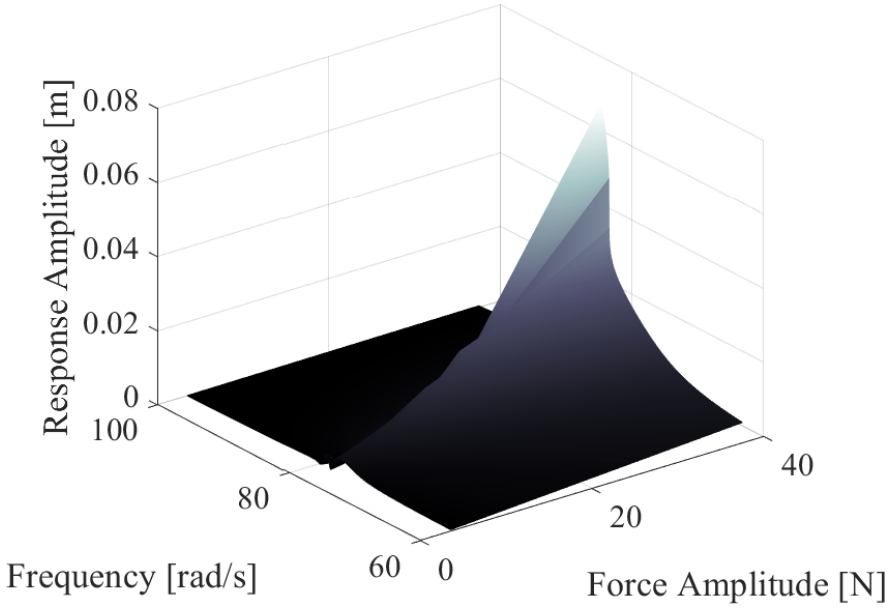

Figure 3-25. Harmonic Force Surface- Cubic Stiffness Example 2

The resultant harmonic force surface is cut using constant displacement amplitudes to obtain indirect quasi-linear frequency response functions (FRFs). Six constant displacement planes are utilized to extract the quasi-linear FRFs with displacement values ranging from 5 mm to 23 mm. The extracted quasi-linear FRFs are listed in

Figure 3-26. It is observed that the quasi-linear FRFs exhibit stepped shapes on the right-hand side of the natural frequency due to the cubic stiffness displaying the hardening behavior of the system, leading to a jump at these forcing levels. That results in the stepped shapes while extracting quasi-linear FRFs from the interpolated HFS. However, modal identification should not be performed based on these parts of the RCT FRF plots since it may lead to incorrect results. A modal curve fitting to these quasi-linear FRFs can be performed using equation (3.10) to identify the modal parameters accurately. A custom curve fitting equation is defined, and MATLAB's curve fitting *fit* function is used to perform the curve fitting. The curve-fitted quasi-linear FRFs are shown in Figure 3-27. The modal parameters are then identified using these curves using the peak-picking method. These results provide valuable insights for further analysis.

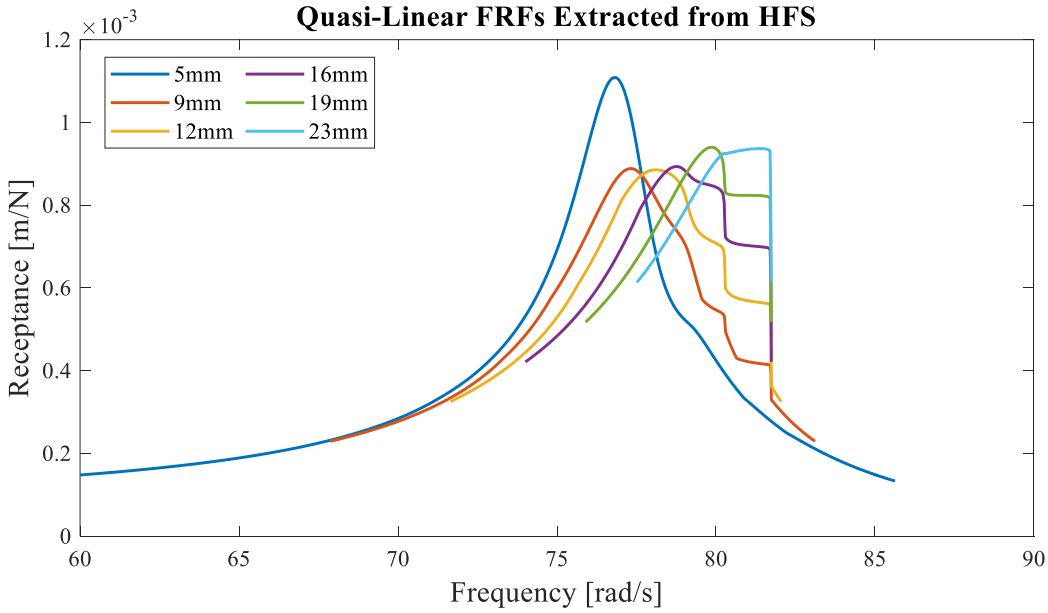

Figure 3-26. Quasi-Linear FRFs Extracted from HFS- Cubic Stiffness Example 2

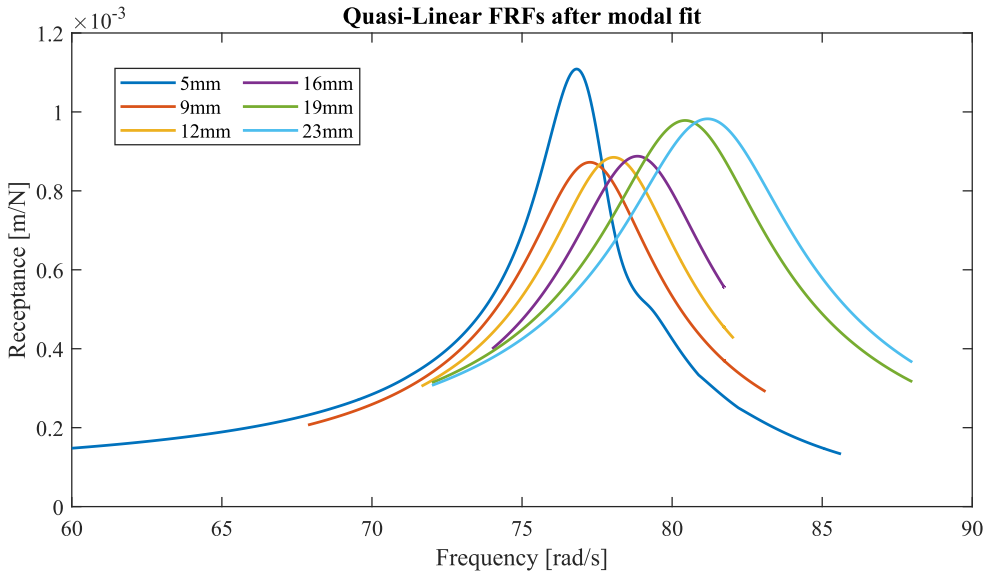

Figure 3-27. Quasi-Linear FRFs Modal Fit- Cubic Stiffness Example 2

The identified modal parameters are shown in Figure 3-28. The force-controlled FRF curves are synthesized using a smoothing spline curve fit of the modal parameters. The original frequency-response amplitude curves are obtained and compared using these modal parameters in Figure 3-29. A good agreement between the original and the synthesized FRFs is observed, especially near resonance frequencies.

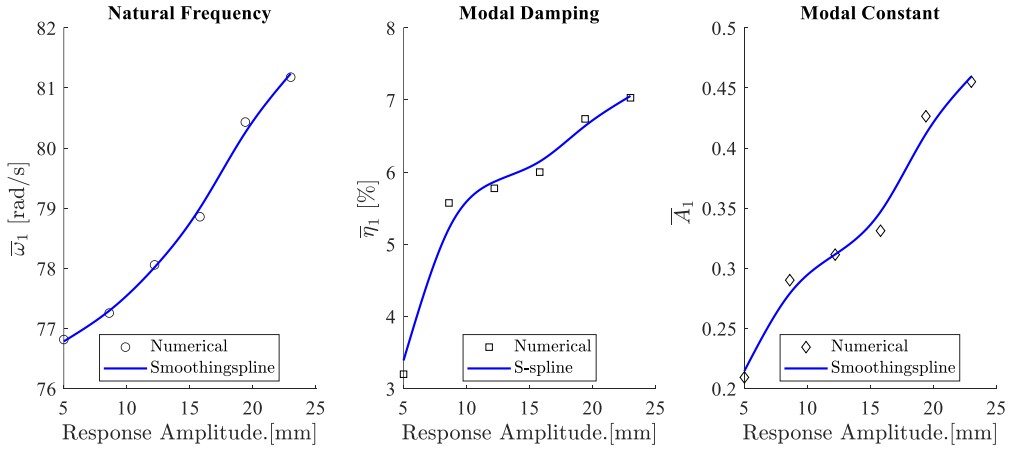

Figure 3-28. Identified Modal Parameters- Cubic Stiffness Example 2

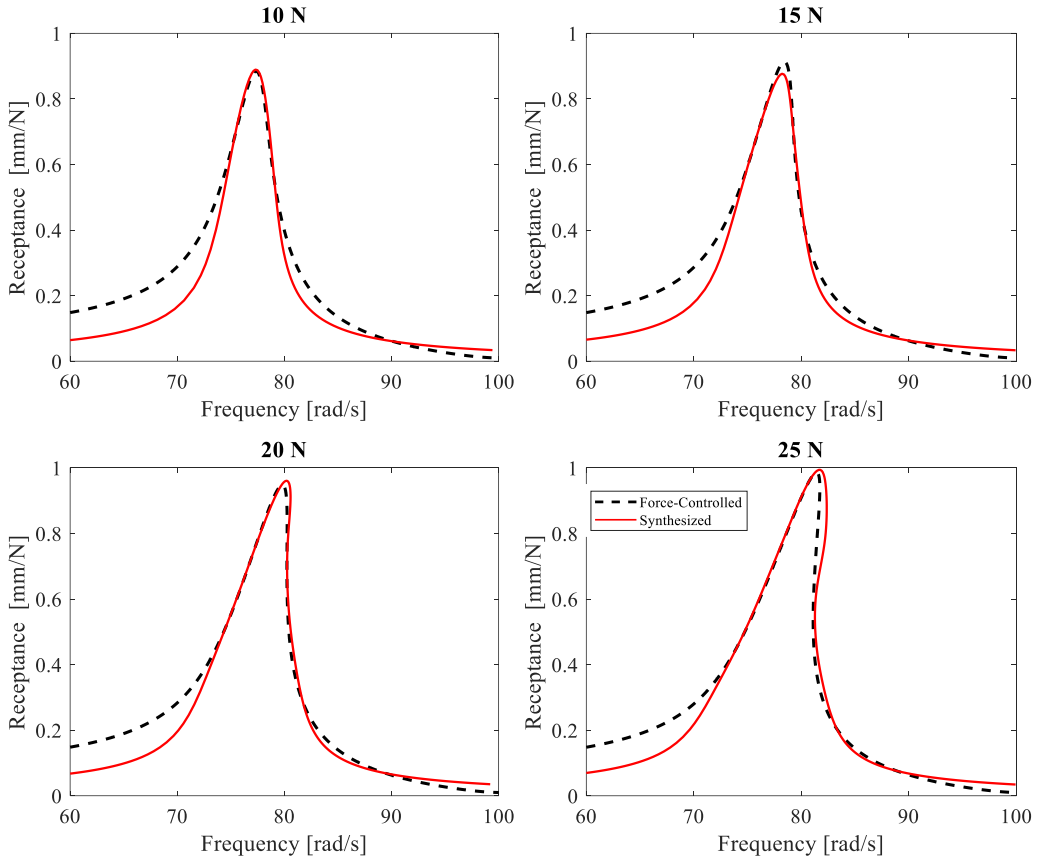

Figure 3-29. Comparison of Measured and Synthesized Frequency- Response Amplitude Curves-Cubic Stiffness Example 2

Some valuable insights and suggestions can be drawn from this example, which are as follows:

- Incorporating frequency response functions with jump phenomena into the FCT-HFS analysis leads to stepped quasi-linear FRFs, making modal identification challenging.
- Several techniques are available to determine the modal parameters of quasi-linear frequency response functions (FRFs), here peak-picking and curve fitting are used.
- An alternative approach to addressing the issue of stepped shapes observed in quasi-linear FRFs involves fitting a polynomial or exponential function to the part of the FRF that does not present jump behavior. This method offers a viable solution to the challenge of modeling quasi-linear FRFs accurately.

- Modal parameters can be directly determined from quasi-linear FRFs extracted from the HFS by applying the *lsqcurvefit* function of MATLAB.
- As understood throughout the text, the proposed technique is not as successful as it is desired in the case of the jump.

3.3 Summary

Chapter 3 of the thesis discusses the RCT-HFS method and its procedure using a simple SDOF system. The strategy behind the new framework is explained using two and three DOF discrete systems. Only a few numerical applications are presented in this chapter which should be enough to explain the proposed methodology. The following chapter focuses on real experimental applications, where those conducting the experiments can better understand the new framework's importance. This chapter concludes with a flowchart that outlines the method's procedure.

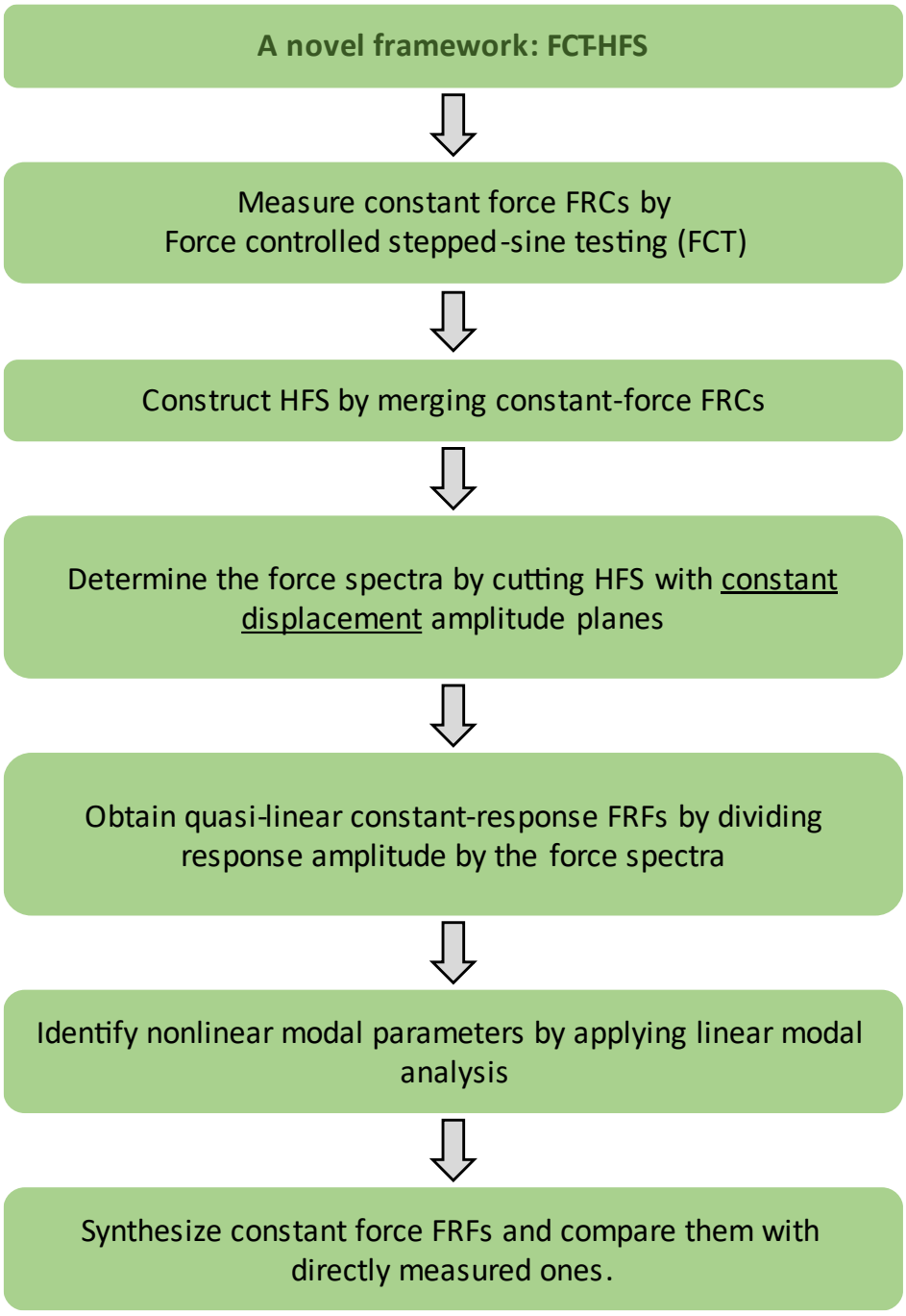

Figure 3-30. Flowchart of the Proposed Nonlinear System Identification Method

CHAPTER 4

EXPERIMENTAL APPLICATIONS OF THE FCT-HFS FRAMEWORK

In Chapter 3, the RCT-HFS and FCT-HFS methods are reviewed, and their procedures are explained in detail using cubic stiffness nonlinearity as an example. It is important to note that the newly developed FCT-HFS method is primarily intended for experimental purposes. This chapter of the thesis verifies the proposed methods through experimental data where some of the data are obtained from literature and some of them are collected from test setups designed for the thesis.

Experiments with the bolted joint connections are utilized as an experimental setup. Those are the indispensable parts of the mechanical systems of manmade structures. Furthermore, these jointed structures introduce friction, gap, and preload nonlinearities. Moreover, modeling and understanding these types of nonlinearities are inconvenient due to the modeling difficulty of their nature. Here, the term understanding is used to find out the modal parameters of the system due to those nonlinearities. Determined modal parameters can then describe the behavior of the system. Therefore, modeling and understanding the nonlinear behavior of those systems are crucial in engineering. To this end, several nonlinear system identification methods have been developed as stated in Chapter 1. Hence, the proposed methodology is verified and validated using such a system with a challenging behavior.

Different joint structures utilized will be explained in the following paragraphs. Hands-on experiments were conducted at TÜBİTAK-SAGE using the Brake-Reuß Beam (BRB) [61, 62]. This beam has become a benchmark across the engineering society for nonlinear mechanical systems. Therefore, the former and latter reasons led to using this beam as a testing specimen. Its dimensions and properties are given in detail in the upcoming section, but it can be summarized as follows with brevity.

Two L-shaped beams, each 42 cm, are connected with three bolted joints where the interface is 12 cm. Besides the test, three experimental applications from the literature verify and validate the method using their experimental data. Firstly, the data of the Orion Beam [63] is utilized to validate and verify the proposed method. The configuration of the designed beam can be summarized as follows. Two beams, each 200 mm, are connected to each other with three bolted joints with the 30 mm interface.

Furthermore, the setup is positioned vertically to the ground. The paper's originality is that it introduced a new lap-joint configuration with high repeatability, and this new configuration separates the correlation between the resonance frequency, maximum amplitude, and half-power bandwidth. That allows this system to be used as a reference while developing methods. Therefore, the force-controlled FRF results that have recently been presented are used to validate and verify the developed method. Details of the experimental setup and the data are presented in a related section. Secondly, the data of the Length Modified Brake-Reuß Beam [64] is also used to validate the proposed method. It is the modified version of the original Brake-Reuß Beam by increasing the beams' length and contact area to 1080 mm and 120 mm, respectively. Finally, the data of the Half Brake-Reuß Beam [65] is utilized. It is designed so that the width of the beam is decreased from 1" to 0.5". All other related and required details of the structures are given in their sections. The summary of each experimental setup, i.e., dimensions, number of connections, and position of the experimental setup, is provided in Table 4-1.

Table 4-1. Summary of the Experimental Setups

	Individual Dimensions of Beams	Number of Connections to Each Other	Position of the Test Setup
The Brake-Reuß Beam	72 x 2.5 x 2.5 cm	3	Horizontal
The Orion Beam	200 x 30 x 2 mm	3	Vertical
The Length Modified Brake-Reuß Beam	42.5 x 1 x 1 inch	3	Horizontal
The Half Brake-Reuß Beam	28.35 x 0.50 x 1.00 inch	3	Horizontal

4.1 Brake-Reuß Beam Tests Conducted in TÜBİTAK SAGE

4.1.1 Test Setup

The test setup of the Brake-Reuß Beam is manufactured and assembled in TÜBİTAK SAGE and it is shown in Figure 4-1. Two L-shaped beams are connected with bolted joints and tightened with a torque wrench to the desired torque level. To ensure the gap at each side of the connection, a 30 μm shim is used during the assembly process, where the Brake-Reuß beam is held with two monolithic beams to ensure linearity. MB Dynamic Modal 110 modal shaker with forcing amplitude and frequency capacities of 500 N and 5000 Hz, respectively is used for exciting the system. A stinger is used as the connection between the beam and the shaker. A PCB Piezotronics 208C03 ICP load cell is attached to the connection of the stringer and beam to monitor forcing at the excitation location and the measured force data is used by the embedded controller of Siemens LMS. In addition, MB Dynamics

MB500VI is used as the power amplifier. LMS SCADAS Mobile is used as the data acquisition system, and the collected data is monitored using a desktop computer. A detailed photo of the test setup is shown in Figure 4-2. The shaker is connected to the metal block, and a rigid body connection is assumed between the shaker and the metal block. Six ICP accelerometers of PCB Piezotronics 352A73 are used to measure the data, and the positive measurement direction is shown in Figure 4-2. Accelerometers 1,3, 5, and 6 are placed along the +z direction half of the beam (+z direction is shown on Figure 4-2). In contrast, the others are placed on the -z direction half of the beam. Data acquired from the first accelerometer and load cell are used to provide the feedback acceleration and forcing measurements for the response-controlled stepped-sine testing controller. So, the rigid L-shaped beam is assumed to demonstrate the same motion on the load cell and accelerometer sides. Through this thesis, the data measured by accelerometer one is used only. Finally, to ensure the free-free condition of the Brake-Reuß Beam, fish lines are used to suspend the test beam as shown in Figure 4-3. Two data sets are recorded using this setup at different tightening torques of 10 and 25 Nm. Initially, the 10 Nm case is examined, then the 25 Nm case.

Data is measured through accelerometers and acceleration data is recorded with LMS Data Acquisition System. The data acquisition system transforms this measured data from the time domain to the frequency domain. This procedure is performed by the built-in feature of the LMS Testlab. LMS Testlab determines the FRF by dividing the cross-power spectrum (S_{xy}) of the input (x) and output (y) by the auto power spectrum (S_{xx}) of the input.

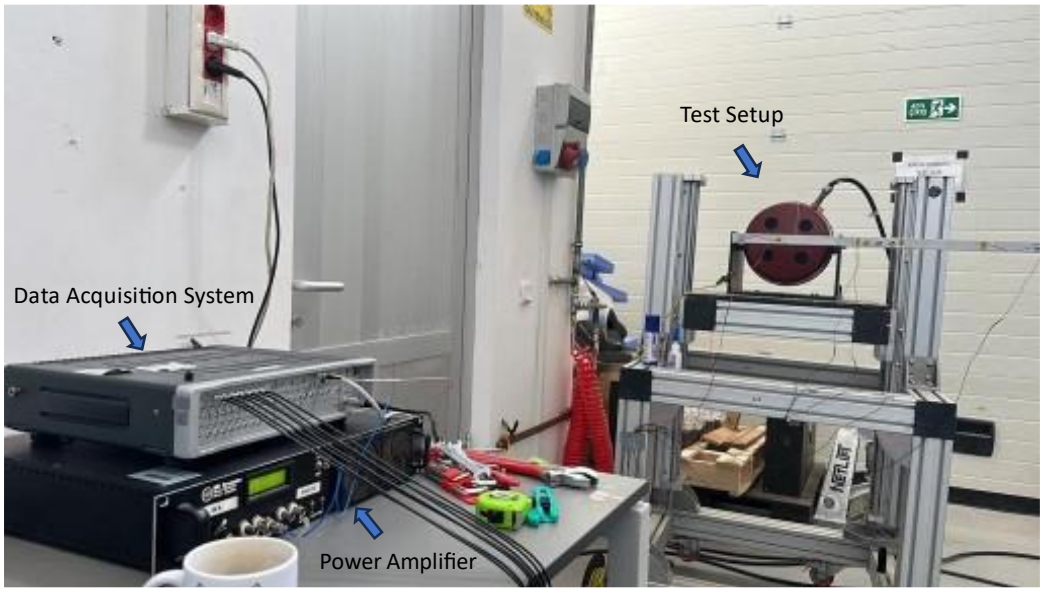

Figure 4-1. Whole Test Setup Including Data Acquisition, Power Amplifier and Test Specimen

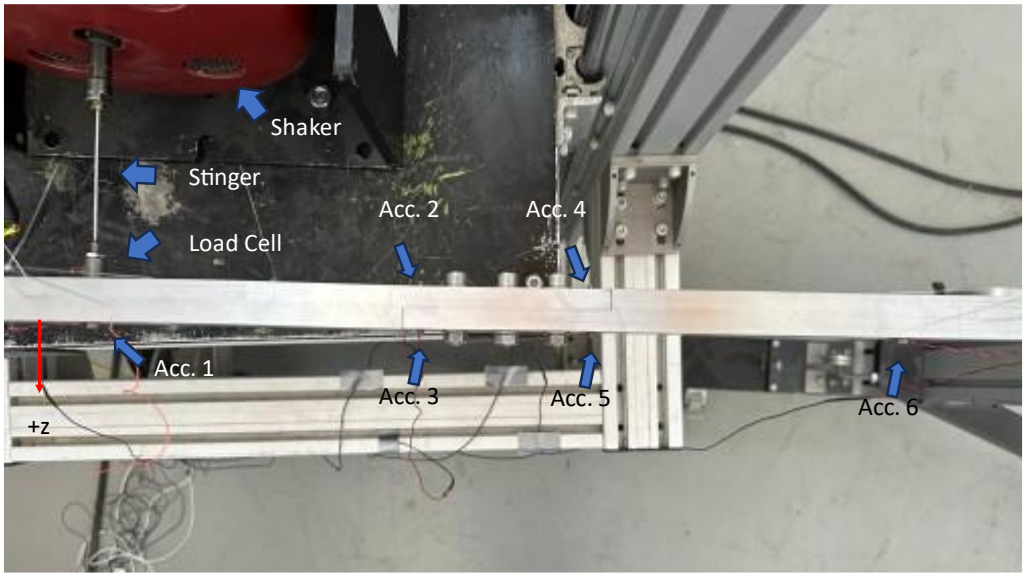

Figure 4-2. Detailed View of Test Setup Photo of Brake-Reuß Beam test setup in TÜBİTAK-SAGE

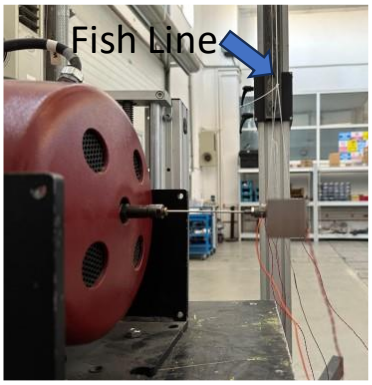

Figure 4-3. Fish Line of The Setup

4.1.2 Test 1: Test with Tightening Torque of 10 Nm

In test 1, two data sets are examined. During each test, force-controlled stepped sine testing is utilized. Even numbers of forcing amplitudes are employed in data set 1, while the other odd numbers of forcing amplitude levels are used in data set 2. During both measurements, stepped sine testing is performed between 133 Hz and 144 Hz which covers the first natural frequency of the beam structure.

4.1.2.1 Data Set 1

First, a force-controlled data set is collected from 2 N to 20 N with an increment of 2 N at each test run. Furthermore, stepped-sine testing is conducted with a frequency increment of 0.125 Hz between 133 and 147 Hz frequencies. In the LMS SCADAS desktop application, the constant force frequency response amplitude curves are measured as shown in Figure 4-4. The measured unit of FRF is in g (m/s^2) and the measured acceleration data is converted to displacement in the frequency domain. These frequency-response amplitude curves are plotted in MATLAB as shown in Figure 4-4b.

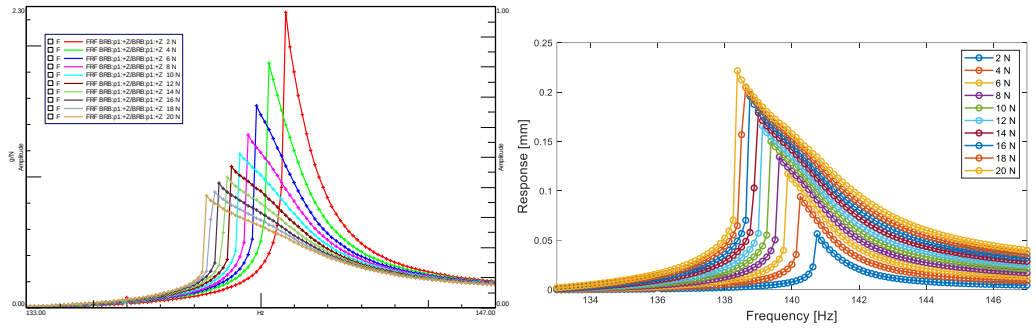

Figure 4-4. Constant Force Response Amplitude Curves of Data Set 1 of Test 1 of BRB a) Accelerance data from LMS b) MATLAB plot using displacement data

It is observed that a jump phenomenon occurred during measurements. Without commenting on this (it is to be discussed in Chapter 5), let's continue to the formal procedure of the FCT-HFS framework. The next step is to construct a harmonic force surface using these frequency-response amplitude curves.

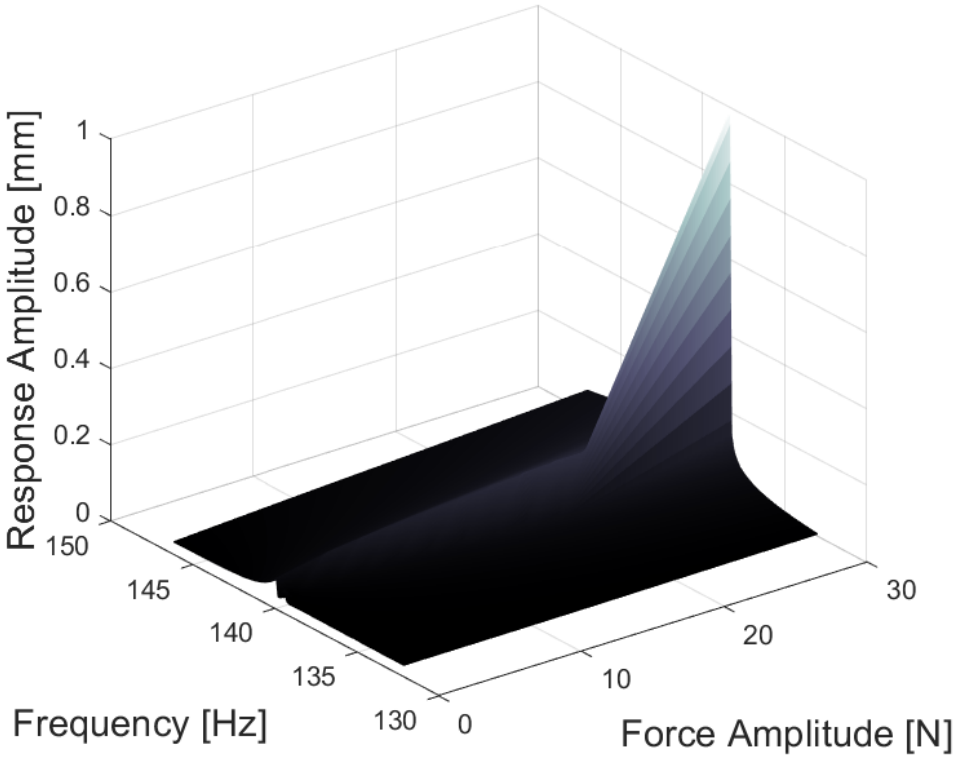

Figure 4-5. Harmonic Force Surface of Data Set 1 of Test 1 of BRB

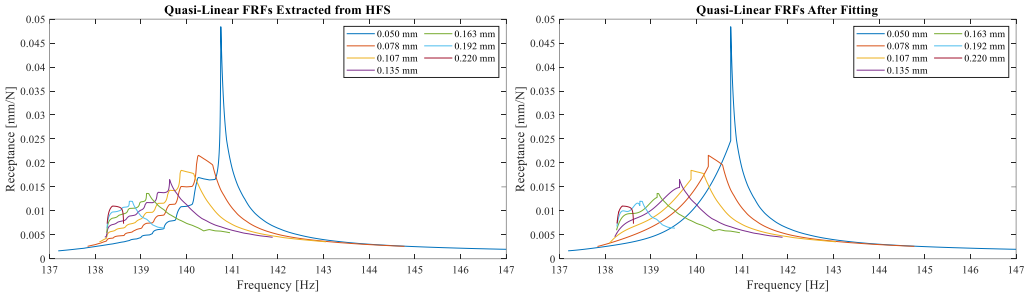

Figure 4-6. a) Quasi-Linear FRFs Extracted from HFS b) Applied Curve Fitting of Data Set 1 of Test 1 of BRB-Curve Fit Type 1

The harmonic force surface of test 1 of BRB is illustrated in Figure 4-5. Extraction of quasi-linear FRFs from the HFS between upper and lowermost displacement amplitude levels of 0.050 mm and 0.220 mm are performed. As shown in Figure 4-6, a stepped curve is observed at the left-hand side of each curve's peak. This stepped response behavior is expected since jumps are observed in the measured frequency-response amplitude plots. A similar stepped curve behavior was observed in the numerical simulation case study with jump behavior which was presented in the previous chapter. Before directly attempting the peak-picking method for these types of shapes, it is worth looking at the shape of the FRFs. The left-hand sides of the curves are stepped, but the right-hand sides are smooth and in the desired behavior. Furthermore, keeping in mind that these are the experimental results, the aim is to get a quasi-linear shape to predict modal parameters from the curves. Two different types of curve fitting can be considered here.

4.1.2.1.1 Curve Fit Type 1 (Peak-picking algorithm)

First, a curve fitting to the left-hand side of the quasi-linear FRFs is applied for that purpose, Figure 4-6a. Now, it is possible to estimate modal parameters using the peak-picking method.

The identified modal parameters from these curves and curve fit of the identified modal parameters are given in Figure 4-7. From these curve fits, constant force FRFs are synthesized and compared with the measured ones in Figure 4-8. The results are

in good agreement around resonance and minor deviations are observed near resonance frequencies. However, one should be cautious while applying this FCT-HFS to the force-controlled FRFs where the jump is observed since the result of an infinite slope causes stepped quasi-linear FRFs. That makes extracting modal parameters difficult using the peak-picking method. On the other hand, it is worth noting that the FCT-HFS framework is easier and more straight-forward to apply for weakly nonlinear cases where FRFs have no jumps. Furthermore, note that although the jump makes the analysis difficult, good agreement between the force-controlled stepped sine testing of measured and synthesized ones are observed near resonance frequencies even when the jump occurs.

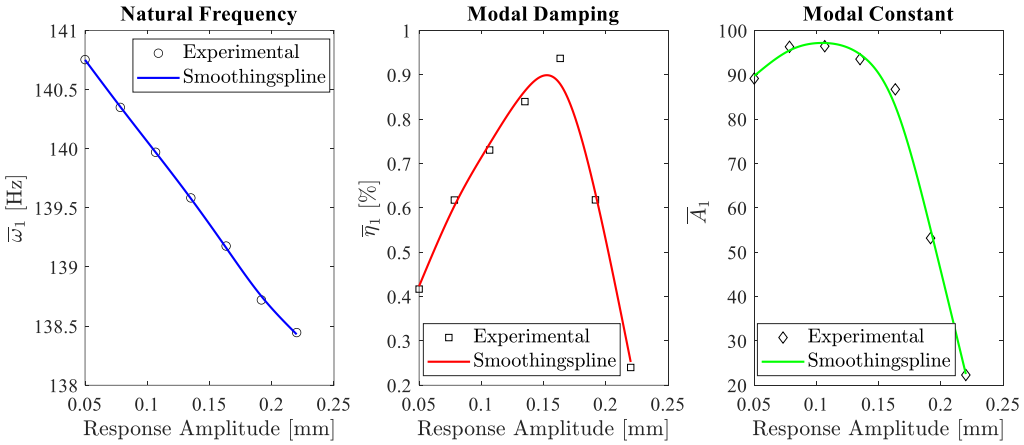

Figure 4-7. Identified Modal Parameters of Data Set 1 of Test 1 of BRB-Curve Fit Type 1

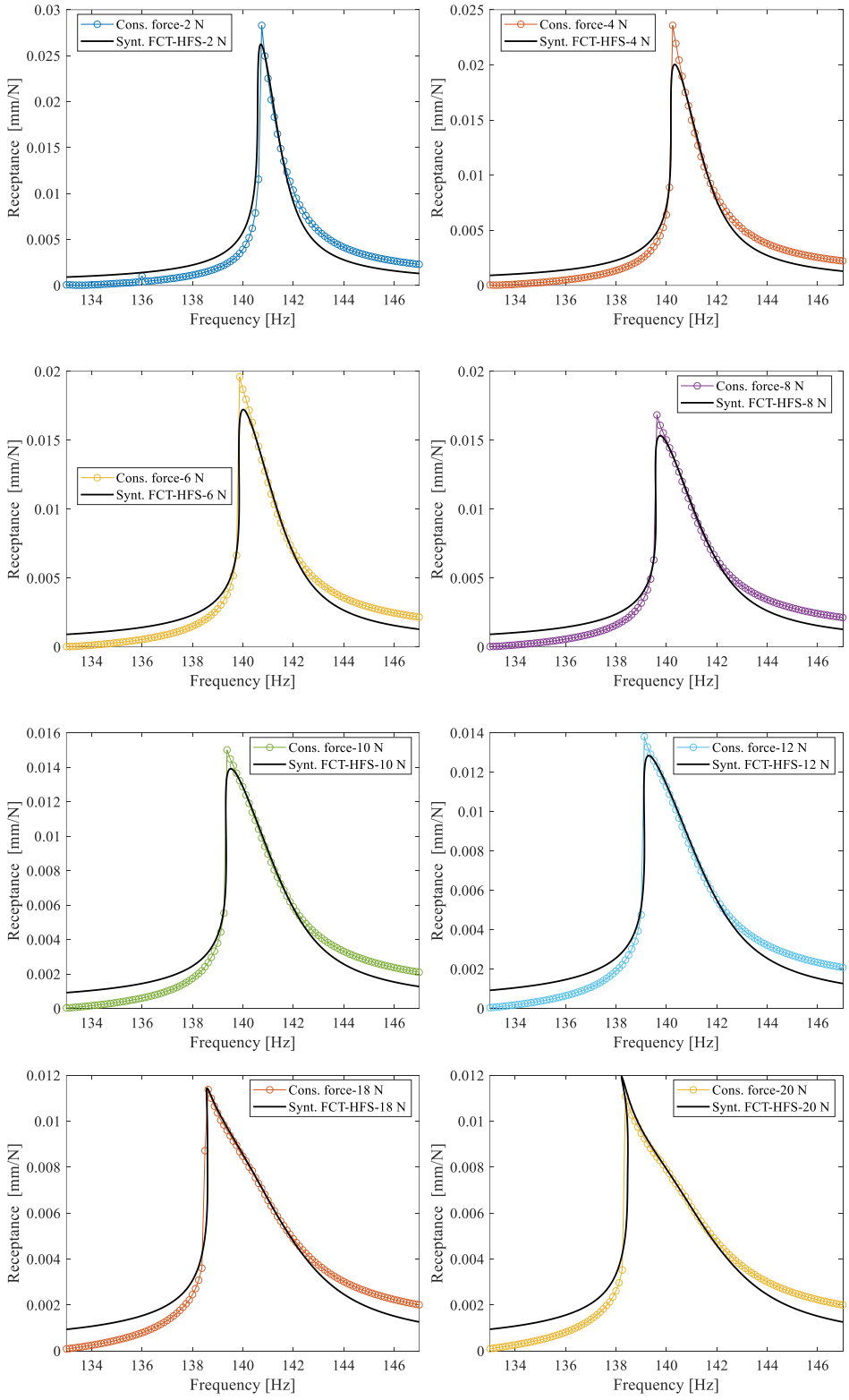

Figure 4-8. Comparison of Synthesized FRFs and Measured Ones of Data Set 1 of Test 1 of BRB-Curve Fit Type 1

4.1.2.1.2 Curve Fit Type 2 (Curve fitting and spline fitting algorithms)

Another approach to handle the stepped shape in the extracted quasi-linear FRFs is using the *lsqcurvefit* function of MATLAB [66] with the modal equation. First, it is meant from the modal equation is the single nonlinear normal mode equation with response amplitude dependent modal parameters as

$$\boldsymbol{x} = \frac{\overline{\boldsymbol{\phi}}(q_r)_r \overline{\boldsymbol{\phi}}(q_r)_r^T \boldsymbol{f}}{\left(-\omega^2 + i\eta_r(q_r)\omega_r^2(q_r) + \omega_r^2(q_r)\right)} \tag{4.1}$$

The working principle of the algorithm can be summarized as follows. First, *lsqcurvefit* is a nonlinear least-square solver that minimizes the error between the measured and fitted data, as shown in equation (4.2). Here, equation (4.1) is used as the function that should be used in equation (4.2).

$$min\left(\sum_i (f(x, xdata_i) - ydata_i)^2\right) \tag{4.2}$$

In contrast to the peak-picking method, here, the modal parameters of the modal equation are tried to be found with this algorithm.

Using this function, it is possible to identify modal parameters by curve fitting to the extracted quasi-linear FRFs. Therefore, the peak-picking method is not used in this approach.

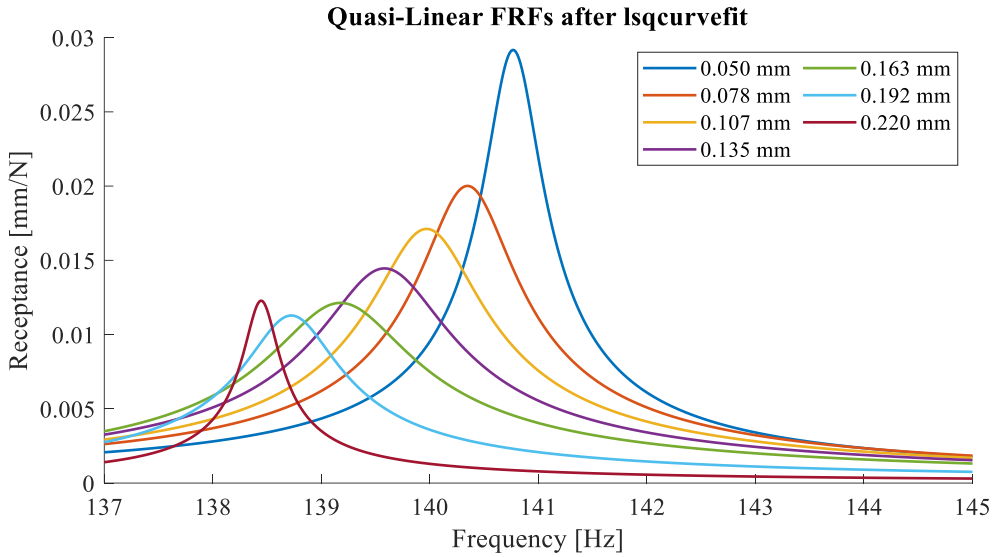

Figure 4-9. Quasi-Linear FRFs after *lsqcurvefit*-Curve Fit Type 2

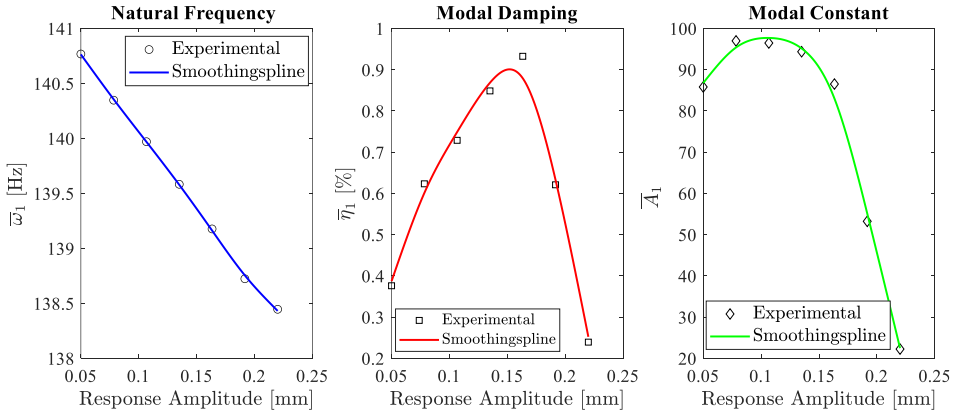

Figure 4-10. Identified Modal Parameters of Data Set 1 of Test 1 of BRB-Curve Fit Type 2

The identified modal parameters and corresponding *smoothingspline* fits are shown in Figure 4-10.The mathematical formulation of smoothingspline can be written as

$$p\sum_i w_i\left(y_i - s(x_i)\right)^2 + (1-p)\int\left(\frac{d^2s}{dx^2}\right)^2 dx \tag{4.3}$$

Where $w_i, p\ and\ s$ are weight, smoothing parameter and smoothing spline, respectively. Generally, p is taken as 1.

Using the modal parameters obtained from spline-fit, the constant force FRFs are synthesized again and compared with the original ones in Figure 4-11. Examining the synthesized FRFs for curve fit types 1 and 2 shows that both approaches are satisfactory except for lower force levels. The cause of this deviation is the modal damping at the lower displacement amplitude levels.

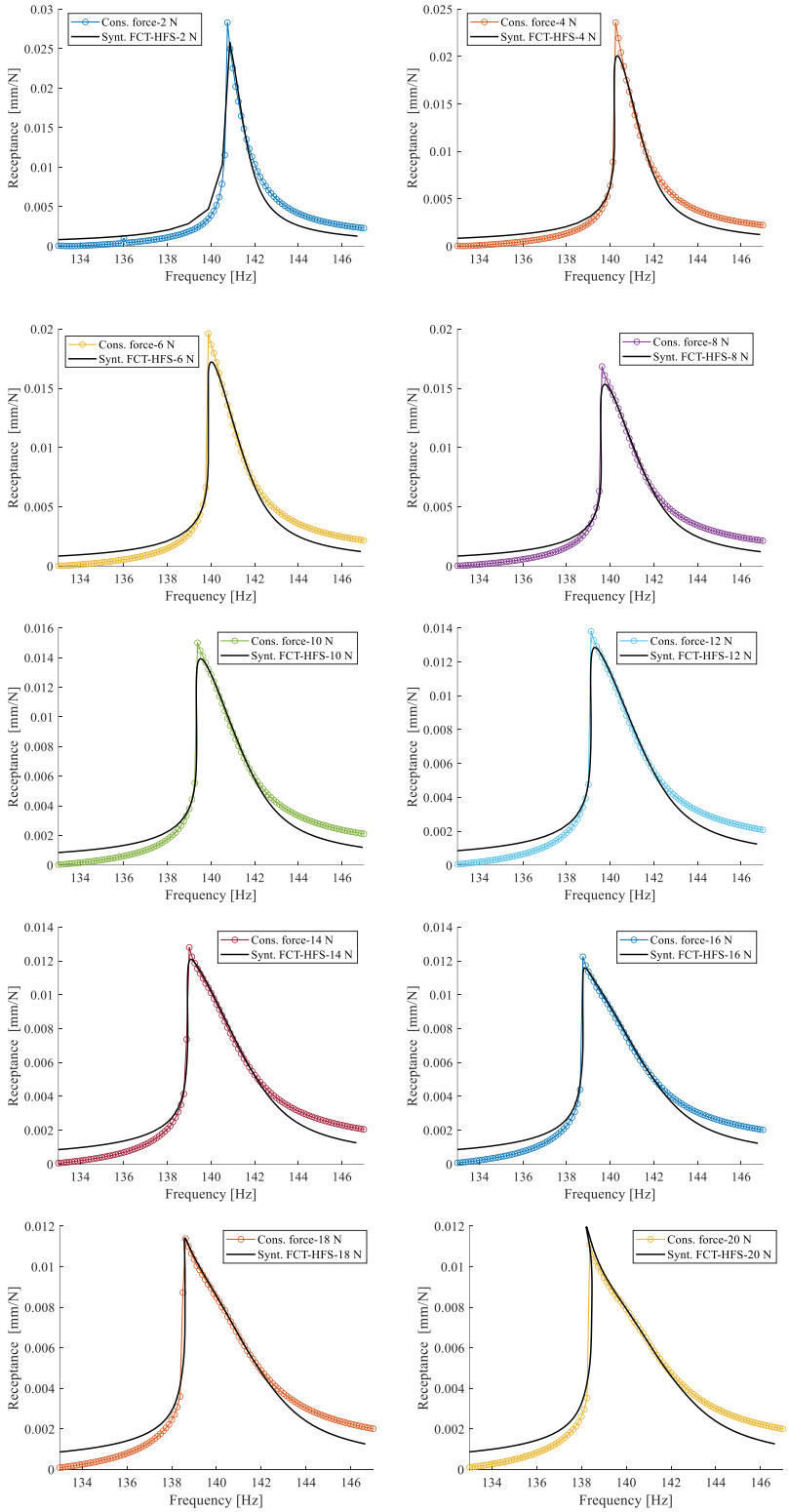

Figure 4-11. Comparison of Synthesized FRFs and Measured Ones of Data Set 1of Test 1 of BRB-Curve Fit Type 2

4.1.2.2 Data Set 2

Another data set with a jump phenomenon is conducted from 1 to 21 N with an increment of 2 N. Furthermore, the forced controlled test uses stepped sine testing with a 0.125 Hz frequency increment. A good match between the measured and synthesized ones is observed similar to the results obtained in Data Set 1. The extracted quasi-linear FRFs have also got a stepped shape at the left-hand side of the peak, and the same method as the preceding one is utilized where the quasi-linear FRFs are extracted from 0.026 mm to 0.220 mm from the HFS surface plot.

4.1.2.2.1 Curve Fit Type 1 (Peak-picking algorithm)

The same data set 1 curve fit type 1 is applied to the quasi-linear FRFs. Using the identified modal parameters (Figure 4-15), consistent FRFs are synthesized as shown in Figure 4-16.

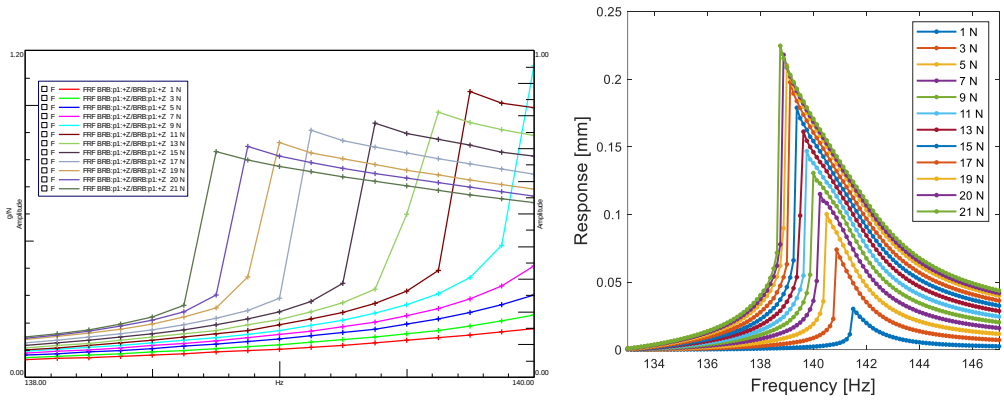

Figure 4-12. Constant Force Response Amplitude Curves of Data Set 2 of Test 1 of BRB a) from LMS (detailed view) b) from MATLAB

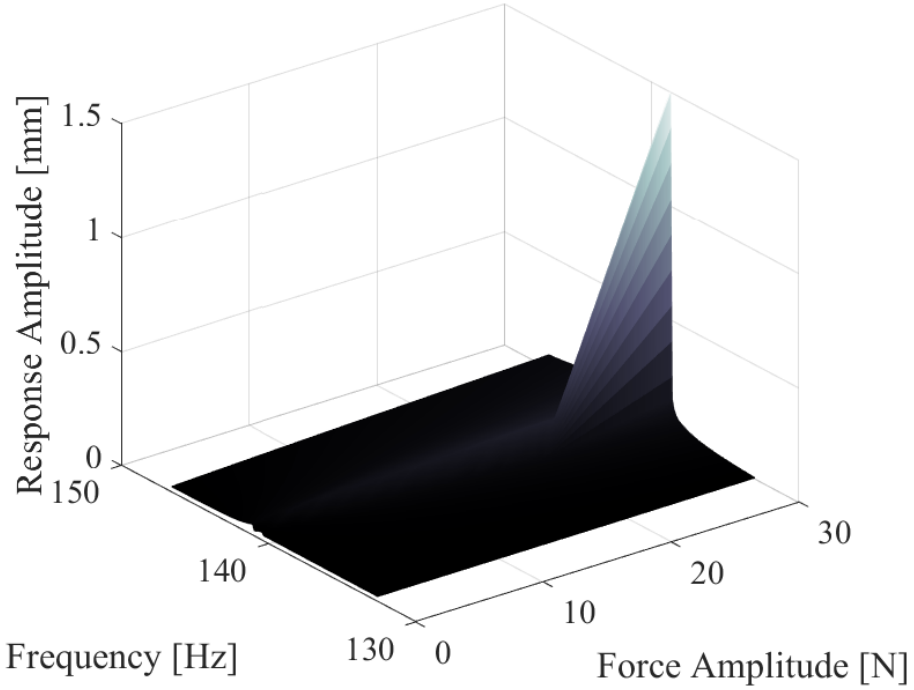

Figure 4-13. Harmonic Force Surface of Data Set 2 of Test 1 of BRB

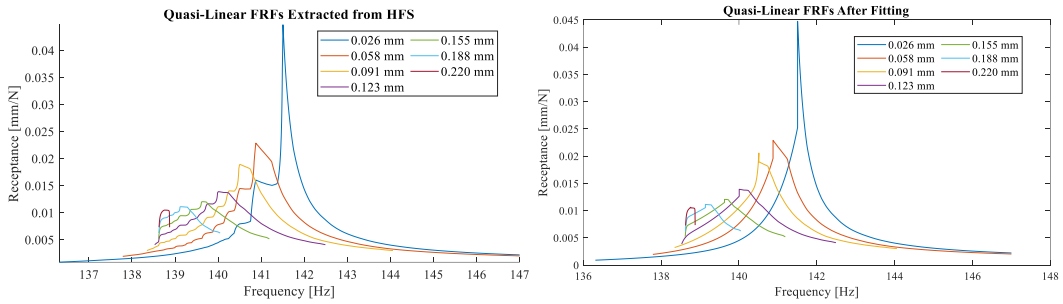

Figure 4-14. a) Quasi-Linear FRFs Extracted from HFS b) Applied Curve Fitting to Data Set 2 of Test 1 of BRB

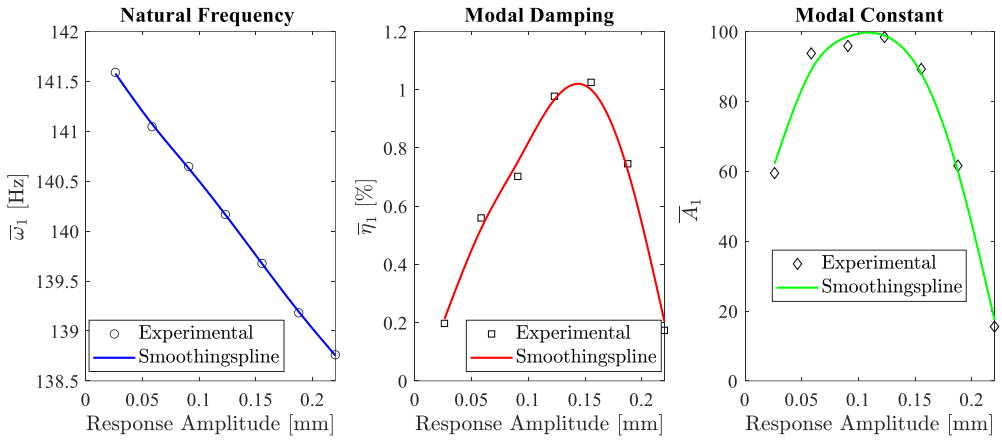

Figure 4-15. Identified Modal Parameters of Data Set 2 of Test 1 of BRB- Curve Fit Type 1

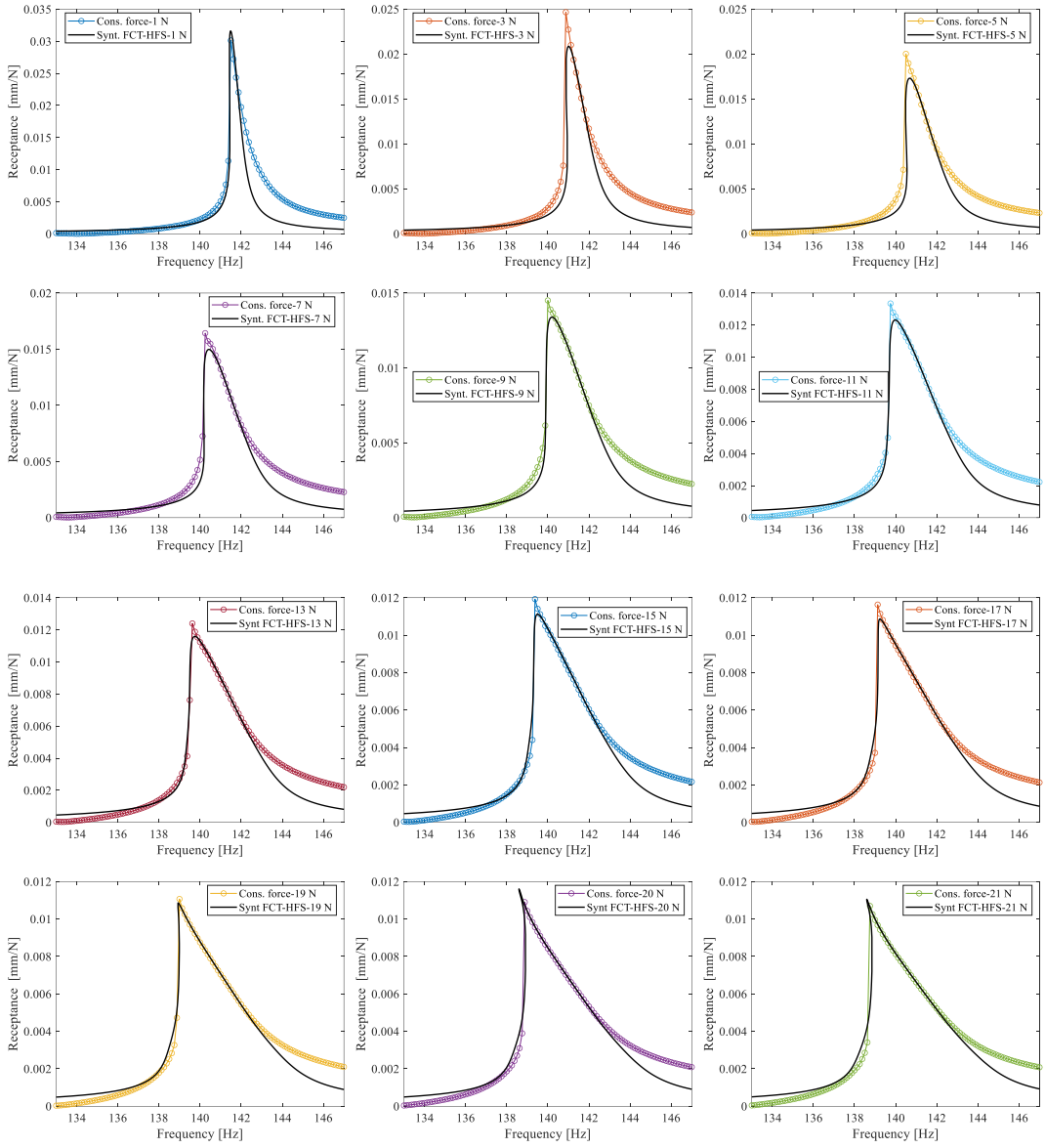

Figure 4-16. Comparison of Synthesized FRFs and Measured Ones of Data Set 2 of Test 1 of BRB- Curve Fit Type 1

4.1.2.2.2 Curve Fit Type 2

The *lsqcurvefit* function in MATLAB is used to identify the modal parameters. The quasi-linear FRFs data is inputted into the function, and the modal parameters are determined accordingly. Figure 4-17 shows the final corrected quasi-linear FRFs. The extracted points are then used to determine the modal parameters, and a *smoothingspline* fitting is applied, as seen in Figure 4-18. The synthesized force-controlled FRFs are presented in Figure 4-19, and this approach provides an accurate synthesis of force-controlled FRFs.

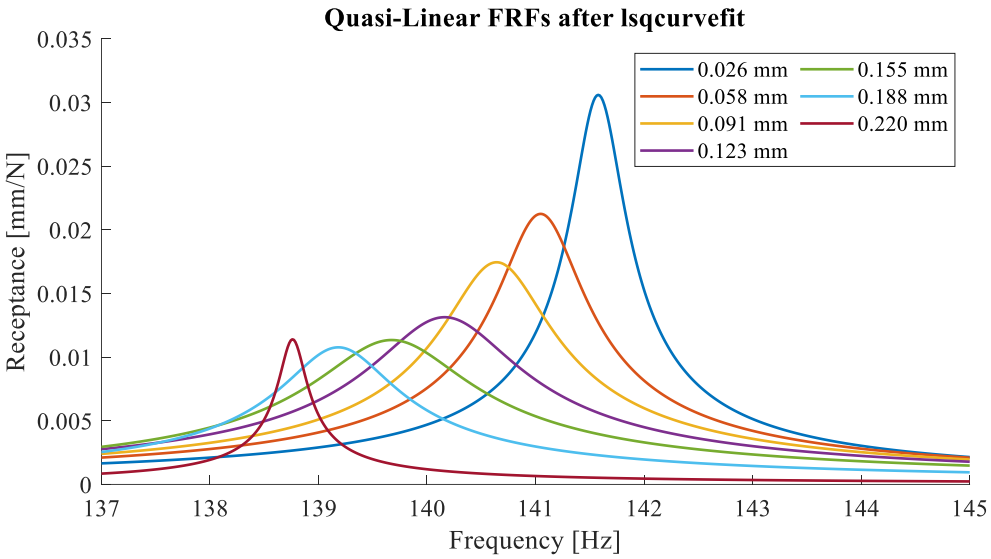

Figure 4-17. Quasi-Linear FRFs after *lsqcurvefit*-Curve Fit Type 2

It is essential to exercise caution when interpreting jump constant force testing results. Even if unstable branches associated with nonlinear frequency response functions can be tracked during measurements, one should remain vigilant. In cases like these, consider the RCT-HFS method.

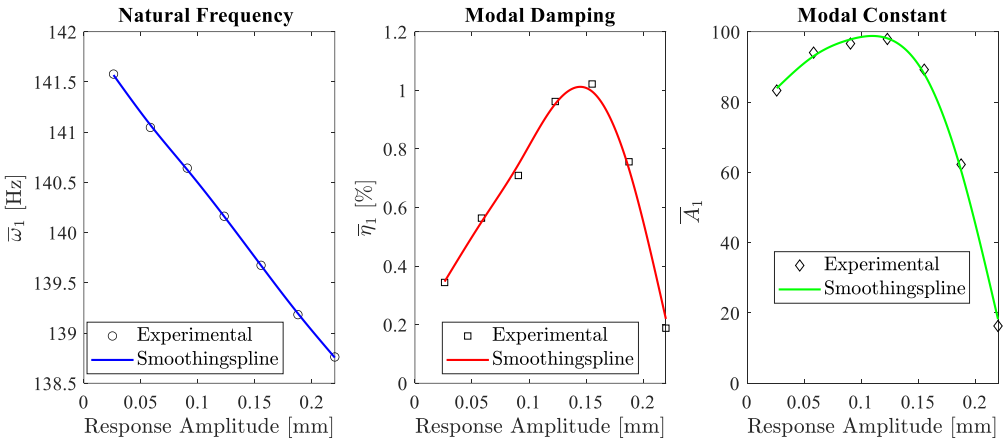

Figure 4-18. Identified Modal Parameters of Data Set 1 of Test 2 of BRB-Curve Fit Type 2

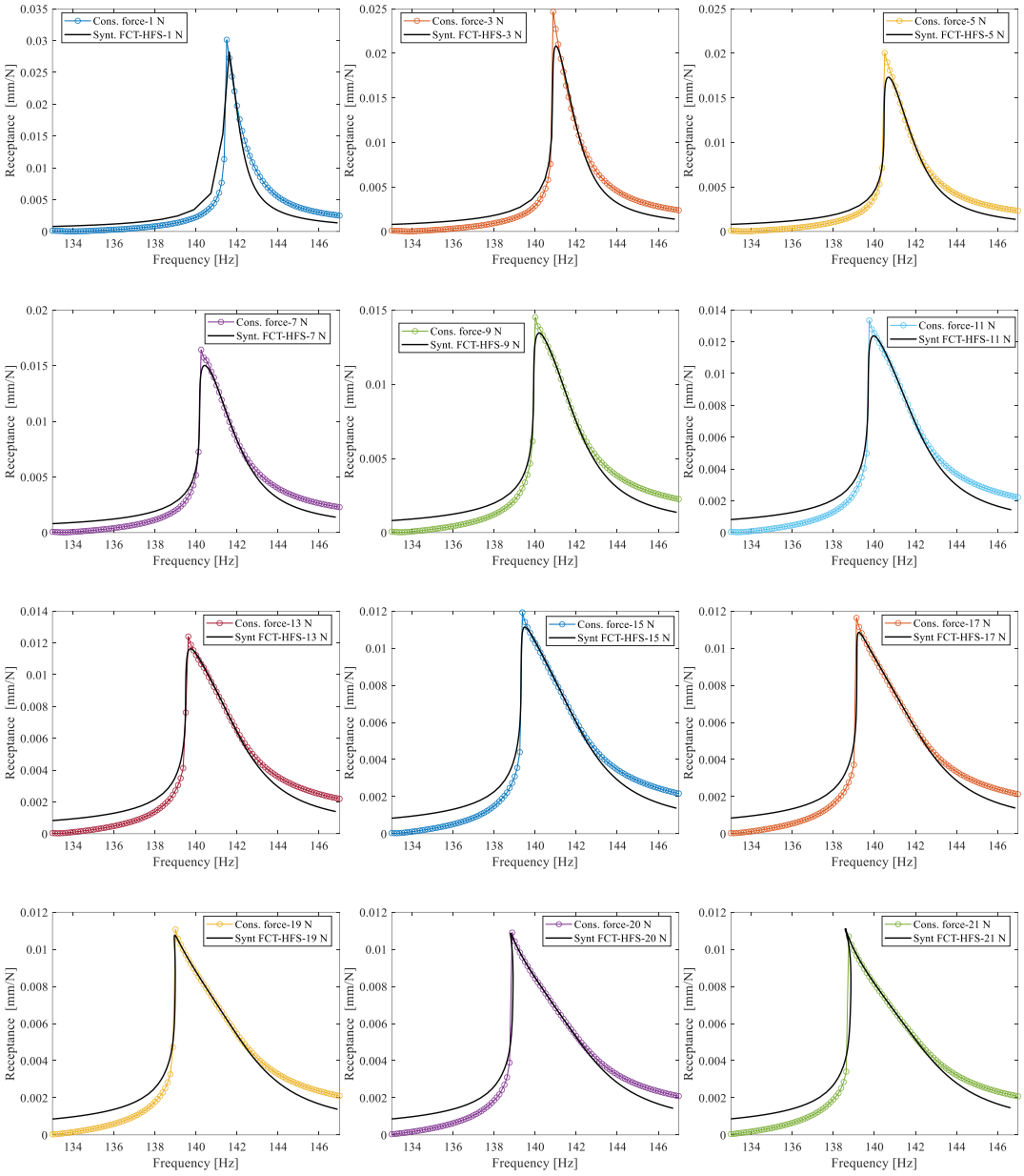

Figure 4-19. Comparison of Synthesized FRFs and Measured Ones of Data Set 2 of Test 1 of BRB- Curve Fit Type 2

4.1.3 Test 2: Test with Tightening Torque of 25 Nm

The effect of a jump in FRF on the accuracy of the RCT-based modeling is aimed to be investigated in this test. The same experimental setup is replicated, and the tightening torque is raised from 10 Nm to 25 Nm to eliminate the FRF jump behavior which complicates the modal data fitting procedure. Furthermore, the accuracy of synthesized RCT-based FCT-HFS models is tested in the absence of a jump. The subsequent trial involved a constant force examination, with amplitudes ranging from 1 N to 7 N and spaced 1 N apart. Step-sine tests are executed from 140 Hz to 150 Hz, sampling at 0.125 Hz.

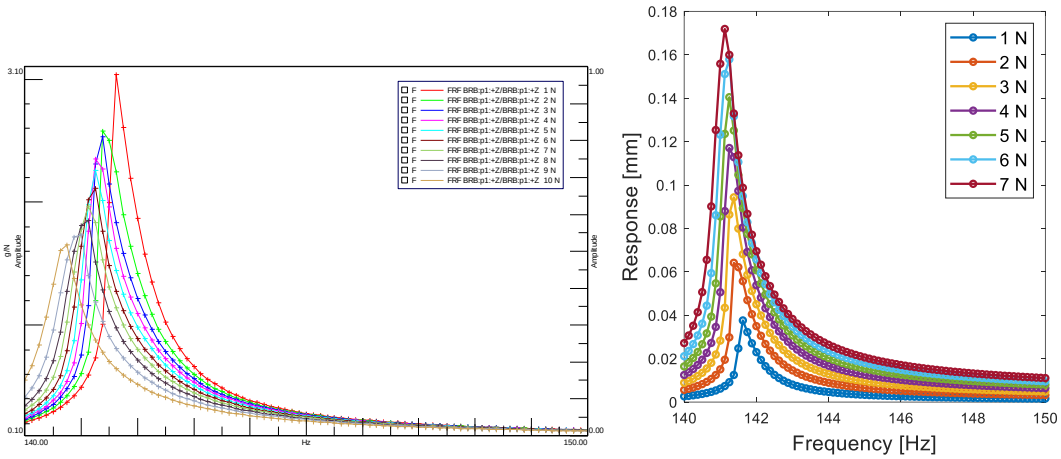

Figure 4-20. Constant Force Response Amplitude Curves of Test 2 of BRB a) from LMS b) from MATLAB

From Simcenter Testlab, experimental measurements of FRFs are tabulated in Figure 4-20.a in g/N, those are converted to the response amplitude in mm in Figure 4-20.b. Then, these response amplitude curves are used to synthesize the harmonic force surface in Figure 4-21a. The HFS is cut with constant displacement amplitude planes between 0.030 mm and 0.170 mm. Figure 4-21b shows that extracted quasi-linear FRFs are not in stepped shape, and those FRFs can be used to perform peak-picking analysis.

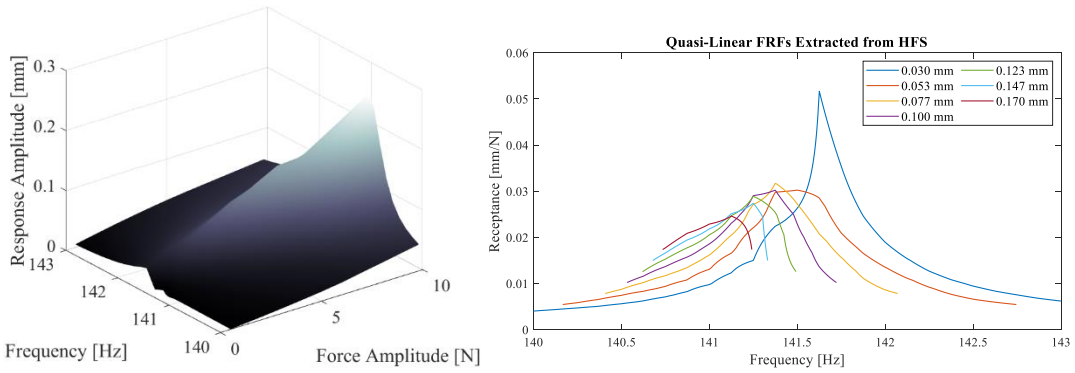

Figure 4-21. a) Harmonic Force Surface b) Quasi-Linear FRFs Extracted from HFS of Test 2 of BRB

Modal parameters at the specified displacement amplitude levels are determined Using the simple peak-picking algorithm in Figure 4-22. Then, smoothing spline curve fitting is applied to the modal parameters shown in the same figure.

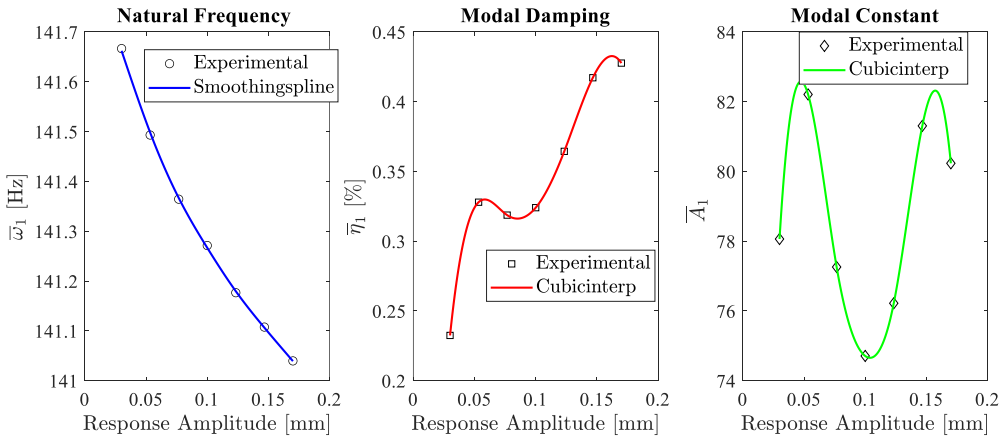

Figure 4-22. Identified Modal Parameters of Test 2 of BRB

Afterward, the constant force FRFs are synthesized using the arclength continuation algorithm to compare with the original ones. Figure 4-23 gives an insight into this comparison. One can observe that this comparison is better than the previous one with the jump FRFs since the force controlled FRFs do not have a jump. Therefore, extracted quasi-linear FRFs from the HFS give more accurate results of modal properties due to the shape of the quasi-linear FRFs.

Also, this experimental study clearly demonstrates the difficulty of testing and identifying the nonlinear behavior of bolted joints. Changing the tightening torque results in completely different modal fit parameters. This high sensitivity of identified modal parameters to tightening torque makes the measurement and identification process of such bolted systems challenging.

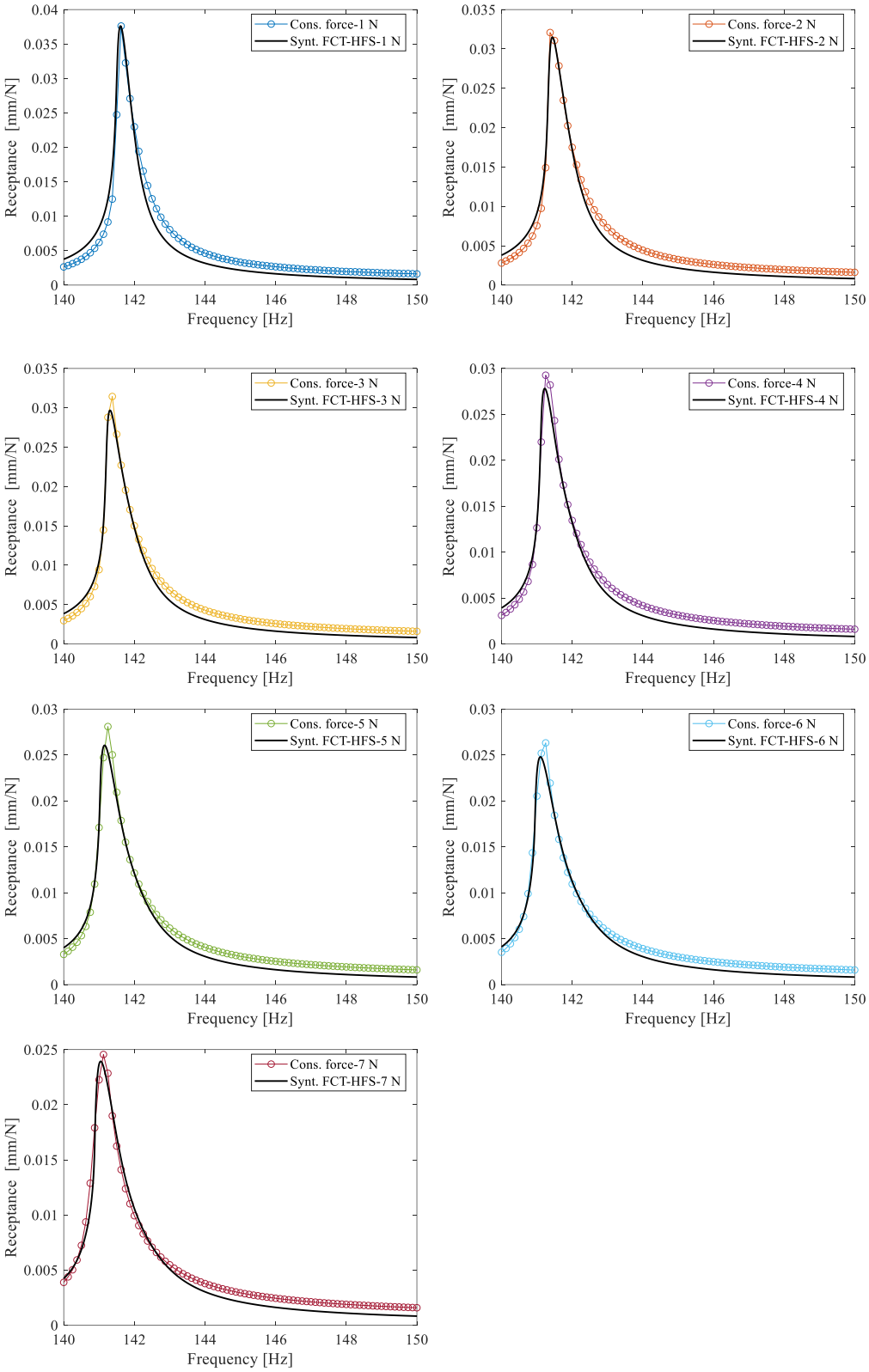

Figure 4-23. Comparison of Synthesized and Measured FRFs of Test 2 of BRB

4.2 The Orion Beam

Recently, a new beam called the Orion Beam has been proposed [63]. Two thin beams are connected with three bolted joints. The experimental setup is shown in Figure 4-24. The effect of the design of the beam on the repeatability issue during the experiments is analyzed by changing the tightening torques and excitation force [67]. Repeatability can be summarized as measurement-to-measurement differences in the same experimental setup [62]. The experiments used two data sets: constant force-testing and random tests. A feedback controller is developed to implement the constant force testing around the beam's third and sixth bending modes to employ the FCT-HFS method. For measurement purposes, a laser vibrometer is used. Further details about the structure and the experiments can be found in [63]. Here, the third and sixth bending mode force-controlled step sine testing results are employed for validation and verification.

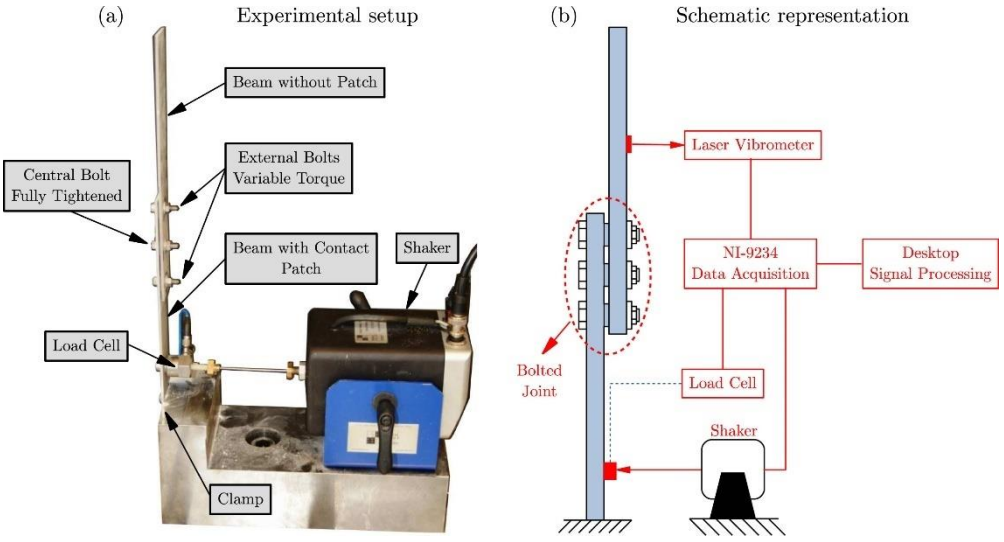

Figure 4-24. Orion Beam a) Experimental Setup b) Schematic Representation

4.2.1 Third Bending Mode

This subsection uses data from the third bending mode of the Orion beam. The related tests are employed between the 280 and 300 Hz frequencies with a frequency

increment of 0.3906 Hz. Furthermore, the tests are performed at the different tightening torque levels of 20 and 80 cNm. In addition, five different forcing levels are handled at these two tightening torques, where the forcing levels are the same at each torque level. The forcing levels are 10, 50, 100, 150 and 200 mN.

4.2.1.1 20 cNm Tightening Torque

Measured constant force frequency-response amplitude graphs are given in Figure 4-25a. Adding force as a third axis and creating the harmonic force surface of the related experiment is shown in Figure 4-25b.

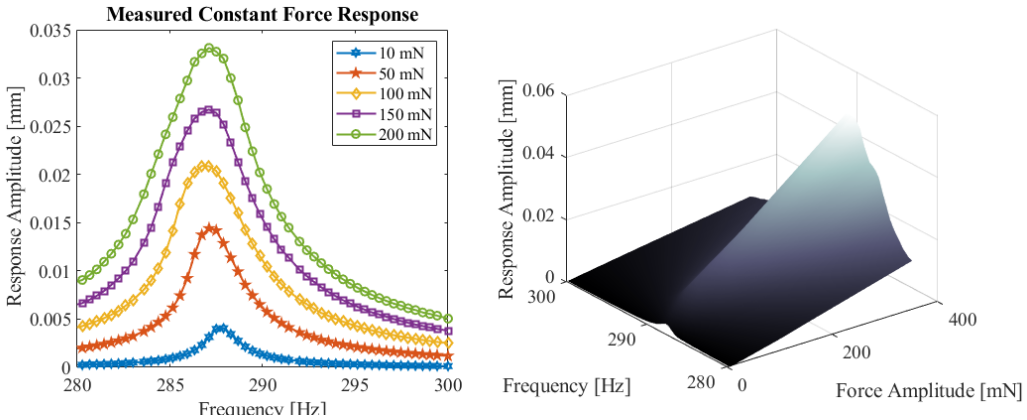

Figure 4-25. a) Measured Constant Force Frequency-Response Amplitude Curves b) Harmonic Force Surface- The Orion Beam Third Bending Mode 20 cNm Torque

Afterward, relevant quasi-linear frequency response functions are obtained using HFS, cut with constant displacement amplitude planes ranging from 0.003 to 0.037 mm, as shown in Figure 4-26. These eighteen quasi-linear FRFs are then used to identify displacement-dependent nonlinear modal parameters, as illustrated in Figure 4-27. A second-order polynomial fit is used for modal natural frequency and modal constant. Additionally, modal damping is smoothed using a smoothing spline. The change in modal damping is significant with the changing displacement amplitude.

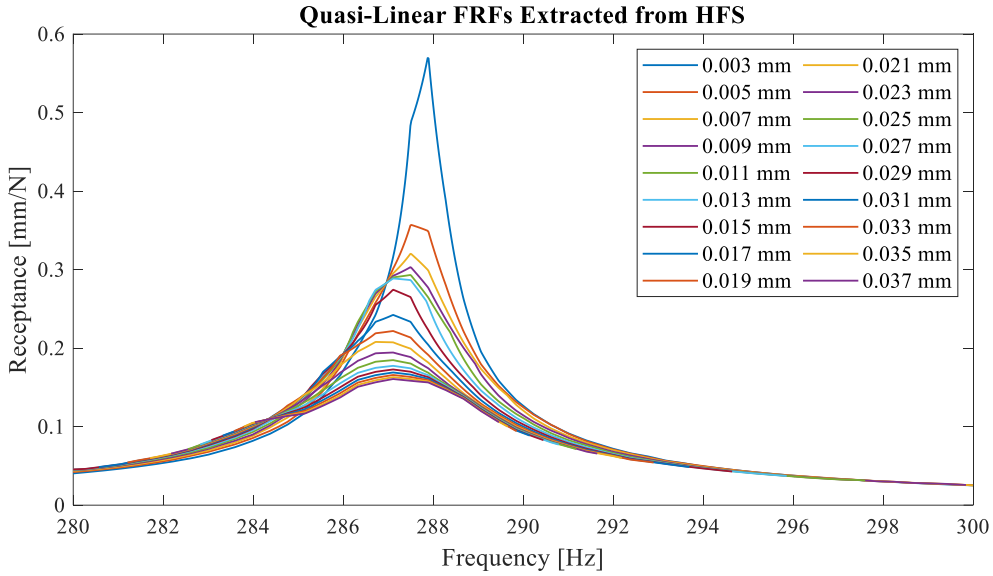

Figure 4-26. Quasi-Linear FRFs Extracted from HFS- The Orion Beam Third Bending Mode 20 cNm Torque

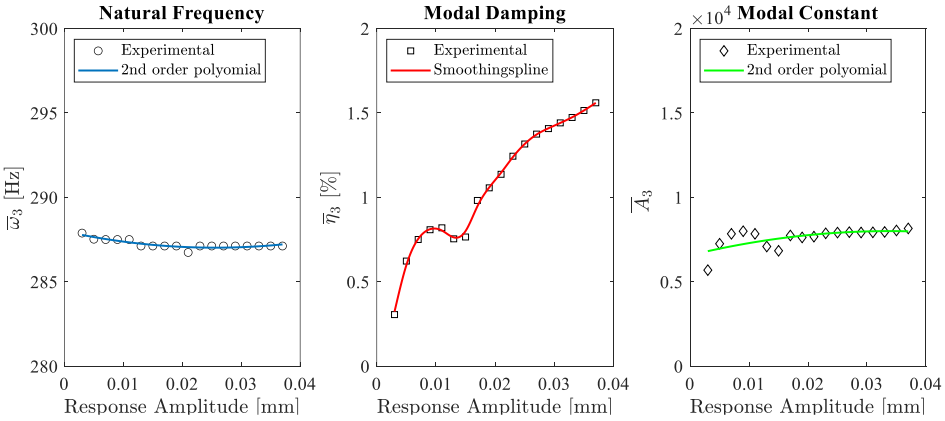

Figure 4-27. Identified Modal Parameters- The Orion Beam Third Bending Mode 20 cNm Torque

Subsequently, constant force frequency-response amplitude plots are synthesized using these displacement-dependent modal parameters and compared to the measured ones in Figure 4-28. Markers are the measured data points, and the solid lines are the synthesized ones. The consistency between the measured and the synthesized constant force amplitude responses is almost perfect.

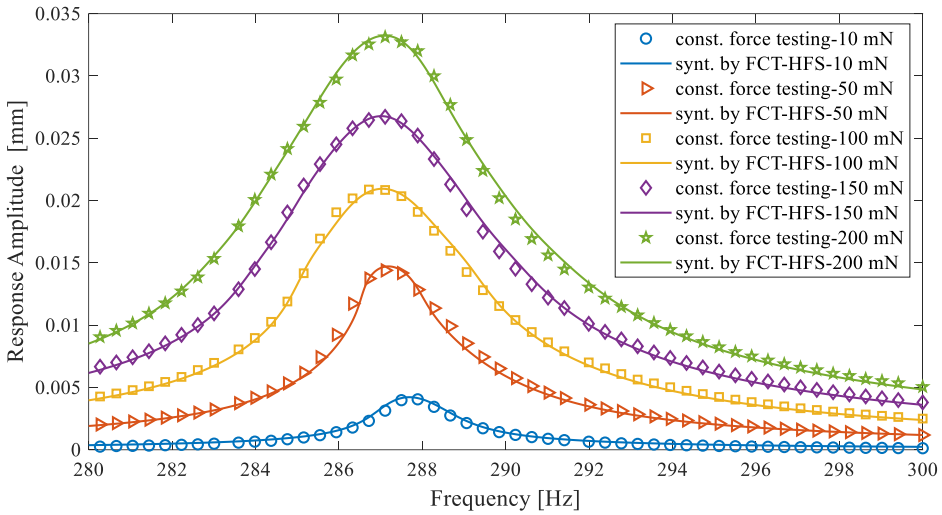

Figure 4-28. Comparison of Measured and Synthesized Frequency-Response Amplitude Curves- The Orion Beam Third Bending Mode 20 cNm Torque

4.2.1.2 80 cNm Tightening Torque

Measured constant force frequency-response displacement amplitude plots are given in Figure 4-29a. Merging these constant force frequency-response amplitude plots generates the harmonic force surface, as shown in Figure 4-29b.

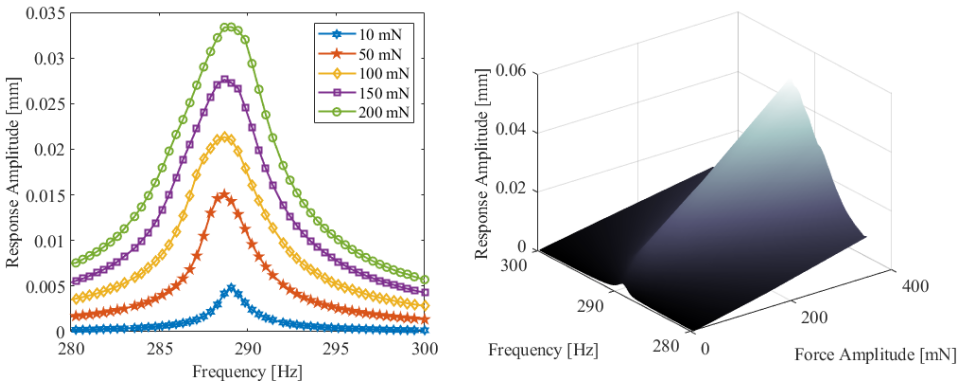

Figure 4-29. a) Measured Constant Force Frequency-Response Amplitude Curves b) Harmonic Force Surface- The Orion Beam Third Bending Mode 80 cNm Torque

Afterward, quasi-linear frequency response functions are obtained using HFS, cut with constant displacement amplitude planes ranging from 0.004 to 0.037 mm,

Figure 4-30. Displacement-dependent nonlinear modal parameters are determined using these eighteen quasi-linear FRFs, Figure 4-31. A second-order polynomial fit is exploited to modal natural frequency and modal constant. Furthermore, a smoothing spline is used for the modal damping. In addition, the frequency shift due to the tightening torque is observed comparing Figure 4-27 and Figure 4-31, which is an expected outcome of increasing the tightening torque [68].

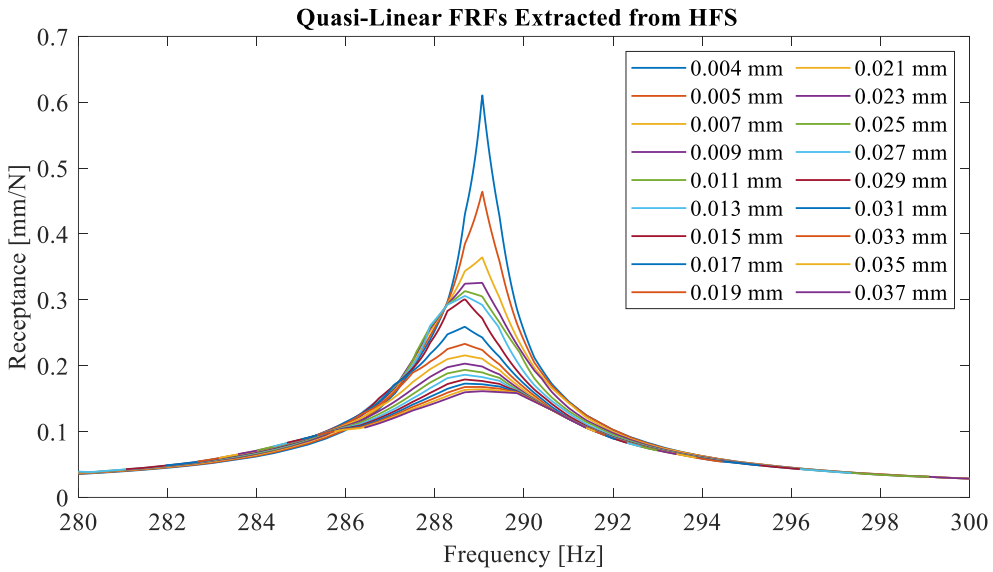

Figure 4-30. Quasi-Linear FRFs Extracted from HFS- The Orion Beam Third Bending Mode 80 cNm Torque

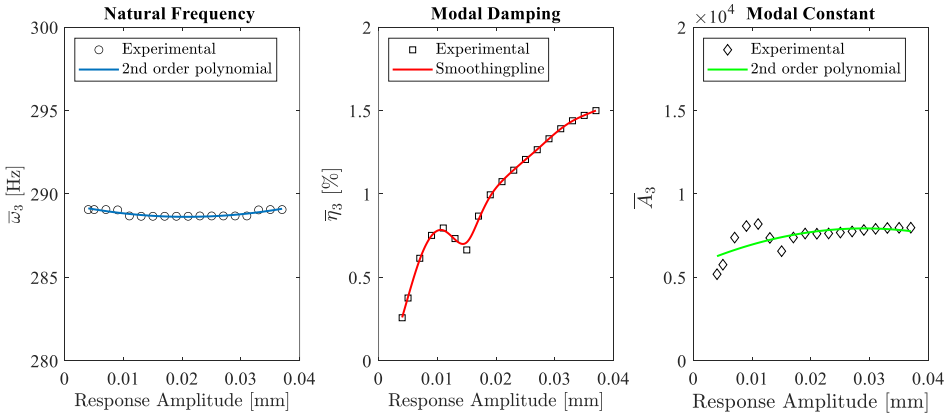

Figure 4-31. Identified Modal Parameters- The Orion Beam Third Bending Mode 80 cNm Torque

Consequently, the constant force frequency-response amplitude plots are re-constructed using these displacement-dependent modal parameters and compared to the measured ones in Figure 4-32. Data points and the solid lines measure marked ones are the re-constructed ones. The agreement between the measured and the synthesized ones is perfect indeed.

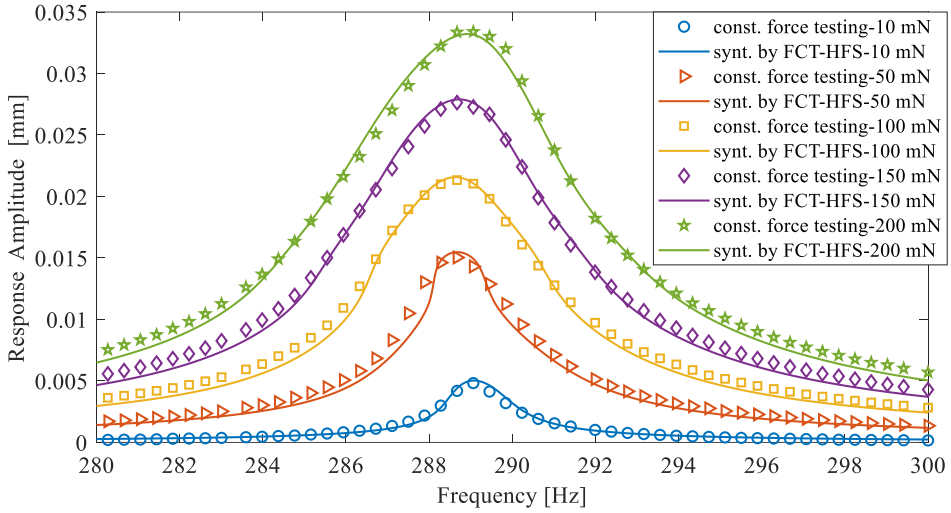

Figure 4-32. Comparison of Measured and Synthesized Frequency-Response Amplitude Plots- The Orion Beam Third Bending Mode 80 cNm Torque

4.2.2 Sixth Bending Mode

This subsection uses data from the sixth bending mode of the Orion beam. The tests are employed at several tightening torques: 10, 20, 30, 80, and 1000 cNm. In addition, six different forcing levels are handled at these five tightening torques, where the forcing levels are the same at each torque level. The forcing levels are 10, 50, 100, 150, 200 and 250 mN. Frequency sweep covers the range from 1700 to 1775 Hz with an increment of 1 Hz. The procedure for constructing the FCT-HFS method is followed at each torque level, and the results are compared accordingly.

4.2.2.1 10 cNm Tightening Torque

It is worth noting that starting from the forcing level of 100 mN, the left-hand side of the resonance is hardly visible due to the excitation frequency used during testing not covering all the resonance regions. After merging the measured frequency-response amplitude curves, the quasi-linear FRFs are obtained indirectly. The quasi-linear FRFs are presented in Figure 4-34. Fourteen constant displacement amplitude planes are generated from 0.0002 to 0.0012 mm for modal identification of the constant displacement amplitude receptances.

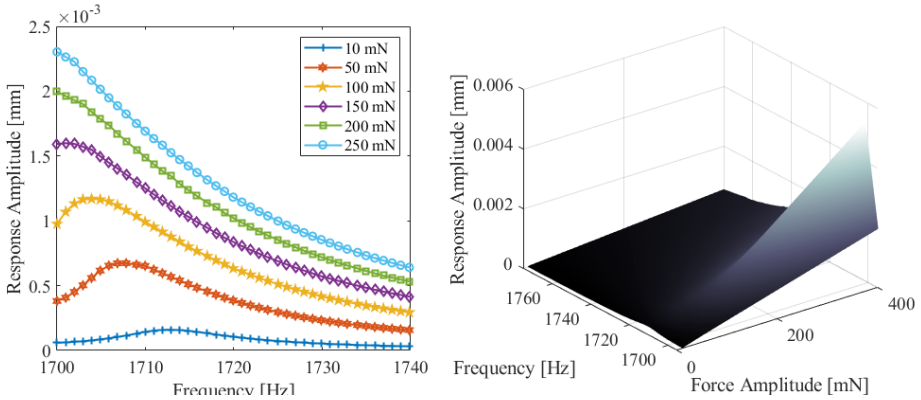

Figure 4-33. a) Measured Constant Force Frequency-Response Amplitude Curves b) Harmonic Force Surface- The Orion Beam Sixth Bending Mode 10 cNm Torque

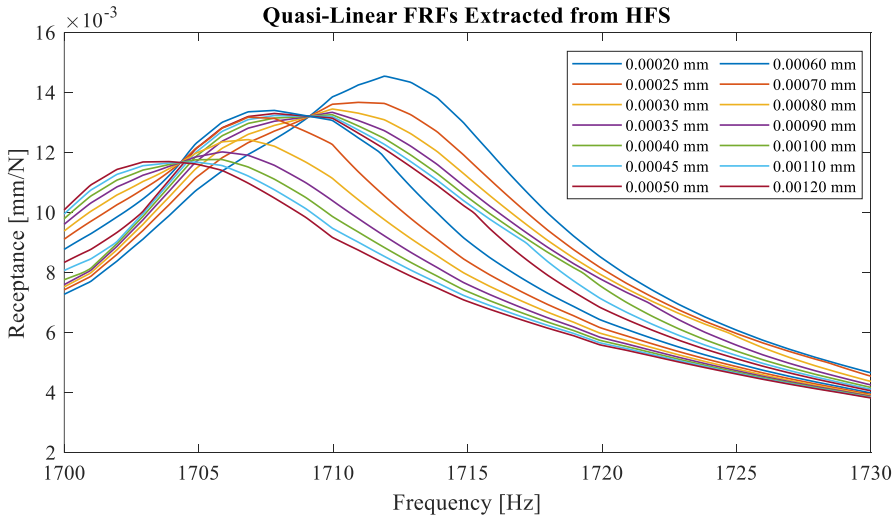

Figure 4-34. Quasi-Linear FRFs Extracted from HFS -The Orion Beam Sixth Bending Mode 10 cNm Torque

Displacement-dependent modal parameters are determined using the peak-picking method. Figure 4-35 shows that the modal natural frequencies at the lower displacement amplitude level decrease by increasing the displacement amplitude level. The other conclusion is that displacement-dependent modal damping oscillates between 0.75 % and 0.85 %.

MATLAB's *smoothingspline* property of a fit function is used for all displacement-dependent modal parameters (modal natural frequency, modal damping, and modal constant) as shown in Figure 4-35.

Thereafter, the constant force frequency-response amplitude curves are reproduced using those modal parameters the curve fits Figure 4-36. Again, a good agreement between the measured and re-produced ones is seized.

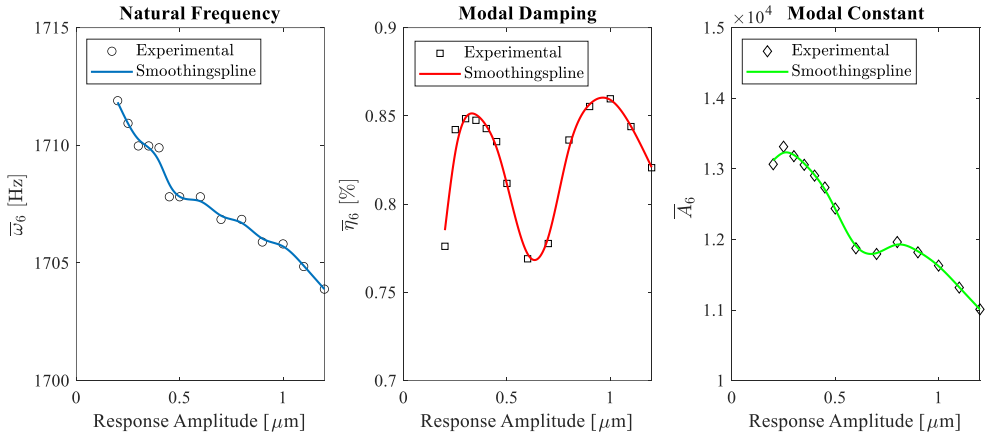

Figure 4-35. Identified Modal Parameters - The Orion Beam Sixth Bending Mode 10 cNm Torque

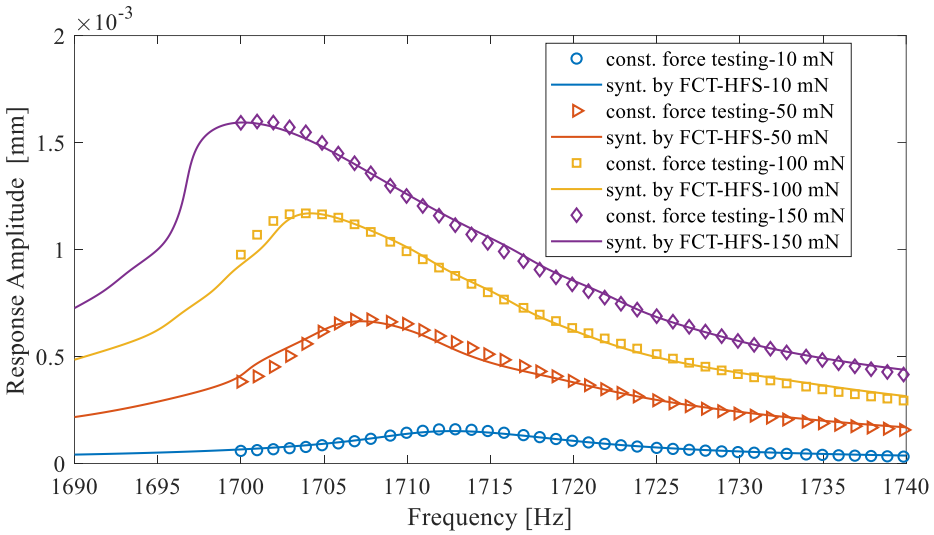

Figure 4-36. Comparison of Measured and Synthesized Frequency-Response Amplitude Curves-The Orion Beam Sixth Bending Mode 10 cNm Torque

4.2.2.2 20 cNm Tightening Torque

Different from the 10 cNm tightening torque level, thirty-four quasi-linear FRFs are extracted from the HFS between the lower and upper bounds of the displacement amplitudes 0.2 and 3.5 μm, respectively.

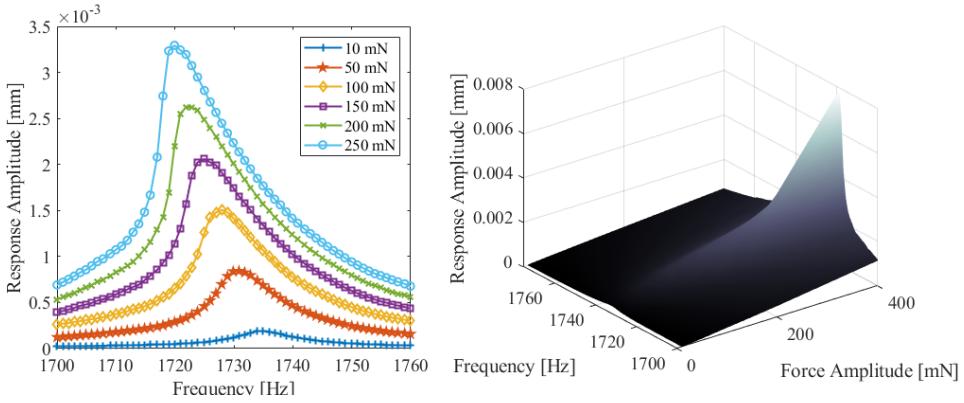

Figure 4-37. a) Measured Constant Force Frequency-Response Amplitude Curves b) Harmonic Force Surface- The Orion Beam Sixth Bending Mode 20 cNm Torque

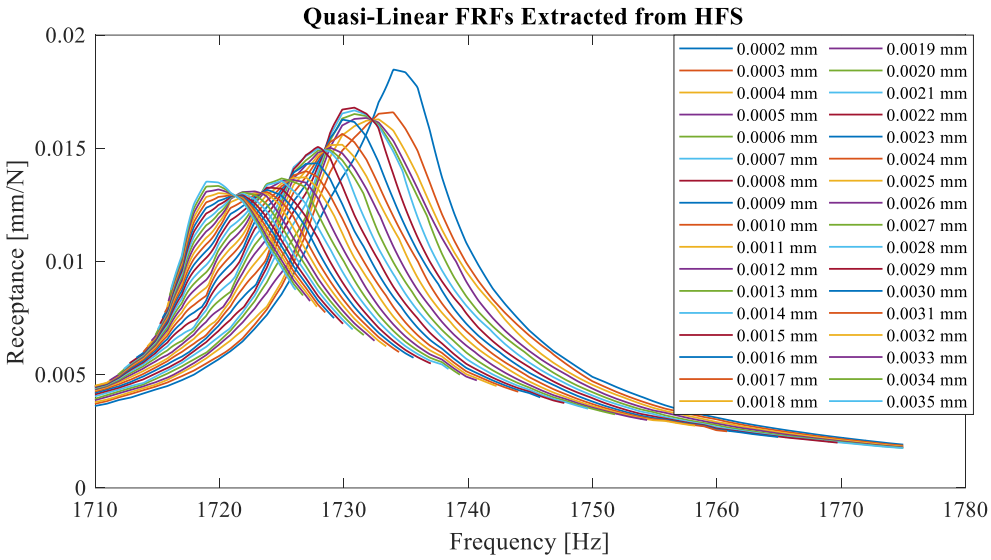

Figure 4-38. Quasi-Linear FRFs Extracted from HFS -The Orion Beam Sixth Bending Mode 20 cNm Torque

Extracted modal parameters are tabulated with markers in Figure 4-39. The trend of the modal natural frequency is like a first-order polynomial, so a first-order polynomial fit is used. The modal natural frequency is about 1735 Hz at the lowest displacement amplitude level. On the other hand, it decreases monotonically to about 1717 Hz. In addition, smoothing spline is utilized for modal damping and modal constant so as not to lose the information gathered from the experiment.

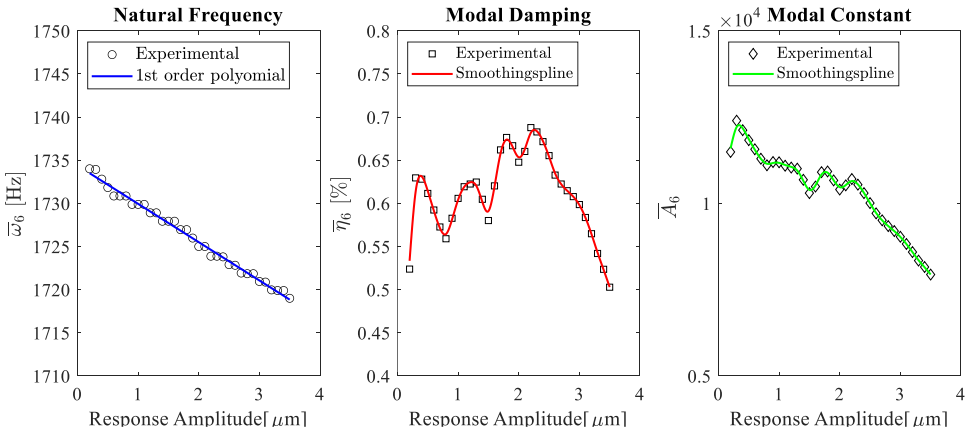

Figure 4-39. Identified Modal Parameters - The Orion Beam Sixth Bending Mode 20 cNm Torque

Constant force frequency-response amplitude plots are reconstructed and compared to the original ones in Figure 4-40 using the fits tabulated in Figure 4-39. Again, an almost perfect match between the measured and the synthesized frequency-displacement curves is obtained.

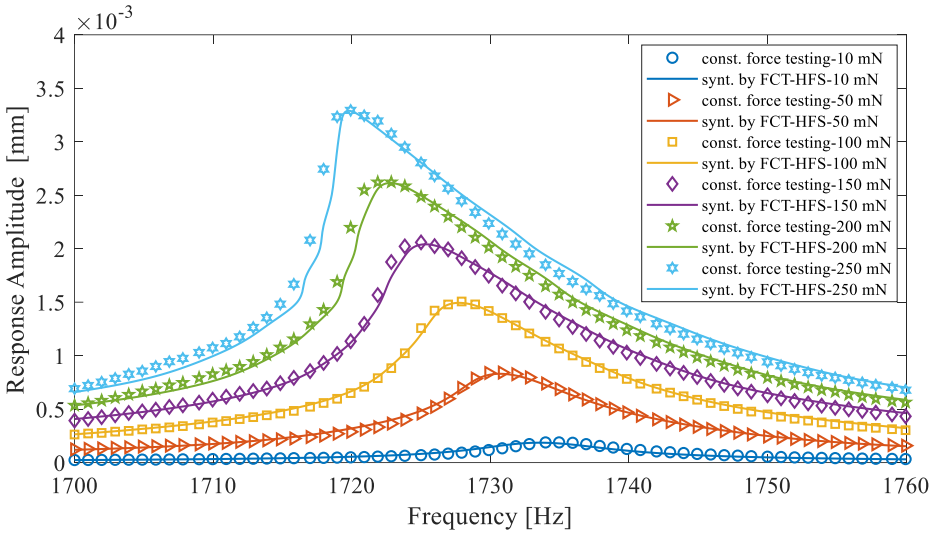

Figure 4-40. Comparison of Measured and Synthesized Frequency-Response Amplitude Curves -The Orion Beam Sixth Bending Mode 20 cNm Torque

4.2.2.3 30 cNm Tightening Torque

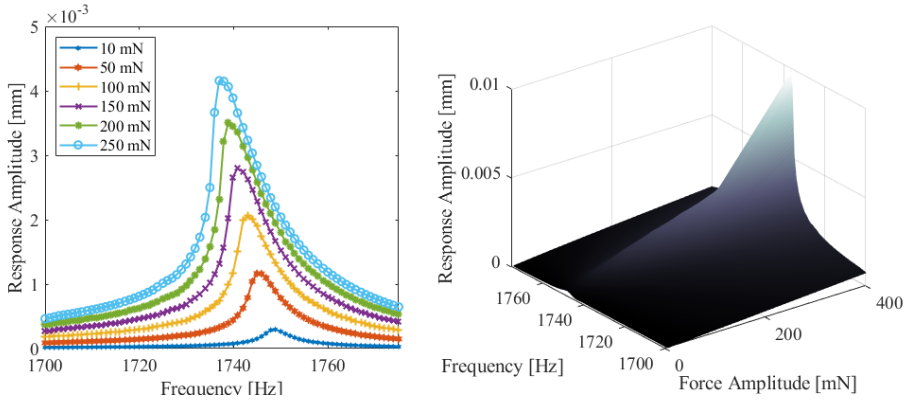

Figure 4-41. a) Measured Constant Force Frequency-Response Amplitude Curves b) Harmonic Force Surface- The Orion Beam Sixth Bending Mode 30 cNm Torque

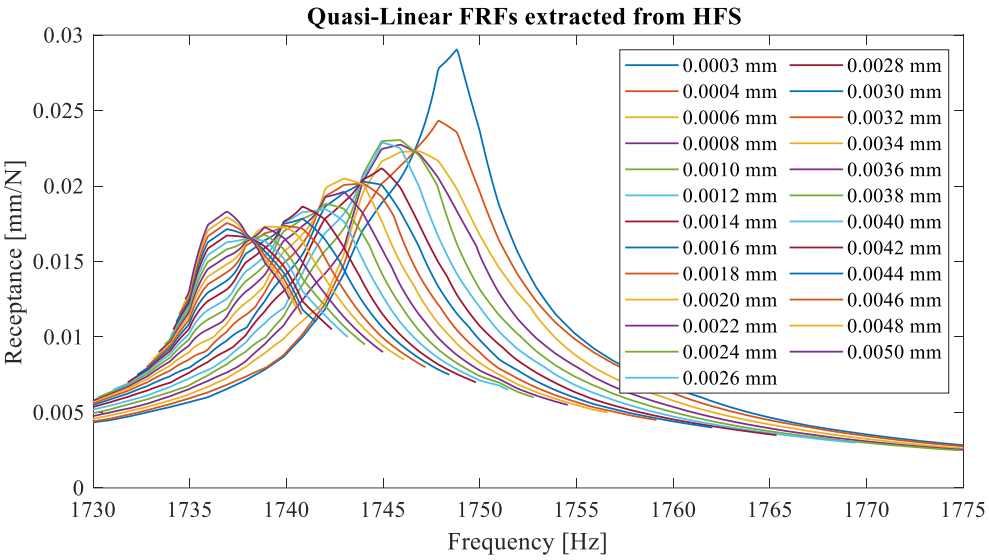

Figure 4-42.Quasi-Linear FRFs Extracted from HFS -The Orion Beam Sixth Bending Mode 30 cNm Torque

After constructing the harmonic force surface associated with the 30 cNm tightening torque, twenty-five constant displacement amplitude planes are used to extract the quasi-linear FRFs of the system, similar to the previous section first order polynomial fit is exploited to the modal natural frequency, and a smoothing spline is employed to the remaining two modal parameters.

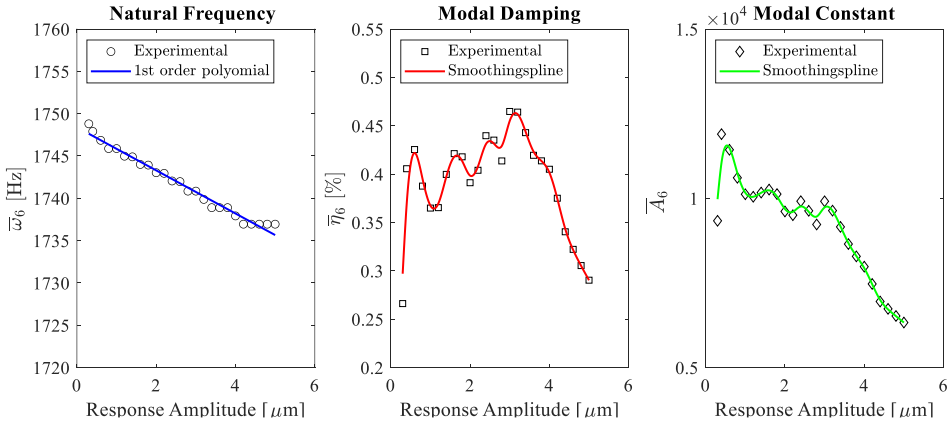

Figure 4-43. Identified Modal Parameters – The Orion Beam Sixth Bending Mode 30 cNm Torque

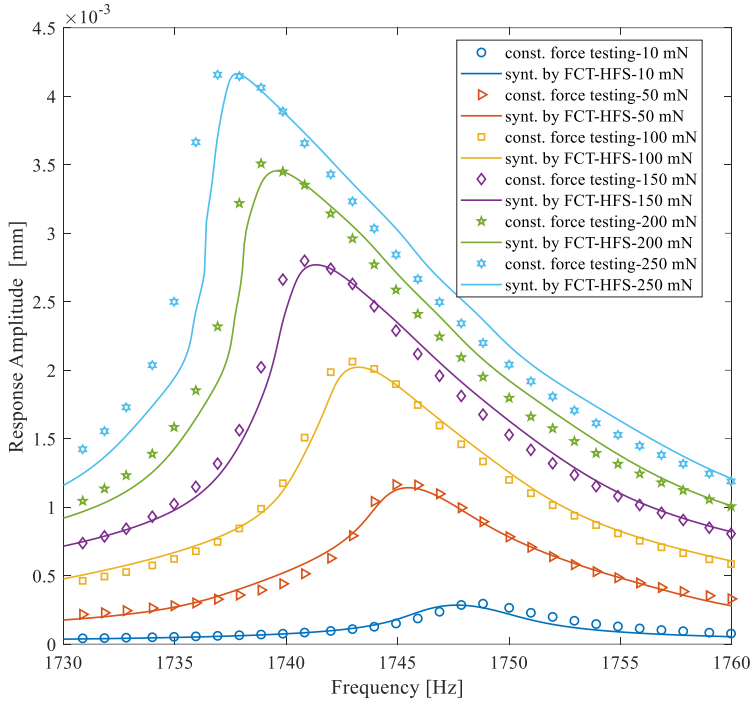

Figure 4-44. Comparison of Measured and Synthesized Frequency-Response Amplitude Curves -The Orion Beam Sixth Bending Mode 30 cNm Torque

As expected, the modal natural frequency increases when the tightening torque of the bolted joints is increased. However, a decrease in the modal natural frequency is observed when the modal displacement amplitude is increased, indicating a softening behavior of the system.

4.2.2.4 80 cNm Tightening Torque

The FCT-HFS method has been applied to another data set at the tightening torque level of 80 cNm. Twenty-nine displacement amplitude planes have been used to determine the experimental quasi-linear FRFs associated with amplitude levels ranging from 0.0003 mm to 0.0058 mm. These FRFs are depicted in Figure 4-46.

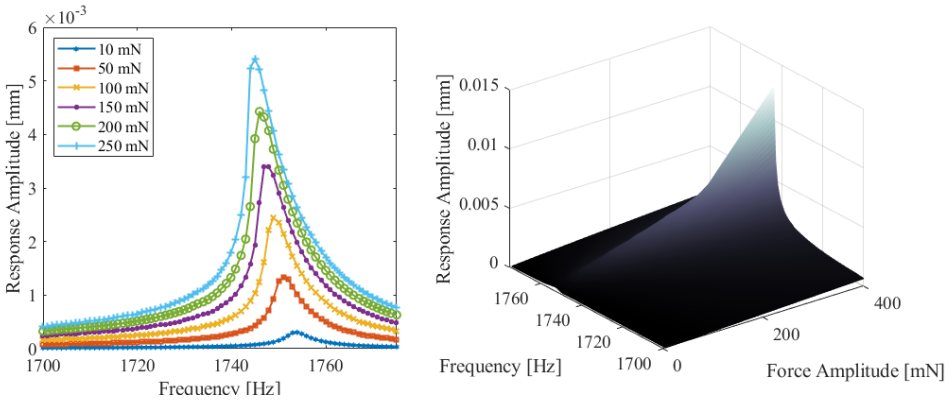

Figure 4-45. a) Measured Constant Force Frequency-Response Amplitude Curves b) Harmonic Force Surface- The Orion Beam Sixth Bending Mode 80 cNm Torque

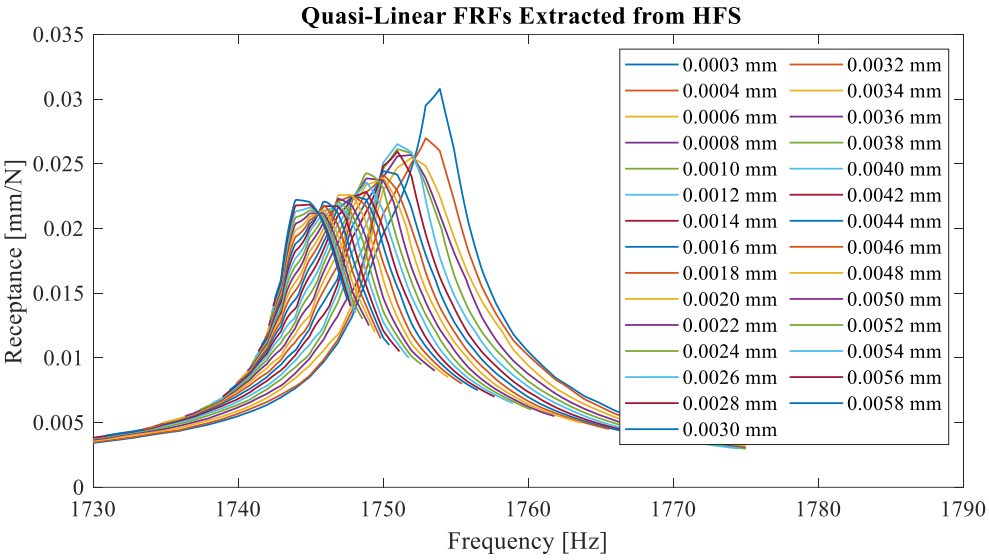

Figure 4-46. Quasi-Linear FRFs Extracted from HFS -The Orion Beam Sixth Bending Mode 80 cNm Torque

Smoothingspline fits are used for modal damping and modal constant parameters, while a first-order polynomial fit is utilized for the modal natural frequency. The constant force frequency-response amplitude curves are synthesized using those fits. A successful match between the experimentally measured constant forcing amplitude responses and the synthesized constant force responses is achieved. The softening behavior of the system is also seen from the frequency-displacement amplitude figure.

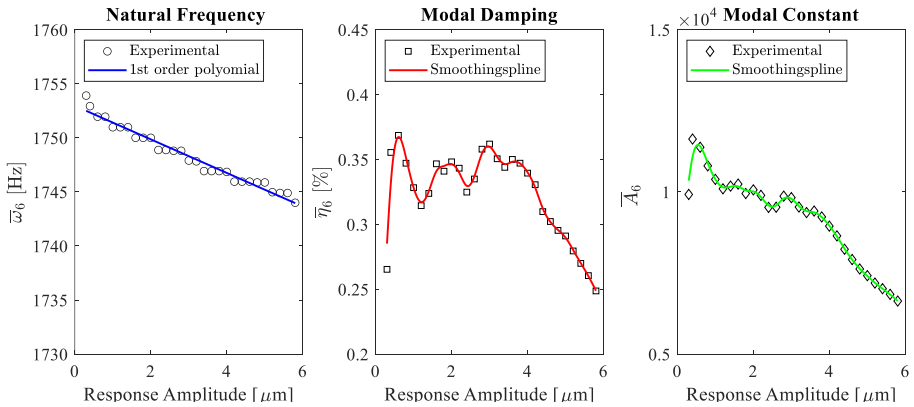

Figure 4-47. Identified Modal Parameters - The Orion Beam Sixth Bending Mode 80 cNm Torque

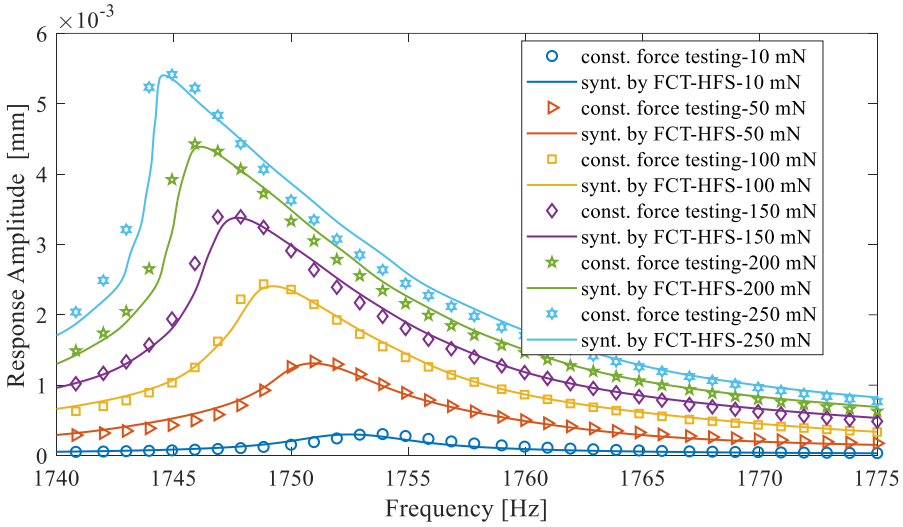

Figure 4-48. Comparison of Measured and Synthesized Frequency-Response Amplitude Curves -The Orion Beam Sixth Bending Mode 80 cNm Torque

4.2.2.5 1000 cNm Tightening Torque (Glued)

The final data set of the Orion beam to utilize the FCT-HFS method is at 1000 cNm tightening torque level. Indeed, it is the glued condition of the joints. Twenty-eight planes are cut from the resultant HFS, and displacement-dependent modal parameters are determined using the peak-picking method.

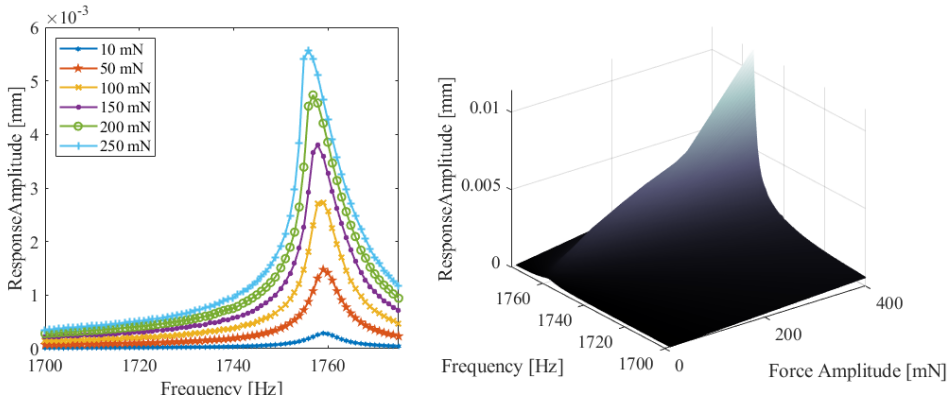

Figure 4-49. a) Measured Constant Force Frequency-Response Amplitude Curves b) Harmonic Force Surface- The Orion Beam Sixth Bending Mode 1000 cNm Torque

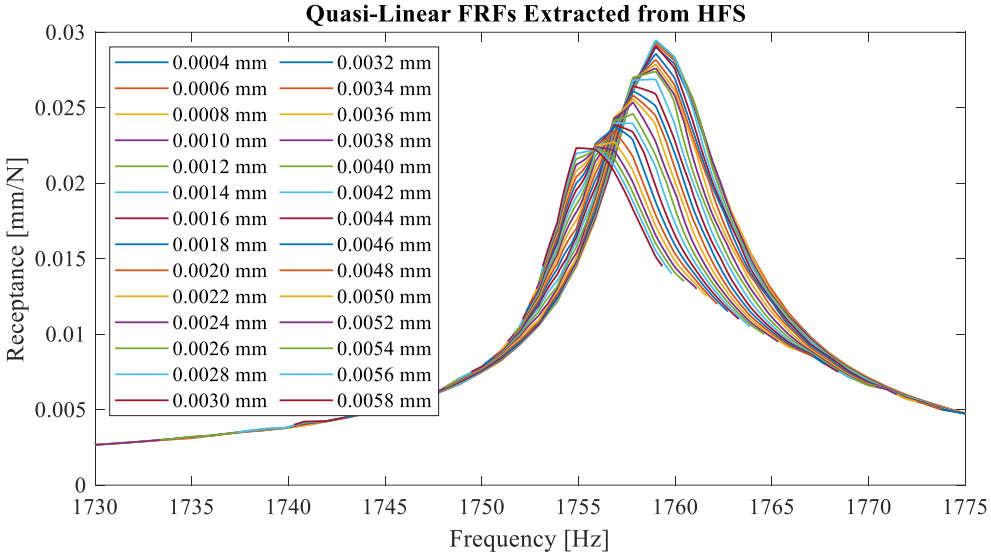

Figure 4-50. Quasi-Linear FRFs Extracted from HFS -The Orion Beam Sixth Bending Mode 1000 cNm Torque

First-order polynomial fit to the modal natural frequency and *smoothingspline* to the remaining two are utilized, Figure 4-51. The modal coefficient fits are used to obtain the synthesized constant forcing amplitude responses and the comparison between the actual constant forcing amplitude experimental data and the synthesized data using FCT-HFS is shown in Figure 4-52.

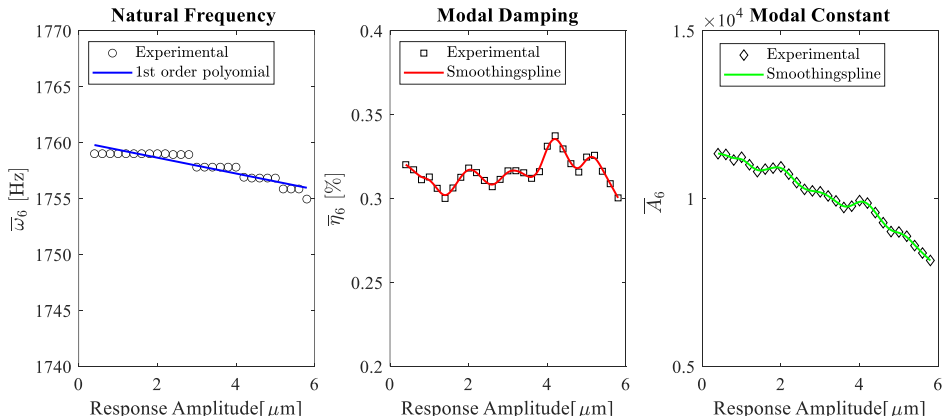

Figure 4-51. Identified Modal Parameters - The Orion Beam Sixth Bending Mode 1000 cNm Torque

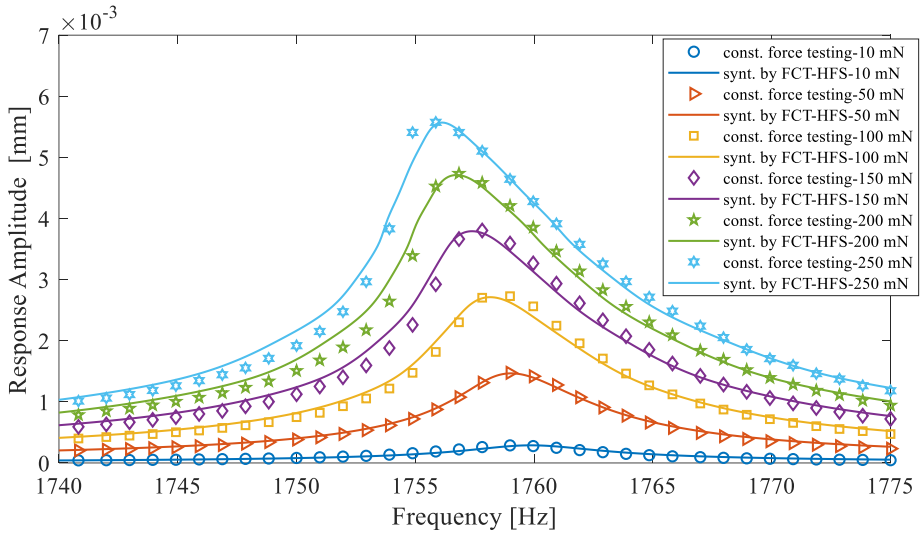

Figure 4-52. Comparison of Measured and Synthesized Frequency-Response Amplitude Curves-The Orion Beam Sixth Bending Mode 1000 cNm Torque

The FCT-HFS method works perfectly well when considering the Orion beam experimental data, even using the simple peak-picking algorithm to obtain modal parameters from the quasi-linear FRFs.

One other observation that someone can make from the Orion beam data is that by increasing the tightening torque level from 10 cNm to 1000 cNm displacement, dependent modal damping decreases nearly four times. To examine this, look at

Figure 4-35 and Figure 4-51, around the sixth bending mode, where most data is shared and the experiment is conducted.

4.3 The Length Modified Brake-Reuß Beam (LBRB)

The other experimental application of the FCT-HFS method is demonstrated on the length-modified Brake-Reuß beam [64]. The experimental data is shared upon request of the author of this thesis. The experimental setup is shown in Figure 4-53. The excitation point and the measurement point are also shown there. The bolted joints are tightened to 20 Nm. The beam is made of stainless steel.

Further, an electrodynamic shaker (GV20-PA100E) is utilized to experiment. The experiment is conducted around the first and second modes of bending using step-sine testing. The details of the experimental setup are in [64].

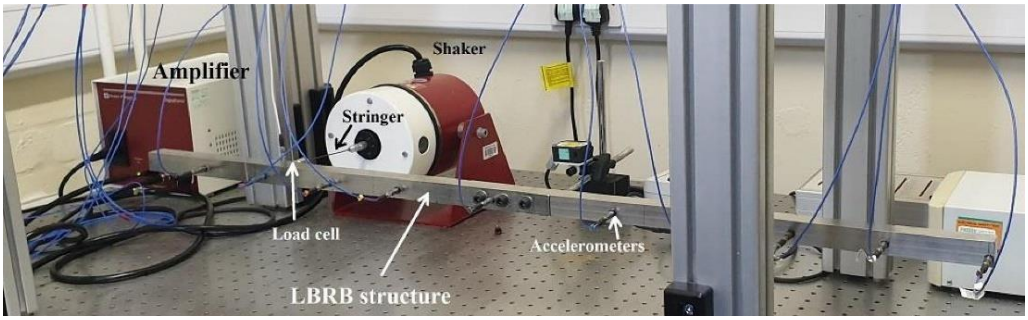

Figure 4-53. The Length Modified Brake-Reuß Beam Setup [64]

4.3.1 Mode 1

The first bending mode of LBRB is considered in this section. At five different forcing levels, the first mode is excited. These are 0.25, 2, 5, 8, and 15 N, and the frequency is between 79.5 and 81.5 Hz with a sampling frequency of 0.03 Hz. The force-controlled test data is used to construct the related harmonic force surface, shown in Figure 4-54. Upper and lowermost displacement amplitude boundaries are determined in such a way that includes all experimental data points.

After that, the harmonic force surface is utilized to extract the quasi-linear frequency-response functions. Eight displacement amplitude planes are exploited from 0.016 to 0.1 mm, Figure 4-55.

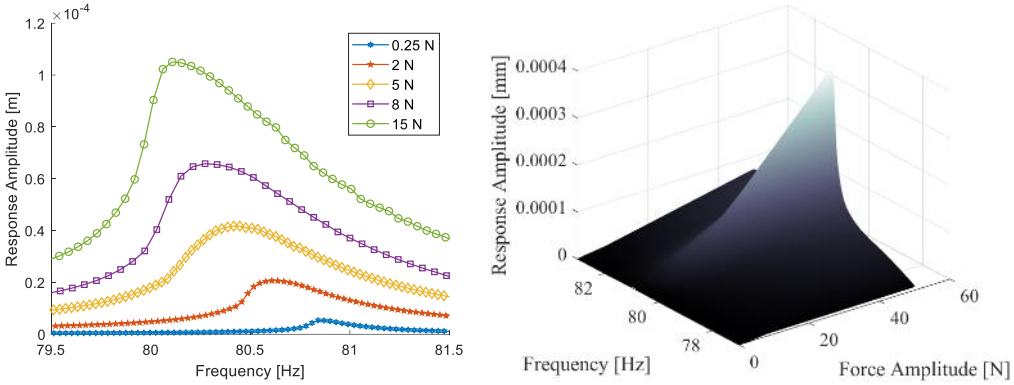

Figure 4-54. a) Measured Constant Force Frequency-Response Amplitude Curves b) Harmonic Force Surface- The Length Modified Brake-Reuß Beam Mode 1

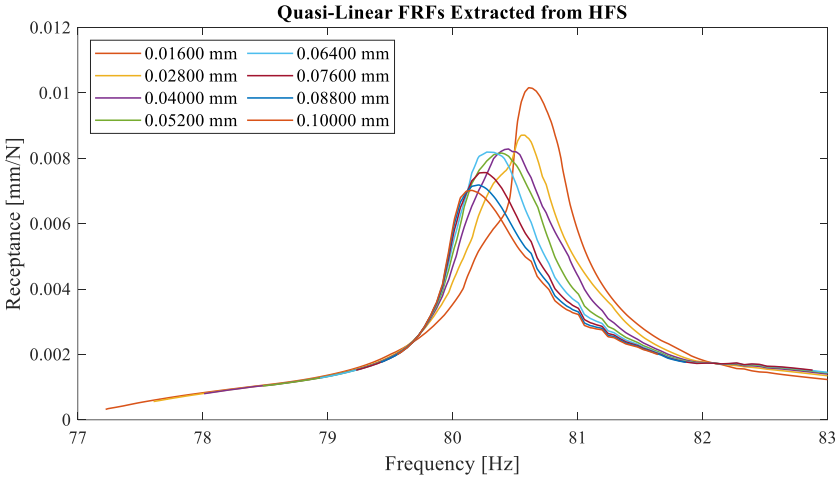

Figure 4-55. Quasi-Linear FRFs Extracted from HFS -The Length Modified Brake-Reuß Beam Mode 1

Experimentally extracted displacement-dependent modal parameters are given as markers in Figure 4-56. Furthermore, smoothingspline to the modal parameters is utilized.

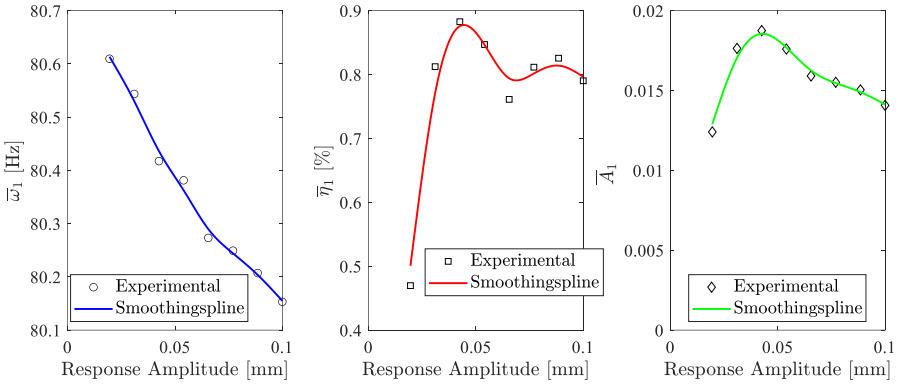

Figure 4-56. Identified Modal Parameters-The Length Modified Brake-Reuß Beam Mode 1

The synthesis is employed except for the lowest force amplitude, and the results are compared in Figure 4-58. The results are almost in perfect agreement except for the 15 N forcing level. Indeed, this identification gives better estimates than the suggested model in the original study [64], tabulated in Figure 4-57. As seen from the plots, the best agreement is achieved between the measured and identified frequency response amplitude curves with the FCT-HFS method (except 15 N forcing level).

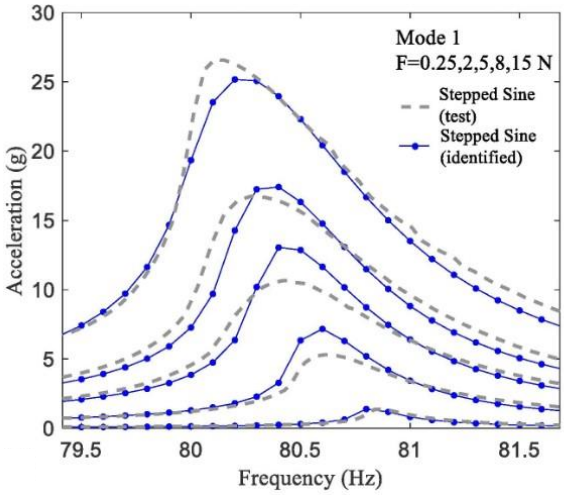

Figure 4-57. Identified Frequency Response Plots from [64]

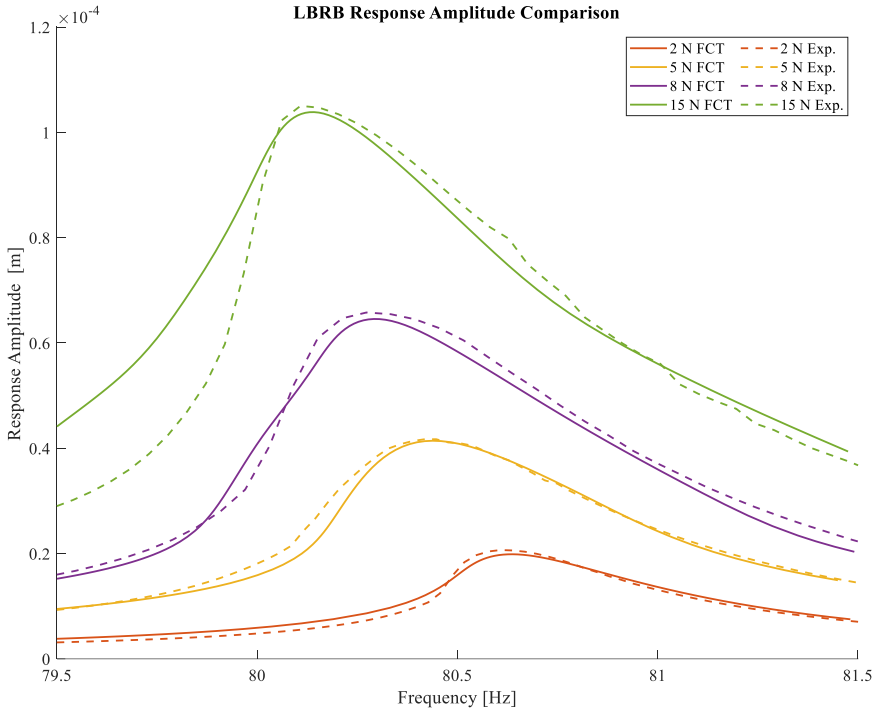

Figure 4-58. Comparison of Measured and Synthesized Frequency-Response Amplitude Curves -The Length Modified Brake-Reuß Beam Mode 1

4.3.2 Mode 2

The second data set of LBRB is the second bending mode, and the test is conducted at 0.25, 1, 2, and 4 N from 280.5 to 283.5 Hz with a sampling rate 0.0405 Hz. The measured frequency-response amplitude curves and resultant harmonic force surface are shown in Figure 4-59. Cutting with five constant displacement planes results in Figure 4-60.

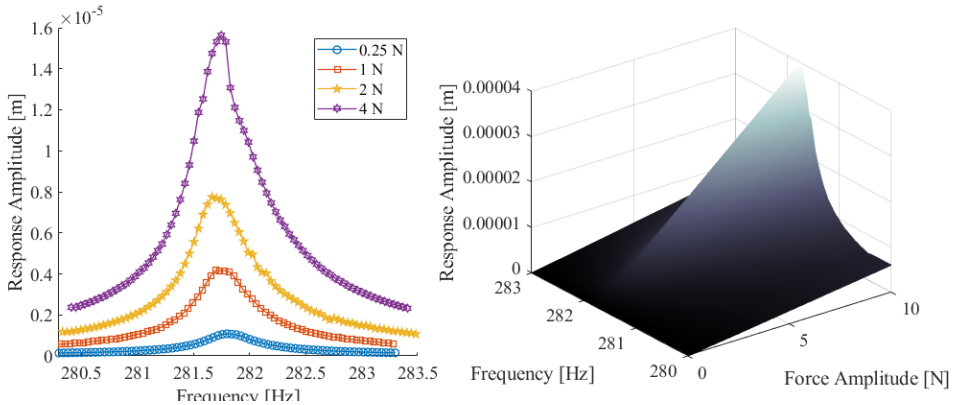

Figure 4-59. a) Measured Constant Force Frequency-Response Amplitude Plots b) Harmonic Force Surface-The Length Modified Brake-Reuß Beam Mode 2

Quasi-linear FRFs of displacement amplitude level from 0.00352 to 0.0156 mm are extracted from the HFS. After modal parameter identification using the peak-picking method, the identified points are shown in Figure 4-61.

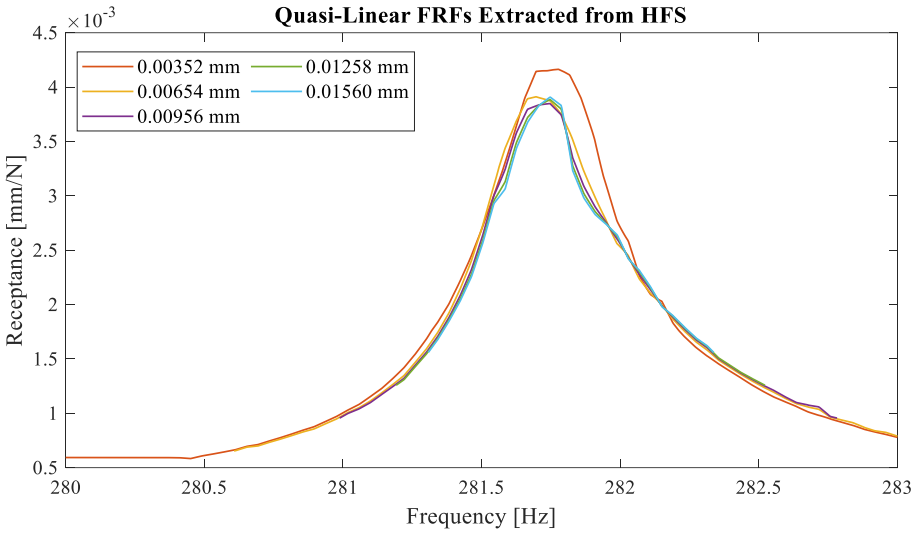

Figure 4-60. Quasi-Linear FRFs Extracted from HFS-The Length Modified Brake-Reuß Beam Mode 2

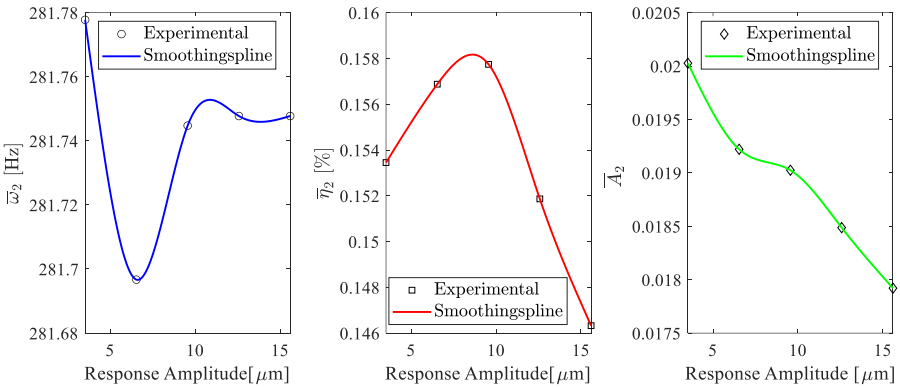

Figure 4-61. Identified Modal Parameters-The Length Modified Brake-Reuß Beam Mode 2

The curve fits of the modal parameters are shown in Figure 4-61. The force-controlled frequency-response amplitude curves are synthesized and compared with the measured ones in Figure 4-62. Ultimately, a good agreement between the measured and the synthesized ones is observed for 2 N and 4 N excitation levels. Note that due to the inability to obtain quasi-linear FRFs at lower response amplitude levels, the other forcing levels are discarded. The 2 N and 4 N response amplitude predictions give better results than the study that originally performed the testing [64].

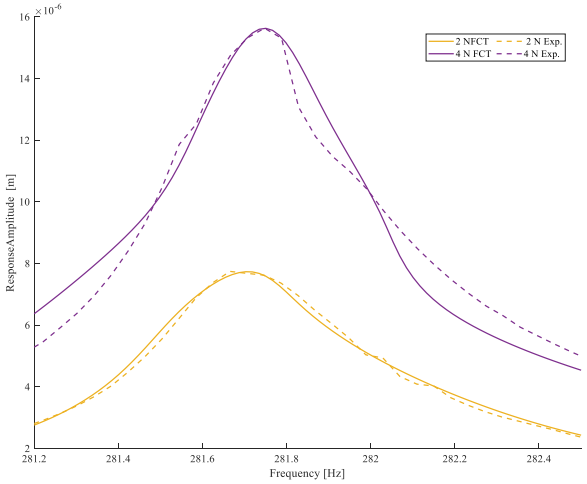

Figure 4-62. Comparison of Measured and Synthesized Frequency-Response Amplitude Curves -The Length Modified Brake-Reuß Beam Mode 2

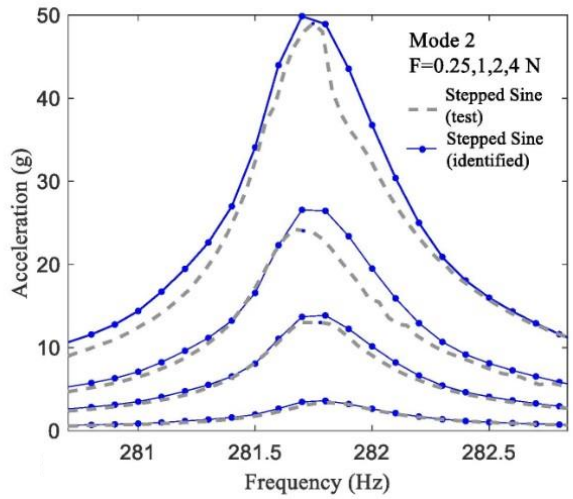

Figure 4-63. Identified Frequency Response Curve from the Literature [64]

4.4 The Half-Brake-Reuß Beam

The half Brake-Reuß beam [65] is the last experimental application of the FCT-HFS framework. Figure 4-64 shows the experimental setup where point 3 is the excitation point and point 1 is the measurement point where the accelerometer is placed. A force-controlled step sine testing is performed at 0.2, 0.5, 1, and 1.5 N within the frequency range 79.2 and 81.2 Hz with a 0.05 Hz sampling rate, the first bending mode of the HBRB. Further details are accessible in [65].

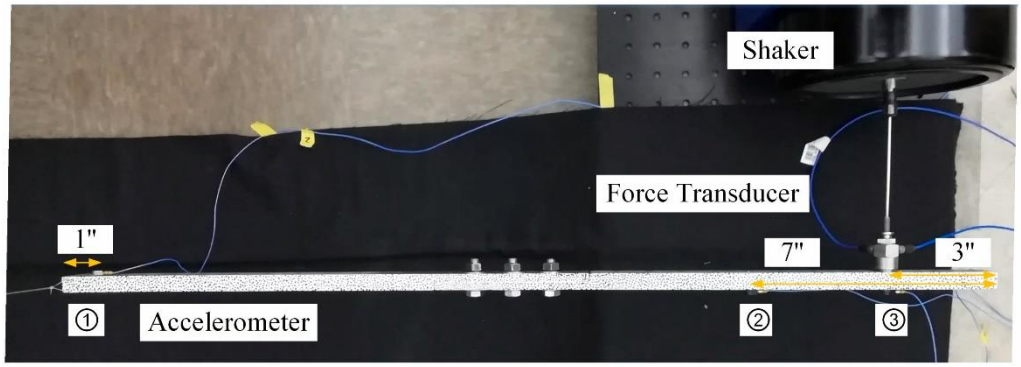

Figure 4-64. Experimental Setup of Forced Control Testing of HBRB[65]

4.4.1 Mode 1

The recorded data is open access, and the author used this data. Since the measured data is in m/s^2, it is converted to m, and the converted frequency-response amplitude plots are given in Figure 4-65. The first examination is lower amplitude forcing response amplitude curves have softening behavior, whereas the others have hardening. This can also be seen in the correspondent harmonic force surface in Figure 4-65. There, two different peaks take shape. Therefore, having two close resonance peaks in the HFS (hence in the constant displacement FRFs) results in difficulty for identifying the modal parameters.

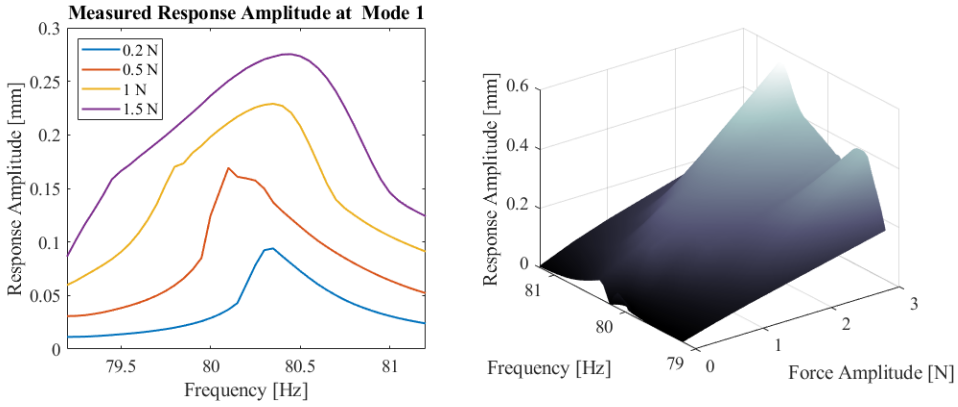

Figure 4-65. a) Measured Constant Force Frequency-Response Amplitude Curves b) Harmonic Force Surface- The Half-Brake-Reuß Beam Mode 1

The quasi-linear FRFs are obtained using the HFS, cut with the constant displacement amplitude planes ranging between 0.066 and 0.296 mm with 24 planes, to perform modal identification as shown in Figure 4-66. However, the synthesis did not result in good agreement due to the sudden change of modal damping values at the lower response amplitude levels. Therefore, the first three response amplitude planes are excluded and the procedure is repeated. After applying peak-picking to the quasi-linear FRFs, the outcomes are plotted frequency versus displacement amplitude in Figure 4-67. Furthermore, the modal parameters are subjected to MATLAB's *smoothingspline* fit.

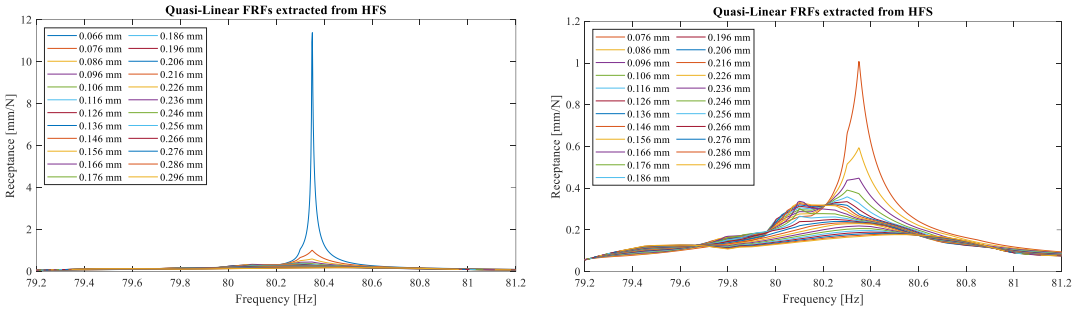

Figure 4-66. Quasi-Linear FRFs Extracted from HFS- The Half-Brake-Reuß Beam Mode 1

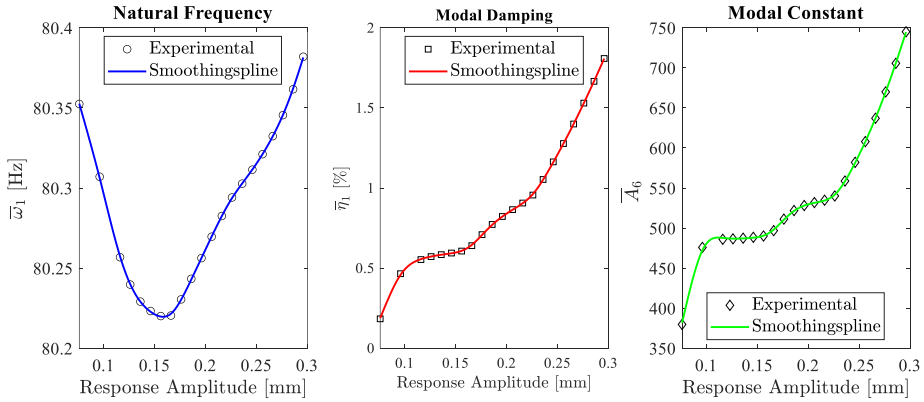

Figure 4-67. Identified Modal Parameters- The Half-Brake-Reuß Beam Mode 1

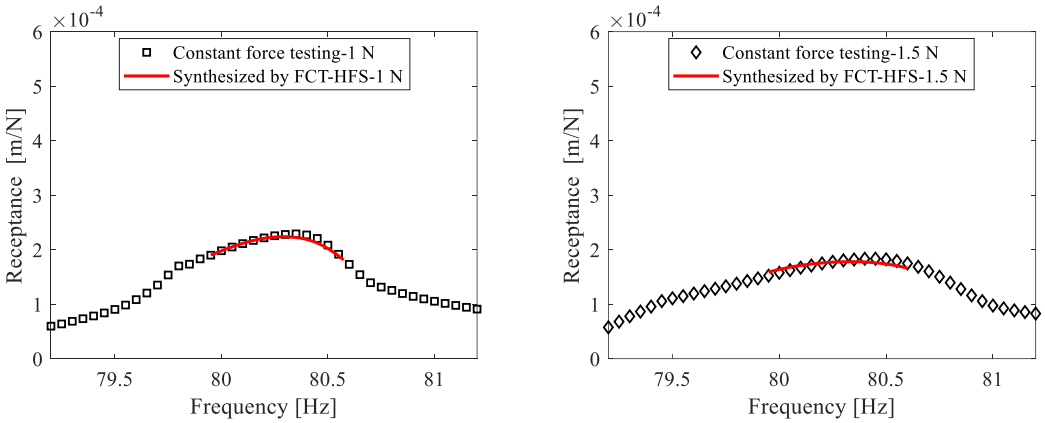

Figure 4-68. Comparison of Measured and Synthesized FRFs - The Half-Brake-Reuß Beam Mode 1

The reconstruction of force-controlled FRF plots is performed using the fits of modal parameters. A good agreement between the experimental curves and the synthesized curves is reported in Figure 4-68 for the highest two forcing levels, at forcing levels

1 N and 1.5 N. The lowest two forcing levels, 0.2 N and 0.5 N are not synthesized since constant response amplitude planes utilized to synthesize the constant force response amplitude plots do not cover the displacement ranges at those forcing levels. This experimental application is the last one presented in this thesis. The next and last chapter summarizes and discusses the FCT-HFS framework developed throughout this thesis

CHAPTER 5

SUMMARY AND DISCUSSION

In this thesis, a novel nonlinear system identification method, the FCT-HFS method, is developed as an extension and leverage of the RCT-HFS framework [40]. The procedure of the method can be summarized as follows:

1. Measuring the constant force amplitude frequency response functions for several different force amplitude values.
2. Merging these constant force FRFs to construct the associated harmonic force surface (HFS).
3. Obtaining quasi-linear frequency response functions corresponding to various values of the displacement response amplitude by cutting the HFS constructed with constant displacement amplitude planes.
4. Determining the modal parameters for each displacement amplitude level using the quasi-linear FRF for that amplitude level by employing the modal identification methods for linear systems.

These four steps can be used to construct a modal model of any nonlinear system, provided that the nonlinearity in the system is not high enough to cause a jump in the frequency response when a force-controlled sine test is applied.

Constructing a modal model using the standard constant force-frequency response functions is the main objective of this study. By applying the FCT-HFS framework proposed in this work, one can construct a modal model using the response model as the RCT-HFS framework works.

The novel framework developed in this study is based on the RCT-HFS framework that has recently proven itself theoretically and experimentally. On the one hand, RCT-HFS exploits the constant response amplitude to construct the harmonic force surface and determine the amplitude-dependent modal parameters that are measured

experimentally. Furthermore, the modal parameters extracted using the RCT-HFS method are obtained from direct measurements. In this study, the FCT-HFS method is employed by merging constant force FRFs to construct the harmonic force surface and then extracting the quasi-linear FRFs from that surface, which is an indirect extraction of the quasi-linear FRFs.

The major advantage of the method developed in this thesis work is constructing a modal model of a nonlinear system by conducting a classical constant force step sine testing where complicated controllers are not required to perform one, unlike the RCT-HFS method. Furthermore, almost all experimentalists are familiar with this classical type of test. In a way, this novel method is an extension and leverage of the RCT-HFS framework.

Some points that should be taken into consideration while employing this method to obtain better results are discussed below:

1. As shown in Chapter 4, where FRFs with jump phenomenon results are obtained while applying the method of FCT-HFS, prudent attempts should be made because the resultant quasi-linear FRFs of the HFS that are constructed using the FRFs with jump behavior results in stepped quasi-linear FRFs.
2. Another vital point is deciding the number of constant displacement amplitude planes to use so that a curve can be fit to the extracted modal parameters. The number of constant displacements that should be included depends on the problem, but 7 to 20 planes are generally adequate.
3. The other point is the decision on the type of curve fitting to the modal parameters extracted from the quasi-linear FRFs. Typically, the first-order polynomial or smoothing spline type of fit of MATLAB's fit function is convenient for exploiting the natural frequency. The smoothing spline method is commonly used in fitting modal damping and modal constants.

4. A further point is the sampling frequency of the experiments. The sampling frequency meticulously affects the accuracy of the results. Therefore, choosing the optimum sampling frequency for the experiment is important.
5. The spacing between the amplitude of forcing levels is another point that affects the accuracy of the results, just like the effect of the sampling frequency.
6. The final observation is that the constant force FRFs should not overlap in the frequency-response plane since these FRFs are used to create harmonic force surface using linear interpolation. If they overlap, the extracted quasi-linear FRFs will have an undesired shape, which makes the peak-picking method difficult and unreliable..

As a future work:

1. The method developed is verified in this study using beams with bolted connections. Therefore, several experimental studies using different structures with different nonlinearities can be performed to study the performance of the method in such applications.
2. Further study can be performed on the cases where a jump is observed in frequency response. Thus, the possibility of using the FCT-HFS framework when a jump occurs can be investigated.
3. One can develop codes for the curve fitting, since the curve fitting functions used here are the built-in functions of MATLAB.

REFERENCES

[1] L. Ljung, *System identification: theory for the user*, 2nd ed. (Prentice Hall information and system sciences series). Upper Saddle River, NJ: Prentice Hall PTR, 1999, p. 609.

[2] G. Kerschen, K. Worden, A. F. Vakakis, and J.-C. Golinval, "Past, present and future of nonlinear system identification in structural dynamics," (in en), *Mechanical Systems and Signal Processing,* vol. 20, no. 3, pp. 505-592, 2006/04// 2006, doi: 10.1016/j.ymssp.2005.04.008.

[3] A. C. Gondhalekar, "STRATEGIES FOR NON-LINEAR SYSTEM IDENTIFICATION," Imperial College London, 2009.

[4] J. P. Noël and G. Kerschen, "Nonlinear system identification in structural dynamics: 10 more years of progress," (in en), *Mechanical Systems and Signal Processing,* vol. 83, pp. 2-35, 2017/01// 2017, doi: 10.1016/j.ymssp.2016.07.020.

[5] X. Wang and G. T. Zheng, "Equivalent Dynamic Stiffness Mapping technique for identifying nonlinear structural elements from frequency response functions," (in en), *Mechanical Systems and Signal Processing,* vol. 68-69, pp. 394-415, 2016/02// 2016, doi: 10.1016/j.ymssp.2015.07.011.

[6] M. W. Sracic and M. S. Allen, "Method for identifying models of nonlinear systems using linear time periodic approximations," (in en), *Mechanical Systems and Signal Processing,* vol. 25, no. 7, pp. 2705-2721, 2011/10// 2011, doi: 10.1016/j.ymssp.2011.03.004.

[7] S. F. Masri and T. K. Caughey, "A Nonparametric Identification Technique for Nonlinear Dynamic Problems," (in en), *Journal of Applied Mechanics,* vol. 46, no. 2, pp. 433-447, 1979/06/01/ 1979, doi: 10.1115/1.3424568.

[8] S. Marchesiello and L. Garibaldi, "A time domain approach for identifying nonlinear vibrating structures by subspace methods," (in en), *Mechanical Systems and Signal Processing,* vol. 22, no. 1, pp. 81-101, 2008/01// 2008, doi: 10.1016/j.ymssp.2007.04.002.

[9] J. P. Noël, S. Marchesiello, and G. Kerschen, "Subspace-based identification of a nonlinear spacecraft in the time and frequency domains," (in en), *Mechanical Systems and Signal Processing,* vol. 43, no. 1-2, pp. 217-236, 2014/02// 2014, doi: 10.1016/j.ymssp.2013.10.016.

[10] D. E. Adams and R. J. Allemang, "A FREQUENCY DOMAIN METHOD FOR ESTIMATING THE PARAMETERS OF A NON-LINEAR STRUCTURAL DYNAMIC MODEL THROUGH FEEDBACK," (in en),

Mechanical Systems and Signal Processing, vol. 14, no. 4, pp. 637-656, 2000/07// 2000, doi: 10.1006/mssp.2000.1292.

[11] M. B. Özer, H. N. Özgüven, and T. J. Royston, "Identification of structural non-linearities using describing functions and the Sherman–Morrison method," (in en), *Mechanical Systems and Signal Processing*, vol. 23, no. 1, pp. 30-44, 2009/01// 2009, doi: 10.1016/j.ymssp.2007.11.014.

[12] J. P. Noël and G. Kerschen, "Frequency-domain subspace identification for nonlinear mechanical systems," (in en), *Mechanical Systems and Signal Processing*, vol. 40, no. 2, pp. 701-717, 2013/11// 2013, doi: 10.1016/j.ymssp.2013.06.034.

[13] D. J. E. A. delli Carri, "Nonlinear identification of a numerical benchmark structure: From measurements to FE model updating," 2014 2014, Leuven, Belgium.

[14] G. V. Demarie, R. Ceravolo, D. Sabia, and P. Argoul, "Experimental identification of beams with localized nonlinearities," (in en), *Journal of Vibration and Control*, vol. 17, no. 11, pp. 1721-1732, 2011/10// 2011, doi: 10.1177/1077546310385287.

[15] L. Heller, E. Foltête, and J. Piranda, "Experimental identification of nonlinear dynamic properties of built-up structures," (in en), *Journal of Sound and Vibration*, vol. 327, no. 1-2, pp. 183-196, 2009/10// 2009, doi: 10.1016/j.jsv.2009.06.008.

[16] M. Witters and J. Swevers, "Black-box model identification for a continuously variable, electro-hydraulic semi-active damper," (in en), *Mechanical Systems and Signal Processing*, vol. 24, no. 1, pp. 4-18, 2010/01// 2010, doi: 10.1016/j.ymssp.2009.03.013.

[17] L. Dos Santos Coelho and M. W. Pessôa, "Nonlinear identification using a B-spline neural network and chaotic immune approaches," (in en), *Mechanical Systems and Signal Processing*, vol. 23, no. 8, pp. 2418-2434, 2009/11// 2009, doi: 10.1016/j.ymssp.2009.01.013.

[18] P. L. Green and K. Worden, "Bayesian and Markov chain Monte Carlo methods for identifying nonlinear systems in the presence of uncertainty," (in en), *Phil. Trans. R. Soc. A.*, vol. 373, no. 2051, p. 20140405, 2015/09/28/ 2015, doi: 10.1098/rsta.2014.0405.

[19] I. Behmanesh, B. Moaveni, G. Lombaert, and C. Papadimitriou, "Hierarchical Bayesian model updating for structural identification," (in en), *Mechanical Systems and Signal Processing*, vol. 64-65, pp. 360-376, 2015/12// 2015, doi: 10.1016/j.ymssp.2015.03.026.

[20] R. M. Rosenberg, "The Normal Modes of Nonlinear n-Degree-of-Freedom Systems," (in en), *Journal of Applied Mechanics*, vol. 29, no. 1, pp. 7-14, 1962/03/01/ 1962, doi: 10.1115/1.3636501.

[21] R. M. Rosenberg, "On Nonlinear Vibrations of Systems with Many Degrees of Freedom," in *Advances in Applied Mechanics*, vol. 9: Elsevier, 1966, pp. 155-242.

[22] R. M. Rosenberg, "Normal Modes of Nonlinear Dual-Mode Systems," (in en), *Journal of Applied Mechanics*, vol. 27, no. 2, pp. 263-268, 1960/06/01/ 1960, doi: 10.1115/1.3643948.

[23] M. F. Platten, J. R. Wright, G. Dimitriadis, and J. E. Cooper, "Identification of multi-degree of freedom non-linear systems using an extended modal space model," (in en), *Mechanical Systems and Signal Processing*, vol. 23, no. 1, pp. 8-29, 2009/01// 2009, doi: 10.1016/j.ymssp.2007.11.016.

[24] M. F. Platten, J. R. Wright, J. E. Cooper, and G. Dimitriadis, "Identification of a Nonlinear Wing Structure Using an Extended Modal Model," (in en), *Journal of Aircraft*, vol. 46, no. 5, pp. 1614-1626, 2009/09// 2009, doi: 10.2514/1.42024.

[25] U. Fuellekrug and D. Goege, "Identification of weak non-linearities within complex aerospace structures," (in en), *Aerospace Science and Technology*, vol. 23, no. 1, pp. 53-62, 2012/12// 2012, doi: 10.1016/j.ast.2011.04.012.

[26] L. Renson, A. Gonzalez-Buelga, D. A. W. Barton, and S. A. Neild, "Robust identification of backbone curves using control-based continuation," (in en), *Journal of Sound and Vibration*, vol. 367, pp. 145-158, 2016/04// 2016, doi: 10.1016/j.jsv.2015.12.035.

[27] L. Renson, D. A. W. Barton, and S. S. Neild, "Experimental Analysis of a Softening-Hardening Nonlinear Oscillator Using Control-Based Continuation," in *Nonlinear Dynamics, Volume 1*, G. Kerschen Ed. Cham: Springer International Publishing, 2016, pp. 19-27.

[28] L. Renson, D. A. W. Barton, and S. A. Neild, "Experimental Tracking of Limit-Point Bifurcations and Backbone Curves Using Control-Based Continuation," (in en), *Int. J. Bifurcation Chaos*, vol. 27, no. 01, p. 1730002, 2017/01// 2017, doi: 10.1142/S0218127417300026.

[29] B. Gomes, I. De Cesare, A. Guarino, M. Di Bernardo, L. Renson, and L. Marucci, "Exploring the Dynamics of Nonlinear Biochemical Systems using Control-Based Continuation," Systems Biology, preprint 2019/07/08/ 2019. Accessed: 2023/10/30/09:51:56. [Online]. Available: http://biorxiv.org/lookup/doi/10.1101/695866

[30] L. Renson, D. A. W. Barton, and S. A. Neild, "Application of Control-Based Continuation to a Nonlinear System with Harmonically Coupled Modes," in *Nonlinear Dynamics, Volume 1*, G. Kerschen Ed. Cham: Springer International Publishing, 2019, pp. 315-316.

[31] G. Abeloos, L. Renson, C. Collette, and G. Kerschen, "Stepped and swept control-based continuation using adaptive filtering," (in en), *Nonlinear Dynamics*, vol. 104, no. 4, pp. 3793-3808, 2021/06// 2021, doi: 10.1007/s11071-021-06506-z.

[32] G. Kleyman, M. Paehr, and S. Tatzko, "Experimental Application of Control-Based-Continuation for Characterization of Isolated Modes on Single- and Multiple-Degree-of-Freedom Systems," in *Nonlinear Structures & Systems, Volume 1*, G. Kerschen, M. R. W. Brake, and L. Renson Eds. Cham: Springer International Publishing, 2021, pp. 135-138.

[33] L. Renson, "Identification of Backbone Curves and Nonlinear Frequency Responses using Control-based Continuation and Local Gaussian Process Regression," in *Nonlinear Structures & Systems, Volume 1*, G. Kerschen, M. R. W. Brake, and L. Renson Eds. Cham: Springer International Publishing, 2021, pp. 83-85.

[34] M. Blyth, K. Tsaneva-Atanasova, L. Marucci, and L. Renson, "Numerical methods for control-based continuation of relaxation oscillations," (in en), *Nonlinear Dynamics*, vol. 111, no. 9, pp. 7975-7992, 2023/05// 2023, doi: 10.1007/s11071-023-08288-y.

[35] S. Peter and R. I. Leine, "Excitation power quantities in phase resonance testing of nonlinear systems with phase-locked-loop excitation," (in en), *Mechanical Systems and Signal Processing*, vol. 96, pp. 139-158, 2017/11// 2017, doi: 10.1016/j.ymssp.2017.04.011.

[36] M. Scheel, T. Weigele, and M. Krack, "Challenging an experimental nonlinear modal analysis method with a new strongly friction-damped structure," (in en), *Journal of Sound and Vibration*, vol. 485, p. 115580, 2020/10// 2020, doi: 10.1016/j.jsv.2020.115580.

[37] V. Denis, M. Jossic, C. Giraud-Audine, B. Chomette, A. Renault, and O. Thomas, "Identification of nonlinear modes using phase-locked-loop experimental continuation and normal form," (in en), *Mechanical Systems and Signal Processing*, vol. 106, pp. 430-452, 2018/06// 2018, doi: 10.1016/j.ymssp.2018.01.014.

[38] S. Schwarz, L. Kohlmann, A. Hartung, J. Gross, M. Scheel, and M. Krack, "Validation of a Turbine Blade Component Test With Frictional Contacts by Phase-Locked-Loop and Force-Controlled Measurements," (in en), *Journal*

of Engineering for Gas Turbines and Power, vol. 142, no. 5, p. 051006, 2020/05/01/ 2020, doi: 10.1115/1.4044772.

[39] S. Peter, F. Schreyer, and R. I. Leine, "Experimental and Numerical Nonlinear Modal Analysis of a Beam with Impact: Part II – Experimental Investigation," in *Nonlinear Dynamics, Volume 1*, G. Kerschen Ed. Cham: Springer International Publishing, 2019, pp. 183-185.

[40] T. Karaağaçlı and H. N. Özgüven, "Experimental modal analysis of nonlinear systems by using response-controlled stepped-sine testing," (in en), *Mechanical Systems and Signal Processing*, vol. 146, p. 107023, 2021/01// 2021, doi: 10.1016/j.ymssp.2020.107023.

[41] Ö. Ö. H. N. Arslan, "Modal identification of non-linear structures and the use of modal model in structural dynamic analysis," 2008 2008, in In: Conference Proceedings of the Society for Experimental Mechanics Series.

[42] W. Szemplińska-Stupnicka, "The modified single mode method in the investigations of the resonant vibrations of non-linear systems," (in en), *Journal of Sound and Vibration*, vol. 63, no. 4, pp. 475-489, 1979/04// 1979, doi: 10.1016/0022-460X(79)90823-X.

[43] W. Szemplinska-Stupnicka, "“Non-linear normal modes” and the generalized Ritz method in the problems of vibrations of non-linear elastic continuous systems," (in en), *International Journal of Non-Linear Mechanics*, vol. 18, no. 2, pp. 149-165, 1983/01// 1983, doi: 10.1016/0020-7462(83)90042-2.

[44] T. Karaağaçlı and H. N. Özgüven, "Experimental Identification of Backbone Curves of Strongly Nonlinear Systems by Using Response-Controlled Stepped-Sine Testing (RCT)," (in en), *Vibration*, vol. 3, no. 3, pp. 266-280, 2020/09/07/ 2020, doi: 10.3390/vibration3030019.

[45] T. Karaağaçlı and H. N. Özgüven, "Experimental Quantification and Validation of Modal Properties of Geometrically Nonlinear Structures by Using Response-Controlled Stepped-Sine Testing," (in en), *Exp Mech*, vol. 62, no. 2, pp. 199-211, 2022/02// 2022, doi: 10.1007/s11340-021-00784-9.

[46] A. Koyuncu, T. Karaağaçlı, M. Şahin, and H. N. Özgüven, "Experimental Modal Analysis of Nonlinear Amplified Piezoelectric Actuators by Using Response-Controlled Stepped-Sine Testing," (in en), *Exp Mech*, vol. 62, no. 9, pp. 1579-1594, 2022/11// 2022, doi: 10.1007/s11340-022-00878-y.

[47] T. Karaağaçlı and H. Nevzat Özgüven, "Experimental Modal Analysis of Structures with High Nonlinear Damping by Using Response-Controlled Stepped-Sine Testing," in *Nonlinear Structures & Systems, Volume 1*, M. R.

W. Brake, L. Renson, R. J. Kuether, and P. Tiso Eds. Cham: Springer Nature Switzerland, 2024, pp. 125-132.

[48] E. Ceren Ekinci, M. Bülent Özer, and H. Nevzat Özgüven, "A Novel Approach for Local Structural Modification of Nonlinear Structures," in *Nonlinear Structures & Systems, Volume 1*, M. R. W. Brake, L. Renson, R. J. Kuether, and P. Tiso Eds. Cham: Springer Nature Switzerland, 2024, pp. 155-160.

[49] H. Nevzat Özgüven, "Structural modifications using frequency response functions," (in en), *Mechanical Systems and Signal Processing,* vol. 4, no. 1, pp. 53-63, 1990/01// 1990, doi: 10.1016/0888-3270(90)90040-R.

[50] M. F. Gürbüz, T. Karaağaçlı, M. B. Özer, and H. N. Özgüven, "Bypassing the Repeatability Issue in Nonlinear Experimental Modal Analysis of Jointed Structures by Using the RCT-HFS Framework," in *Nonlinear Structures & Systems, Volume 1*, M. R. W. Brake, L. Renson, R. J. Kuether, and P. Tiso Eds. Cham: Springer Nature Switzerland, 2024, pp. 75-80.

[51] O. Tanrikulu, B. Kuran, H. N. Ozguven, and M. Imregun, "Forced harmonic response analysis of nonlinear structures using describing functions," *AIAA Journal,* vol. 31, no. 7, pp. 1313-1320, 1993/07// 1993, doi: 10.2514/3.11769.

[52] B. D. Yang and C. H. Menq, "Modeling of Friction Contact and Its Application to the Design of Shroud Contact," (in en), *Journal of Engineering for Gas Turbines and Power,* vol. 119, no. 4, pp. 958-963, 1997/10/01/ 1997, doi: 10.1115/1.2817082.

[53] B. Sun, Y. Zhang, D. Dai, L. Wang, and J. Ou, "Seismic fragility analysis of a large-scale frame structure with local nonlinearities using an efficient reduced-order Newton-Raphson method," (in en), *Soil Dynamics and Earthquake Engineering,* vol. 164, p. 107559, 2023/01// 2023, doi: 10.1016/j.soildyn.2022.107559.

[54] N. Arie de, "Step-size control and corrector methods in numerical continuation of ocean circulation and fill-reducing orderings in multilevel ILU methods," University of Groningen, 2002.

[55] M. A. Crisfield, "A fast incremental/iterative solution procedure that handles “snap-through”," (in en), *Computers & Structures,* vol. 13, no. 1-3, pp. 55-62, 1981/06// 1981, doi: 10.1016/0045-7949(81)90108-5.

[56] G. Formica, F. Milicchio, and W. Lacarbonara, "A Krylov accelerated Newton–Raphson scheme for efficient pseudo-arclength pathfollowing," (in en), *International Journal of Non-Linear Mechanics,* vol. 145, p. 104116, 2022/10// 2022, doi: 10.1016/j.ijnonlinmec.2022.104116.

[57] T. Zhu, G. Zhang, C. Zang, H. Cui, and M. I. Friswell, "Arclength-based response matching of multivalued frequency responses to update models with strong nonlinearities," (in en), *Mechanical Systems and Signal Processing*, vol. 204, p. 110777, 2023/12// 2023, doi: 10.1016/j.ymssp.2023.110777.

[58] T. Zhu, G. Zhang, C. Zang, and M. I. Friswell, "Global correlation analysis of strongly nonlinear frequency responses using the arclength-based separation and the Correlation-Map," (in en), *Journal of Sound and Vibration*, vol. 569, p. 117998, 2024/01// 2024, doi: 10.1016/j.jsv.2023.117998.

[59] E. Ferhatoglu, E. Cigeroglu, and H. N. Özgüven, "A novel modal superposition method with response dependent nonlinear modes for periodic vibration analysis of large MDOF nonlinear systems," (in en), *Mechanical Systems and Signal Processing*, vol. 135, p. 106388, 2020/01// 2020, doi: 10.1016/j.ymssp.2019.106388.

[60] E. Ferhatoglu, E. Cigeroglu, and H. N. Özgüven, "A new modal superposition method for nonlinear vibration analysis of structures using hybrid mode shapes," (in en), *Mechanical Systems and Signal Processing*, vol. 107, pp. 317-342, 2018/07// 2018, doi: 10.1016/j.ymssp.2018.01.036.

[61] M. R. Brake, P. Reuss, D. J. Segalman, and L. Gaul, "Variability and Repeatability of Jointed Structures with Frictional Interfaces," in *Dynamics of Coupled Structures, Volume 1*, M. Allen, R. Mayes, and D. Rixen Eds. Cham: Springer International Publishing, 2014, pp. 245-252.

[62] M. R. W. Brake, C. W. Schwingshackl, and P. Reuß, "Observations of variability and repeatability in jointed structures," (in en), *Mechanical Systems and Signal Processing*, vol. 129, pp. 282-307, 2019/08// 2019, doi: 10.1016/j.ymssp.2019.04.020.

[63] R. D. O. Teloli, P. Butaud, G. Chevallier, and S. Da Silva, "Good practices for designing and experimental testing of dynamically excited jointed structures: The Orion beam," (in en), *Mechanical Systems and Signal Processing*, vol. 163, p. 108172, 2022/01// 2022, doi: 10.1016/j.ymssp.2021.108172.

[64] S. Safari and J. M. Londoño Monsalve, "Data-driven structural identification of nonlinear assemblies: Structures with bolted joints," (in en), *Mechanical Systems and Signal Processing*, vol. 195, p. 110296, 2023/07// 2023, doi: 10.1016/j.ymssp.2023.110296.

[65] W. Chen *et al.*, "Measurement and identification of the nonlinear dynamics of a jointed structure using full-field data, Part I: Measurement of nonlinear

dynamics," (in en), *Mechanical Systems and Signal Processing*, vol. 166, p. 108401, 2022/03// 2022, doi: 10.1016/j.ymssp.2021.108401.

[66] "The MathWorks Inc. (2024). MATLAB version: 24.1.0.2568132 (R2024a), Natick, Massachusetts: The MathWorks Inc. https://www.mathworks.com," ed.

[67] R. D. O. Teloli, P. Butaud, G. Chevallier, and S. Da Silva, "Dataset of experimental measurements for the Orion beam structure," (in en), *Data in Brief*, vol. 39, p. 107627, 2021/12// 2021, doi: 10.1016/j.dib.2021.107627.

[68] W. Xu, "Effect of Bolted Joint Preload on Structural Damping," University of South Florida, 2013.

APPENDICES

A. Conference Paper

BYPASSING THE REPEATABILITY ISSUE IN NONLINEAR EXPERIMENTAL MODAL ANALYSIS OF JOINTED STRUCTURES BY USING THE RCT-HFS FRAMEWORK

M. Fatih Gürbüz[1], Taylan Karaağaçlı[2], M. Bülent Özer[1], H. Nevzat Özgüven[1]

[1] Department of Mechanical Engineering, Middle East Technical University, 06800 Ankara, Turkey

[2] The Scientific and Technological Research Council of Turkey, Defense Industries Research and Development Institute, TÜBİTAK-SAGE, P.K. 16, 06261 Mamak, Ankara, Turkey

ABSTRACT

Mechanical joints, which are indispensable for almost all mechanical systems, are often an important source of nonlinearity due to frictional, backlash and/or preload effects. Recent studies have shown that the contact pressure distribution at bolted joint interfaces is the key parameter that governs joint friction and, therefore, the nonlinear damping mechanism in these systems. The problem is that this pressure distribution is susceptible to several different factors: bolt preload, bolt tightening order, surface roughness, surface flatness, and misalignments during the assembly process. These issues lead to considerable variability and repeatability problems in the nonlinear dynamics of jointed structures. Consequently, the accurate identification of nonlinear damping in jointed structures is still a challenging task. The combined use of the response- controlled stepped-sine testing (RCT) and the harmonic force surface concept (HFS) constitutes a framework that determines

frequency response curves from the same measurement in two different ways; either by directly measuring them or by synthesizing them from the identified nonlinear modal parameters. Since any possible discrepancy of the frequency response curves obtained from the same measurement cannot be attributed to the repeatability issue, the RCT-HFS framework validates the accuracy of the identified nonlinear modal parameters in a sense bypassing the repeatability problem. In this study, this novel feature of the RCT-HFS framework is used in identifying and validating the accuracy of the modal model of a benchmark beam with a bolted lap joint.

Keywords: Joint nonlinearity, friction nonlinearity, response-controlled stepped-sine testing, harmonic force surface, repeatability

1. REPEATABILITY ISSUE

Vibration responses of jointed structures repeatedly measured under the same excitation condition can be very different from each other [1]. This poor repeatability in measurements makes it difficult to understand the nonlinear dynamics of mechanical joints and to develop a reliable and accurate mathematical model from experiments. Remarkable studies have been published recently that clarify the causes of the repeatability issue in jointed structures (e.g. [2-3]). In these studies, it is shown that the interfacial contact pressure distribution is the key metric that affects the nonlinear dynamics of mechanical joints as well as the measurement repeatability. It is also shown that this pressure distribution is very sensitive to various factors such as the topography of the contact interface (flatness and surface roughness), bolt tightening order, bolt preload, and alignment issues during the assembly process. Some of these factors change considerably not only in the case of disassembly/reassembly but even in the case of the repeated measurements of the same assembly, which highly affects the contact pressure and therefore the measurement repeatability. In [2], it is demonstrated that a well-controlled assembly procedure can highly improve measurement repeatability. Furthermore, it is revealed that lower surface roughness considerably reduces the sensitivity of the contact

pressure to bolt preload and bolted tightening order, which also results in better repeatability.

Although significant progress has been made in understanding the nonlinear characteristics of mechanical joints and improving repeatability as discussed above, developing an accurate mathematical model for joints still remains a challenging problem. In a recent joint work [4], the nonlinear dynamics of a jointed beam have been studied by applying several different identification methods such as the Hilbert Transform method, Peak Finding and Fitting method to the free decay response data measured by impact testing and shaker ringdown testing. In the same work, a significant discrepancy was reported between the backbone curves and nonlinear modal damping curves identified from these methods with the ones obtained from classical force-controlled stepped sine testing. Whether this discrepancy is due to the theoretical/practical limitations of the studied identification methods or the repeatability issue remains ambiguous. On the other side, since the modal damping obtained from force-controlled testing is identified indirectly by assuming the input energy provided by the shaker is equal to the energy dissipated by bolted joints of the beam, it is also disputable whether this modal damping constitutes an accurate reference to validate other identification techniques.

An important advantage of the RCT-HFS identification framework [5] compared to the aforementioned identification methods is that it is capable of determining frequency response curves from the *same measurement* data set in two different ways; either by extracting them from the HFS or by synthesizing them from the identified nonlinear modal parameters based on the Single Nonlinear Mode (SNM) theory [6]. Since any possible discrepancy of the frequency response curves reproduced from the same measurement by two different approaches cannot be attributed to the repeatability issue, the RCT- HFS framework provides a reliable mean of validating its theoretical foundation, i.e. the SNM theory, in a sense bypassing the repeatability problem. Of course, if the structure suffers from poor repeatability, the problem is still there and can be studied separately by applying the RCT-HFS framework on repeated measurements and obtaining uncertainty

bounds of identified nonlinear modal parameters as shown in the case of a real missile in [5].

In a short period of time, The RCT-HFS identification framework has been successfully applied to a wide range of nonlinear systems; a T-beam benchmark with local cubic stiffness nonlinearity and a real missile with moderate damping nonlinearity due to bolted joints [5], a metal strip that exhibits strong geometrical (distributed) nonlinearity [7, 8], a nonlinear micro- electromechanical device with stack-type piezo-actuator [9] and the control fin actuation mechanism of a real missile [10]. In this study, the framework is successfully applied to a recently proposed benchmark beam with bolted lap joint, namely the Orion beam [11].

2. APPLICATION OF THE RCT-HFS FRAMEWORK TO THE ORION BEAM

In this study, the RCT-HFS identification method is applied to a benchmark structure, the so-called Orion beam recently proposed in [11]. The structure consists of two thin beams connected by three bolted joints with contact patches on each connecting bolt. In [11], the Orion beam is subjected to a series of constant-force stepped-sine testing by using the experimental setup shown in Fig. 1. The beam is excited by a modal shaker at a point close to its clamped end. The response is measured by a laser vibrometer. All the details about the dimensions of the beam, data acquisition and control strategy can be found in [11]. Frequency response functions (FRFs) measured at different levels of excitation force amplitude and tightening torque are also provided in [12] as an open-source dataset to help different research groups to test the identification methods they have developed.

In the RCT-HFS framework, the usual practice is to conduct a series of response-controlled stepped-sine testing by keeping the displacement amplitude of a selected control point (usually the driving point) constant and to measure constant-response receptances which turn out to be quasi-linear even in the case of strongly nonlinear systems [5, 7-10]. Then, these receptances are processed by using standard linear modal analysis techniques to extract response-level dependent nonlinear modal

parameters (natural frequency, modal damping ratio, and modal constant). On the other side, the HFS is constructed by using harmonic force spectra measured at different constant displacement amplitude levels. By cutting the HFS with constant force planes, one can extract constant-force frequency response curves including unstable branches if there are any. Finally, the accuracy of the identified nonlinear modal parameters is validated by comparing constant-force receptances synthesized from these parameters (in a Newton-Raphson solution scheme) with the ones extracted from the HFS. However, [11, 12] provide only the constant-force FRFs for the Orion beam but not the constant-response FRFs. In this study, this issue is solved by using the HFS concept in a novel way different than its usual implementation as explained below.

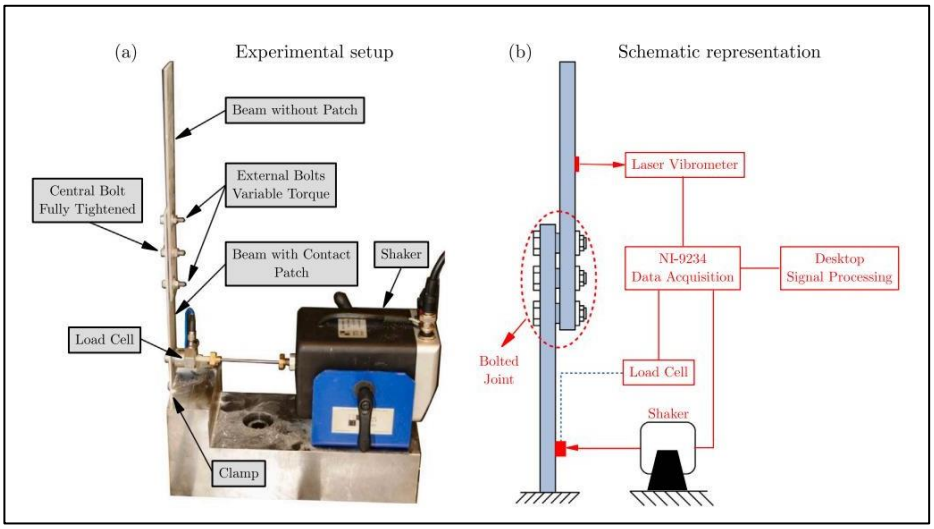

Fig. 1. Orion beam experimental setup [11]

In [12], constant-force mobility (velocity/force) data are measured around the 3rd mode of the Orion beam at 20 cNm tightening torque level. These data are converted into frequency response curves as shown in Fig. 2(a). Since the nonlinearity is relatively weak, the frequency response curves do not exhibit any jump and are very smooth. Consequently, these curves are merged to construct a smooth HFS as shown in Fig. 2(b). Cutting this HFS with constant displacement amplitude planes gives V-shaped harmonic force spectra. Finally, dividing selected constant displacement

amplitudes with corresponding harmonic force spectra gives the quasi-linear constant-response FRFs as shown in Fig 3. It is important to note that the main motivation behind the invention of the HFS was accurately identifying unstable branches and turning points of constant-force FRFs that exhibit the jump phenomenon in the case of classical constant-force testing. Therefore, in the case of strongly nonlinear systems, the HFS is used to obtain constant-force FRFs from the measured constant-response measurements. However, as shown in this study, this procedure can be reversed in the case of weakly nonlinear systems. This novel implementation of the HFS concept can be very useful to identify the model parameters of nonlinear structures very accurately as shown below.

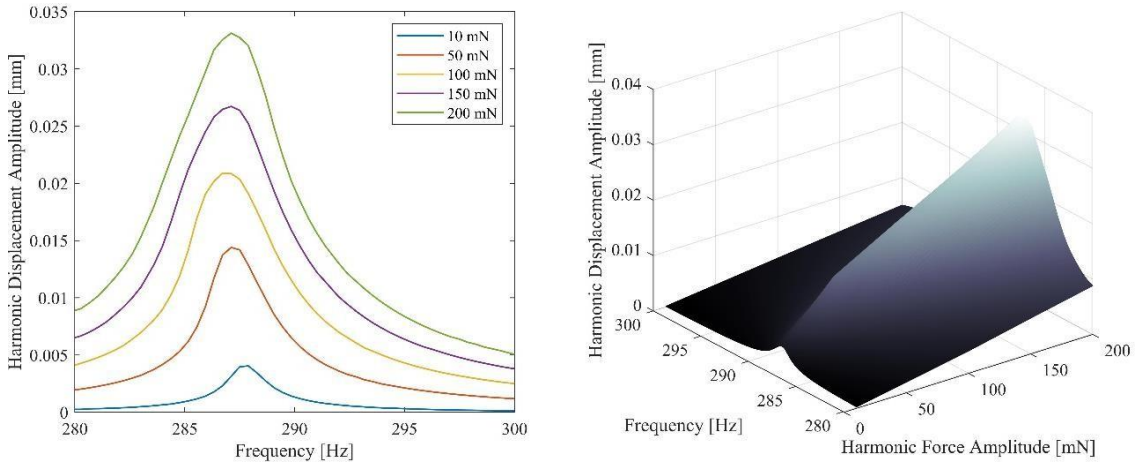

Fig. 2. Construction of the HFS from the constant-force frequency response curves for the 3rd bending mode at 20 cNm tightening torque: (a) constant-force frequency response curves (b) Harmonic Force Surface (HFS)

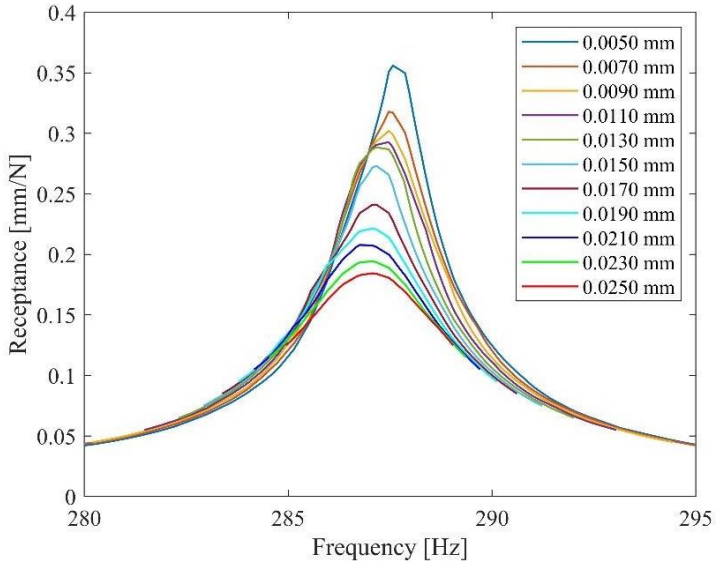

Fig. 3. Extraction of the quasi-linear constant-displacement FRFs from the HFS for the 3rd bending mode at 20 cNm tightening torque

Once the quasi-linear constant-response FRFs are obtained from the HFS as shown in Fig. 3, they can be processed by using standard linear modal analysis techniques to extract modal parameters corresponding to each displacement amplitude level. In this study, constant-response FRFs are processed by using the simple pick-picking algorithm, and response level depended nonlinear modal parameters are obtained as shown in Fig. 4. An important advantage of the RCT-HFS framework over most of the state-of-the-art identification techniques is that it identifies accurate modal models of nonlinear structures without necessitating the apriori knowledge of the location and/or the type of nonlinearity, and it can be used even for distributed nonlinearity. In [11], a Duffing-Van der Pol oscillator model is assumed for the Orion beam, and the parameters of that model are determined iteratively by using the measured constant-force FRFs. The issue with such parametric modeling is that it can be computationally expensive or not possible at all in the case of complex engineering systems

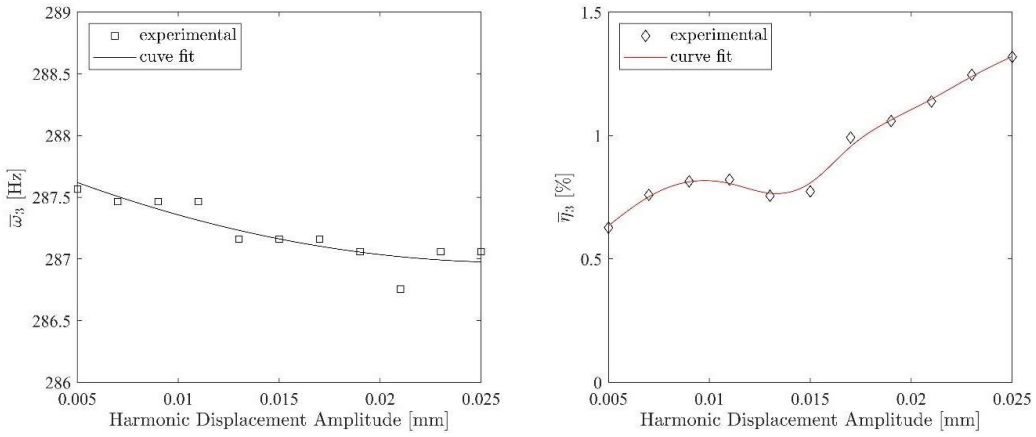

Fig. 4. Variation of modal parameters with response amplitude: (a) natural frequency (b) modal damping ratio

The final step of the RCT-HFS framework is the demonstration of the accuracy of the identified nonlinear modal parameters. To achieve this goal, constant-force FRFs are synthesized from the identified nonlinear modal model by using the SNM theory [6] and the Newton-Raphson solution scheme. These synthesized FRFs are compared with the ones directly measured by constant-force testing [11-12] in Fig. 5. As can be seen from the figure, the match between the synthesized and directly measured data is perfect, which proves the accuracy of the identified nonlinear modal model.

A very interesting and important observation that can be made from Fig. 4 and Fig. 5 is that although the nonlinear model parameters were experimentally obtained for the displacement levels between 0.005 mm and 0.025 mm as seen in Fig. 4, the constant-force FRFs corresponding to the 10mN and 200 mN covering response amplitudes below 0.005 mm and above

0.025 mm are also very accurately synthesized as shown in Fig. 5. This is achieved by a successful curve fitting and extrapolation process using the *fit* function of Matlab. A second-order polynomial is fitted to the natural frequency and smoothing spline curves are fitted to the modal damping ratio and modal constant, which satisfactorily extrapolates the modal parameters at amplitude levels below 0.005 mm and above 0.025 mm.

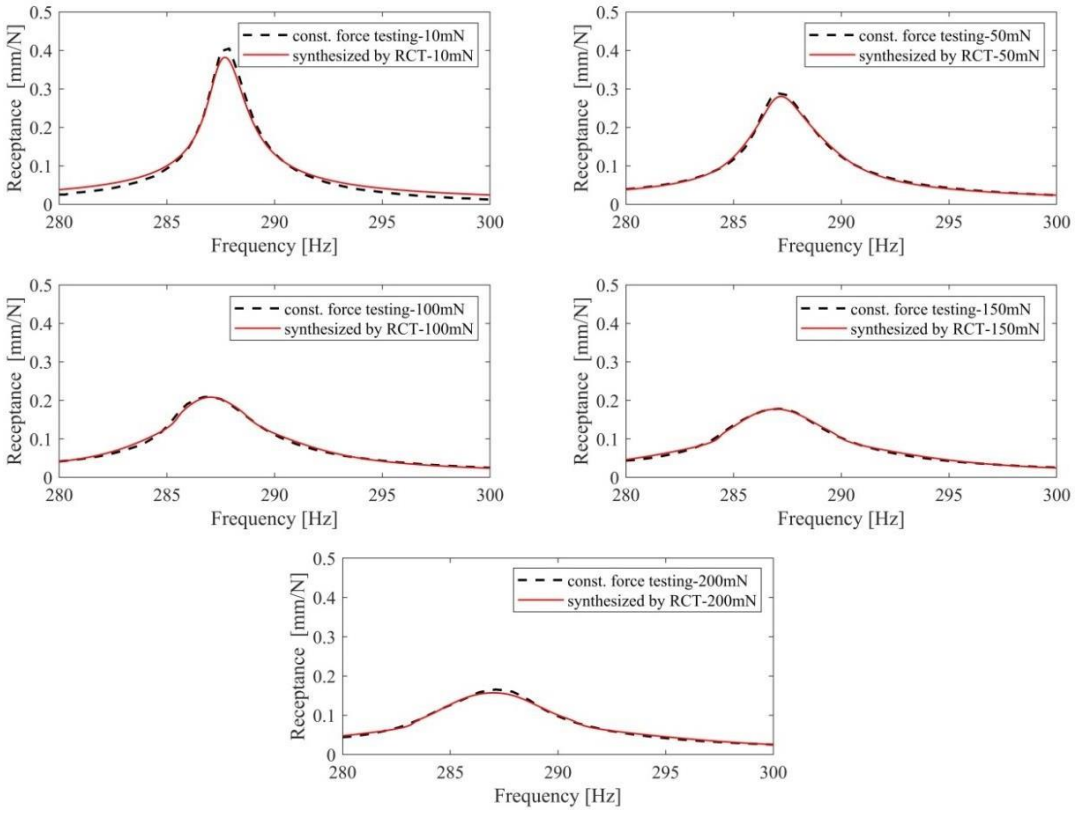

Fig. 5. Validation of the identified nonlinear modal parameters by comparing constant-force FRFs synthesized from these parameters with the ones directly measured by constant-force testing

3. DISCUSSIONS AND CONCLUSIONS

Poor repeatability in measurements of jointed structures makes it a challenging task to understand the nonlinear dynamics of mechanical joints and to develop reliable and accurate mathematical models from experiments. In this study, the RCT-HFS framework, which has been successfully applied to a wide range of structures in a short period of time, is applied for the nonlinear modal identification of a recently proposed benchmark beam with a lap joint, the so-called Orion beam. Since the experimental data available in the literature consists of constant-force FRFs, the HFS is constructed in a novel way by merging constant-force frequency response data, contrary to its usual implementation which uses constant-response

measurements. Cutting the HFS with constant displacement amplitude planes gives quasi-linear constant-response FRFs. These FRFs are then processed with a simple peak-picking method to identify nonlinear modal parameters as functions of response amplitude. The perfect match between the constant-force FRFs obtained from direct measurement and the ones synthesized from the identified nonlinear modal parameters demonstrates the accuracy of the RCT-HFS method. Since the constant-force FRFs are obtained from the *same measurement* in two different ways, the accuracy of the identified nonlinear modal parameters is shown in a sense bypassing the repeatability problem. Of course, the repeatability problem is still there and can be studied separately by applying the RCT-HFS framework on repeated measurements and obtaining uncertainty bounds of identified nonlinear modal parameters. Also, since the nature of the RCT measurements requires keeping the vibration amplitude of the excitation point constant, unlike the constant amplitude forcing testing approach, the system does not move into an uncontrolled high amplitude oscillation regime at and around the resonance frequencies. In an RCT-HFS framework, the resonance is observed with decreased forcing amplitudes only; therefore, it avoids drastic changes in alignments and contact conditions as well as reduces the stress levels around the joint region which is expected to reduce the severity of the repeatability problem in comparison to constant amplitude forcing measurements. This point will be studied in future work.

REFERENCES

Brake, M.R.W. (ed.), The mechanics of jointed structures, Springer, 2018.

Brake, M.R.W., Schwingshackl, C.W., Reuß, P., Observations of variability and repeatability in jointed structures, Mech. Syst. Signal Process., 129, pp. 282-307, 2019.

Dreher, T., Brake, M.R.W., Seeger, B., Krack, M., In situ, real-time measurements of contact pressure internal to jointed interfaces during dynamic excitation of an assembled structure, Mech. Syst. Signal Process., 160, 2021.

Jin, M., Kosova, G., Cenedese, M., Chen, W., Singh, A., Jana, D., Brake, M. R. W. et al., Measurement and identification of the nonlinear dynamics of a jointed structure using full-field data; Part II-Nonlinear system identification, Mech. Syst. and Signal Process., 166, 2022.

Karaağaçlı, T., Özgüven, H. N., Experimental modal analysis of nonlinear systems by using response-controlled stepped-sine testing, Mech. Syst. Signal Process., 146, 2021.

Szemplinska-Stupnicka, W., The modified single mode method in the investigation of the resonant vibration of nonlinear systems, J. Sound and Vib., 63(4), pp. 475-489, 1979.

Karaağaçlı, T., Özgüven, H.N., Experimental quantification and validation of modal properties of geometrically nonlinear structures by using response-controlled stepped-sine testing, Exp. Mech., 62, pp. 199-211, 2022.

Karaağaçlı, T., Özgüven, H.N., Experimental modal analysis of geometrically nonlinear structures by using response-controlled stepped-sine testing, in: Proceedings of the 39th International Modal Analysis Conference (IMAC), Orlando, FL, USA, 2021.

Koyuncu, A., Karaağaçlı, T., Şahin, M., Özgüven, H.N., Experimental modal analysis of nonlinear amplified piezoelectric actuators by using response-controlled stepped-sine testing, Exp. Mech., 62, pp. 1579-1594, 2022.

Karaağaçlı, T., Özgüven, H.N., Experimental modal analysis of structures with high nonlinear damping by using response-controlled stepped-sine testing, in: Proceedings of the 41st International Modal Analysis Conference (IMAC), Austin, TX, USA, 2023.

Teloli, R.O., Butaud, P., Chevallier, G., da Silva, S., Good practices for designing and experimental testing of dynamically excited jointed structures: The Orion beam, Mech. Syst. and Signal Process., 163, 2022.

Teloli, R.O., Butaud, P., Chevallier, G., da Silva, S., Dataset of experimental measurements for the Orion beam structure, Data in Brief, 39, 2021.